EXPLOITING NATURAL CHARACTERISTICS OF PNEUMATIC SERVO-ACTUATION THROUGH MULTI-INPUT CONTROL

By

Xiangrong Shen

Dissertation

Submitted to the Faculty of the

Graduate School of Vanderbilt University

in partial fulfillment of the requirements

for the degree of

DOCTOR OF PHILOSOPHY

in

Mechanical Engineering

May, 2006

Nashville, Tennessee

Approved:

Professor Michael Goldfarb

Professor Eric J. Barth

Professor Robert E. Bodenheimer

Professor Kenneth D. Frampton

Professor Nilanjan Sarkar

TABLE OF CONTENTS

ACKNOWLEDGEMENTS

First of all, I would like to thank my wife and parents for all their love and support in my life. Under my parents' encouragement, I came to the United States five years ago to pursue my dream. Here I struggled through the difficulties in the beginning, met my wife Xiaohui, and is about to start a family. At this point of time when I am about to complete my graduate study and obtain my PhD degree, I am really looking forward to having them attend my graduation ceremony and share this glorious time with me.

I would also like to thank my advisor, Dr. Michael Goldfarb. I won't be able to finish this work without his instruction and support. As both a great mentor and a dedicated researcher, he provides me a perfect example of how to conduct research and make real contributions.

My advisor at University of Nebraska – Lincoln, Dr. Shane Farritor, accepted me as his student when I essentially knew nothing about doing research, and offered great help in getting me started. Thank you, Dr. Farritor, for guiding my research with your brilliant ideas, and tolerating my slow progress.

Other people I want to thank are Dr. Barth, Kevin, Tom, Bobby, Navneet, Tyler, Yong and everybody else in the Center for Intelligent Mechatronics: working with you all was such a great experience. Besides, the valuable feedbacks from Dr. Sarkar, Dr. Frampton, and Dr. Bodenheimer are also greatly appreciated. Wish all of you good luck in your research and career.

LIST OF FIGURES

LIST OF TABLES

Page

CHAPTER I

INTRODUCTION AND SUMMARY

Introduction

Pneumatic actuation systems are widely used in robotics and automation applications due to their multiple advantages, e.g. low cost, high power-weight ratio, cleanness, etc. However, the compressibility of the working fluid and the highly nonlinear nature of the pneumatic systems pose great difficulty in their control. As such, initial application of pneumatic actuation systems was limited to the simple positioning tasks realized with simple on-off control valves and mechanical stops.

Extensive efforts have been expended for the precise positioning control of pneumatic actuation systems, pioneered by Shearer [1-3] in the 1950's. He studied the pneumatic processes in the motion control, and set up a complete mathematical model involving the compressibility of air in the actuator chambers and the characteristics of the airflow through the control valve. This model is still widely used in pneumatic system control. Several researchers also contributed to this topic, including Mannetje [4], Wang et al. [5], Bobrow and McDonell [6], and Richer and Hurmuzlu [7, 8], whose studies involved servocontrol via spool-type four-way servovalves, and Jacobsen et al. [9], Ben-Dov and Salcudean [10], and Henri et al. [11], whose studies involved control via flapper or jet-pipe type servovalves.

The aforementioned works require the use of expensive control valves, and the cost of valves dominates the cost of actuator in almost all cases. This inspires the research

in the first topic of this dissertation. Pulse width modulated (PWM) control offers the ability to provide servo control of pneumatic actuators at a significantly lower cost by utilizing binary solenoid valves in place of proportional servo valves. Instead of continuously varying the resistance of the control valve as in the case of proportional-valve-based systems, PWM-controlled systems meter the power delivered to the actuator discretely by delivering packets or quanta of fluid mass via a valve that is either completely on or completely off. If delivery of these packets of mass occur on a time scale that is significantly faster than the system dynamics (i.e., dynamics of the actuator and load), then the system will respond in essence to the average mass flow rate into and out of the cylinder, in a manner similar to the continuous case.

Despite the prior work on the control of pneumatic servo systems, little work has focused on exploiting the unique characteristics of the pneumatic systems. Different from that of an electromagnetic motor, the behavior of a pneumatic actuator is essentially a series elastic actuator, in which the compressed air acts as the elastic element. Thus, the stiffness of this elastic actuator physically exists and can be modulated by controlling the air masses in the actuator chambers. The research in the second and third topic of this dissertation leverages this unique characteristic to simultaneously control the output force and stiffness of a robotic actuator, and enhance the passivity of haptic interfaces, respectively.

Energy efficiency in the control of pneumatic servo systems is another topic that has received little attention before, partly because the compressed air supply in most cases is unlimited, e.g. from a power plant. With the increasing applications of pneumatic actuation in robotics, especially those in mobile robots, energy efficiency is becoming a

more significant issue. As previously mentioned, the behavior of a pneumatic actuator is essentially a series elastic actuator, in which energy can be stored in the elastic element – compressed air in the actuator chambers. If the energy stored in the compressed air can be reused rather than dissipated by exhausting to the atmosphere, a large portion of energy can be saved. This inspires the research in the fourth topic of this research, which achieves energy-saving control of pneumatic servo systems by utilizing cross-chamber flow.

The First Topic: Pulse Width Modulated Sliding Mode Control of Pneumatic Servo Systems

Background

Several researchers have investigated the PWM control of solenoid on/off valves for the servo control of pneumatic actuators. Noritsugu [12, 13] proposed a feedback speed or position control approach by utilizing three automobile-type fuel injection valves operating in a PWM mode, and the PWM signal is generated based on a proportional controller acting on the speed or position tracking error. Kunt and Singh [14] applied Floquet Theory to analyze the dynamic response of the on-off valve controlled pneumatic systems based on the linear time varying (LTV) model. Ye et al. [15] proposed two models for the pneumatic PWM solenoid valves, in which the valves were considered as on-off devices with opening and closing delays. The accuracy of the models was demonstrated with simulation results. Shih and Hwang [16] proposed a fuzzy PWM controller for the position control of a pneumatic robot cylinder, and the modified differential PWM method was used to eliminate the dead zone and improve the

performance. The above-mentioned works incorporate principally heuristic approaches, and they do not provide the stability or performance guarantees of approaches developed within a more rigorous analytical framework.

Some researchers applied the linear control approach to the PWM control of pneumatic systems. van Varseveld et al. [17] proposes the use of discrete time linear controllers for the PWM control of pneumatic servo systems. A PID controller with added friction compensation and position feedback was developed and the performance and robustness were demonstrated in experiments. Barth et al. [18] utilized a linear state-space averaging technique to enable the design of a linear compensator via a loop shaping approach that provides a prescribed degree of stability robustness in addition to a desired closed-loop bandwidth. Both of these works achieved a certain extent of success, however, the pneumatic servo systems are better treated within the nonlinear control framework due to the highly nonlinear nature.

In addition to the works based on the pulse width modulation (PWM) control, Paul et al. [19] proposed a switching controller (not technically a PWM controller) based on a “reduced-order” nonlinear model that provides stability in the sense of Lyapunov. However, in their work they neglected the major nonlinearities of pneumatic systems, i.e. the nonlinearity in the chamber pressure dynamics, the change in pressure boundary conditions that results when switching the direction of control effort (i.e., the upstream and downstream pressures switch from supply and chamber, respectively, to chamber and atmosphere), and the distinction between the choked and unchoked flow regimes through the solenoid valves.

Synopsis of Contribution

In the research of this topic, the nonlinear averaging technique is utilized for the development of an average model of the PWM controlled pneumatic servo systems, which is based on the full (i.e., non-reduced-order) nonlinear description of such systems. Then a sliding mode controller is developed and implemented on a single degree-of-freedom pneumatic servo system, and the effectiveness of the method verified by experimental trajectory tracking.

The Second Topic: Simultaneous Force and Stiffness Control of a Pneumatic Actuator

Background

Modulating the output stiffness of actuators can find a variety of uses in robotic applications, especially those inspired by biological behaviors. For example, largely due to their ability of modulating the joint stiffness independently of the joint torque, humans are capable of interacting with various types of environments in a stable and effective way. As proposed by Salisbury [20] and generalized by Hogan [21], one means of modulating actuator output stiffness is via feedback control. However, like all other feedback control systems, they are subject to several major drawbacks, e.g. limited frequency range, possible instability, etc. In order to develop variable output actuators free of these limitations, several researchers have developed actuators with physically variable stiffness.

Lurin-Kovitz et al. [22] proposed the design of a variable stiffness actuator incorporating two motors for each joint, each actuating opposite ends of a tendon through

a nonlinear spring. This approach is quite similar to the manner in which humans affect motor control – differences in tension between antagonist muscle groups generates a joint torque, while the sum of the muscle tensions determines the joint stiffness.

Koganezawa and Yamazaki [23], Koganezawa and Ban [24] and English and Russell [25, 26] proposed the variable stiffness actuators in similar configurations.

Hurst et al. [27] and Tonietti et al. [28] also proposed their variable stiffness actuator designs with two motors for each degree-of-freedom, but in their design the stiffness is modulated by adjusting the spring pretension with the second motor, in stead of the aforementioned agonist-antagonist approaches.

Synopsis of Contribution

In the research of this topic, a variable stiffness actuator design is proposed by leveraging the open-loop behavior of a pneumatic actuator. This design offers a more compact package with less mechanical complexity than other previously described approaches. Like the agonist/antagonist systems previously described, the actuator force is a function of the difference between the chamber pressures, while the actuator output stiffness is a function of their sum. By decoupling the single four-way valve into a pair of three-way valves, the pressures in each cylinder can be independently controlled, thus the actuator output stiffness can be controlled independently of the actuation force. An approach for the independent stiffness and force control of the pneumatic actuator is presented, along with the experimental results showing the force and stiffness tracking performance.

The Third Topic: On the Enhanced Passivity of Pneumatically-Actuated Impedance-Type Haptic Interfaces

Background

In the haptic simulation of virtual environments, stiffness is a defining characteristic of rigid objects and surfaces. However, the capability of most haptic devices is limited in simulating high stiffness due to the stability issue. Despite the fact that such behavior (i.e. a single value algebraic relationship between force and position) is energetically conservative, impedance-type simulations of haptic surfaces generally result in active behavior, which in turn can result in instability of the device. The active behavior of simulated surfaces is due primarily to the disproportionality between displacement and force introduced by discretization, digital quantization, and phase lag introduced by sensor filtering and the mechanical dynamics of the haptic interface [29], which have been collectively referred to as "energy leaks" [30]. This issue has been studied and treated by several researchers.

Colgate et al. [31] and Colgate and Schenkel [32, 33] derived a condition for the passivity of a discretely simulated wall that indicates that the maximum stiffness to preserve passivity of the haptic interface is proportional to the ratio of open-loop damping in the device to the sampling period of the simulation.

Abbott and Okamura [34] and Diolaiti et al. [35] have generalized this result by additionally considering the Coulomb friction and the effects of quantization.

Love and Book [36] also present an analysis for the stability of a discretely simulated haptic surface, but incorporate a classical stability analysis of the discrete-time characteristic equation rather than a passivity-based approach.

In order to enhance the stability of haptic simulation, a number of control approaches are proposed, among which most works address the problem via software modification.

Based on the passivity analysis presented by Colgate and Schenkel, Colgate et al. [37] proposed the use of a "virtual coupling," which is in essence a filter placed between the haptic device and the simulated environment. The "virtual coupling" in effect modifies the simulated environment to ensure that it preserves passivity of the system (as given by the condition derived in [32, 33]. Adams and Hannaford [38] and Stramigioli et al. [39] further developed virtual coupling methods.

Hannaford and Ryu [40] proposed a time-based approach to the design of a virtual coupling that monitors the net power flow and adjusts the properties of the coupling to ensure energetically passive behavior of the haptic system over time.

Finally, Gillespie and Cutkosky [30], Ellis et al. [41], Goldfarb and Wang [42], and Madill et al. [43] propose other algorithms, not explicitly based on passivity, that compensate for the energy leaks in a haptic simulation.

Based on the conclusion proposed by Colgate et al. [31] and Colgate and Schenkel [32, 33], the maximum stiffness to preserve passivity of the haptic interface is proportional to the ratio of open-loop damping in the device to the sampling period of the simulation. Thus, by adding open-loop damping to the design of the device, higher stiffness simulations can be obtained without sacrificing the dynamic character of the simulation.

Colgate and Brown [29] demonstrated this approach by showing that a mechanical damper coupled to the output shaft of a motor-actuated haptic display increased significantly the range of simulated impedances that maintain passive behavior.

Based on a similar notion, Mehling et al. [44] proposed a variation on this theme that utilized an electrical resistance across the motor leads rather than a mechanical damper.

Synopsis of Contribution

The work proposed in this topic is a related approach to that proposed by Colgate and Schenkel and implemented in various incarnations by Colgate and Brown and Mehling et al., but rather than add open-loop damping to the device, the proposed approach leverages the open-loop stiffness of pneumatic actuators to enhance the passivity of the haptic simulation of a stiff surface. A stability analysis is presented to show that the presence of open-loop stiffness in the pneumatic actuator enhances the range of achievable surface stiffnesses relative to an electric motor actuated system, and additionally show that the system is always stable in free space. Experimental results indicate the enhanced passivity of the proposed approach.

The Fourth Topic: Energy Saving in Pneumatic Servo Control Utilizing Inter-Chamber Cross-Flow

Background

Several control and design approaches have been investigated for the energy saving purpose in the control of pneumatic systems, such as the works proposed by Sanville [45], Quaglia and Gestaldi [46, 47], Pu et al. [48], Wang et al. [49], Kawakami et al. [50], Arinaga et al. [51], and Margolis [52].

Sanville [45] proposed a two-level system, in which a secondary reservoir collects exhaust air and serves as an auxiliary power supply. The analysis showed the possibility of doubling the overall efficiency compared with the equivalent conventional system. However, this approach requires a variable-speed compressor and no experimental results were presented to show the exact effect of the reduction of compressed air consumption.

Quaglia and Gestaldi [46, 47] proposed a novel linear pneumatic actuator design for the energy saving purpose, which incorporated multiple cylinder chambers. This actuator achieves energy saving by controlling the air cross flows between the chambers with control valves so that the high-pressure air can be reused rather than exhausted to the atmosphere. They developed a model for the actuator and verified it in experiments, but motion control was not included in this work.

Pu et al. [48] proposed a new configuration of pneumatic servo system in which a direct flow path between the two chambers of a double-acting cylinder was added. By utilizing the cross flow between the chambers, the compressed air can be reused and the low-pressure chamber can be pressured more rapidly so that the system bandwidth can be improved. A PID controller with mode switching was presented, along with the

simulation and experimental results. Since no energy consumption data was presented, the exact effect of energy saving was unclear.

Wang et al. [49] studied the effect of velocity profile on the energy saving in the point-to-point motion control. They compared three particular shaped profiles and the simulation results showed that the energy efficiency in such tasks could be improved by properly designing the velocity profiles.

Kawakami et al. [50] proposed an approach to reduce the air consumption in the point-to-point driving system with meter-in and meter-out circuits. Arinaga et al. [51] also used metering circuits for point-to-point motions, and in their approach energy can be saved by cutting off the air supply when the piston reaches the end of the stroke.

Al-Dakkan et al. [52] developed a dynamic constraint based energy saving control approach of pneumatic servo systems. In this approach, the four-way valve in the tradition pneumatic servo system was replaced by a pair of two three-way valves and the additional control degree-of-freedom was utilized to satisfy an energy-related dynamic constraint. Their experimental results indicated energy savings of 27% to 45%, depending on desired tracking frequency.

Margolis [53] proposed a position control system with an energy storage actuator. The control system utilized the accumulator in the actuator to store energy when the load is decelerated and reuse the energy when required. Both position control and force control were demonstrated to provide good response by this system, while the exact energy saving effect is not clear since no energy consumption data was presented.

Synopsis of Contribution

Like the work of Al Dakkan et al., the research in this topic proposed an approach to energy saving in the context of a servocontrolled pneumatic actuator. The decoupled configuration (utilized in Al Dakkan et al.) enables independent control of cylinder chamber pressures, but does not enable the reuse or recycling of pressurized air. Unlike that work, the work presented herein utilizes a cross flow configuration rather than a decoupled configuration, such that pressurized air can be recycled. The structural configuration utilized in this work is similar to that used in the work of Pu et al. The control approach, however, is quite different. Specifically, they utilize a linear control approach that assumes for simplicity that the command to the cross flow valve is linearly related to the command for the standard (four-way) valve. Further, the "preliminary" results presented by Pu et al. do not quantify the energy savings provided by their approach (relative to a standard approach), and thus the effectiveness of the proposed approach is unclear. The work presented in this paper incorporates a nonlinear control approach that constrains the valves only by the tracking and energy saving objectives, and experimentally demonstrates the effectiveness of the proposed approach relative to a standard (four-way valve) approach.

References

[1] Shearer, J. L., "Study of Pneumatic Processes in the Continuous Control of Motion with Compresses Air – I," *Transactions of the ASME*, vol. 78, pp. 233-242, 1956.

[2] Shearer, J. L., "Study of Pneumatic Processes in the Continuous Control of Motion with Compresses Air – II," *Transactions of the ASME*, vol. 78, pp. 243-249, 1956.

[3] Shearer, J. L., "Nonlinear Analog Study of a High-Pressure Servomechanism," *Transactions of the ASME*, vol. 79, pp. 465-472, 1957.

[4] Mannetje, J. J., "Pneumatic Servo Design Method Improves System Bandwidth Twenty-fold," *Control Engineering*, vol. 28, no. 6, pp. 79-83, 1981.

[5] Wang, J., Pu, J., and Moore, P., "A practical control strategy for servo-pneumatic actuator systems," *Control Engineering Practice*, vol. 7, pp. 1483-1488, 1999.

[6] Bobrow, J., and McDonell, B., "Modeling, Identification, and Control of a Pneumatically Actuated, Force Controllable Robot," *IEEE Transactions on Robotics and Automation*, vol. 14, no. 5, pp. 732-742, 1998.

[7] Richer, E. and Hurmuzlu, Y., "A High Performance Pneumatic Force Actuator System: Part I-Nonlinear Mathematical Model" *ASME Journal of Dynamic Systems, Measurement, and Control*, vol. 122, no. 3, pp. 416-425, 2000.

[8] Richer, E. and Hurmuzlu, Y., "A High Performance Pneumatic Force Actuator System: Part II-Nonlinear Control Design" *ASME Journal of Dynamic Systems, Measurement, and Control*, vol. 122, no. 3, pp. 426-434, 2000.

[9] Jacobsen, S.C., Iversen E.K., Knutti, D.F., Johnson, R.T., and Biggers, K.B., "Design of the Utah/MIT Dextrous Hand," *IEEE International Conference on Robotics and Automation*, pp. 1520-1532, 1986.

[10] Ben-Dov, D. and Salcudean, S.E., "A Force-Controlled Pneumatic Actuator," *IEEE Transactions on Robotics and Automation*, vol. 11, no. 6, pp. 906-911, 1995.

[11] Henri, P.D., Hollerbach, J.M., and Nahvi, A., "An Analytical and Experimental Investigation of a Jet Pipe Controlled Electropneumatic Actuator," *IEEE Transactions on Robotics and Automation*, vol. 14, no. 4, pp. 601-611, 1998.

[12] Noritsugu, T., "Development of PWM Mode Electro-Pneumatic Servo-mechanism. Part I: Speed Control of a Pneumatic Cylinder," *Journal of Fluid Control*, vol. 17, no. 1, pp. 65-80, 1986.

[13] Noritsugu, T., "Development of PWM Mode Electro-Pneumatic Servo-mechanism. Part II: Position Control of a Pneumatic Cylinder," *Journal of Fluid Control*, vol. 17, no. 2, pp. 7-31, 1986.

[14] Kunt, C., and Singh, R., "A Linear Time Varying Model for On-Off Valve Controlled Pneumatic Actuators," *ASME Journal of Dynamic Systems, Measurement, and Control,* vol. 112, no. 4, pp. 740-747, 1990.

[15] Ye, N., Scavarda, S., Betemps, M., and Jutard, A., "Models of a Pneumatic PWM Solenoid Valve for Engineering Applications," *ASME Journal of Dynamic Systems, Measurement, and Control,* vol. 114, no. 4, pp. 680-688, 1992.

[16] Shih, M., and Hwang, C., "Fuzzy PWM Control of the Positions of a Pneumatic Robot Cylinder Using High Speed Solenoid Valve," *JSME International Journal*, vol. 40, no. 3, pp. 469-476, 1997.

[17] van Varseveld, R. B., and Bone, G. M., "Accurate Position Control of a Pneumatic Actuator Using On/Off Solenoid Valves," *IEEE/ASME Transactions on Mechatronics*, vol. 2, no. 3, pp. 195-204, 1997.

[18] Barth E. J., Zhang, J., and Goldfarb, M., 2003, "Control Design for Relative Stability in a PWM-Controlled Pneumatic System." *ASME Journal of Dynamic Systems, Measurement, and Control*, vol. 125, no. 3, pp. 504-508.

[19] Paul, A. K., Mishra, J. K., Radke, M. G., 1994, "Reduced Order Sliding Mode Control for Pneumatic Actuator," *IEEE Transactions on Control Systems Technology*, vol. 2, no.3, pp. 271-276.

[20] Salisbury, J.K., "Active Stiffness Control of a Manipulator in Cartesian Coordinates," *IEEE Conference on Decision and Control*, pp. 383 – 388, 1980.

[21] Hogan, N., "Impedance Control: An Approach to Manipulation," *Journal of Dynamic Systems, Measurement, and Control*, pp. 1 – 24, 1985.

[22] Laurin-Kovitz, K.F.; Colgate, J.E.; Carnes, S.D.R. "Design of components for programmable passive impedance," *IEEE International Conference on Robotics and Automation*, vol. 2, pp. 1476-1481, 1991.

[23] Koganezawa, K. and Yamazaki, M. "Mechanical stiffness control of tendon-driven joints," *IEEE/RSJ International Conference on Intelligent Robots and Systems*, pp. 818–825, 1999.

[24] Koganezawa, K., Ban, S., "Stiffness Control of Antagonistically Driven Redundant DOF Manipulator," in *Proceedings of the IEEE/RSJ International Conference on Intelligent Robots and Systems*, pp. 2280-2285, 2002.

[25] English, C.E. and Russell, D. “Mechanics and stiffness limitations of a variable stiffness actuator for use in prosthetic limbs,” *Mechanism and Machine Theory*, vol. 34, no. 1, pp. 7-25, 1999.

[26] English, C.E. and Russell, D. “Implementation of variable joint stiffness through antagonistic actuation using rolamite springs,” *Mechanism and Machine Theory*, vol. 34, no. 1, pp. 27-40, 1999.

[27] Hurst, J.W., Chestnutt, J.E., and Rizzi, A.A. “An actuator with physically variable stiffness for highly dynamic legged locomotion,” *IEEE International Conference on Robotics and Automation*, pp. 4662-4667, 2004.

[28] Tonietti, G., Schiavi, R., and Bicchi, A. “Design and control of a variable stiffness actuator for safe and fast physical human/robot interaction,” *IEEE International Conference on Robotics and Automation*, pp. 528-533, 2005.

[29] Colgate, J. E. and Brown, J. M., “Factors affecting the Z-width of a haptic display,” in *Proceedings of the IEEE International Conference on Robotics and Automation*, pp. 3205-3210, 1994.

[30] Gillespie, R. B. and Cutkosky, M. R., “Stable user-specific haptic rendering of the virtual wall,” in *Proceedings of ASME Dynamic Systems and Control Division*, vol. 58, pp. 397-406, 1996.

[31] Colgate, J. E., Grafing, P. E., Stanley, M. C. and Schenkel, G., “Implementation of stiff virtual walls in force reflecting interfaces,” in *Proceedings of IEEE Virtual Reality Annual International Symposium*, pp. 202-207, 1993.

[32] Colgate, J. E. and Schenkel, G., “Passivity of a class of sampled-data systems: Application to haptic interfaces,” in *Proceedings of the American Control Conference*, pp. 3236-3240, 1994.

[33] Colgate, J. E. and Schenkel, G., “Passivity of a class of sampled-data systems: Application to haptic interfaces,” *Journal of Robotic Systems*, vol. 14, no. 1, pp. 37-47, Jan. 1997.

[34] Abbott, J. and Okamura, A., “A sufficient condition for passive virtual walls with quantization effects,” in *Proceedings of 2004 ASME International Mechanical Engineering Congress and Exposition*, pp. 1065-1073, 2004.

[35] Diolaiti, N., Niemeyer, G., Barbagli, F. and Salisbury, J. K., “A criterion for the passivity of haptic devices,” in *Proceedings of the IEEE International Conference on Robotics and Automation*, pp. 2463-2467, 2005.

[36] Love, L. and Book, W., "Contact stability analysis of virtual walls," in *Proceedings of ASME Dynamic Systems and Control Division*, vol. 57, pp. 689-694, 1995.

[37] Colgate, J. E., Stanley, M. C., and Brown, J. M., "Issues in the haptic display of tool use," in *Proceedings of the IEEE/RSJ International Conference on Intelligent Robots and Systems*, vol. 3, pp. 140-145, 1995.

[38] Adams, R. J. and Hannaford, B., "Stable haptic interaction with virtual environments," *IEEE Transactions on Robotics and Automation*, vol. 15, no. 3, pp. 465-474, June 1999.

[39] Stramigioli, S., Secchi, C., van der Schaft, A. and Fantuzzi, C., "A novel theory for sample data system passivity," in *Proceedings of the IEEE/RSJ International Conference on Intelligent Robots and Systems*, pp. 1936-1941, 2002.

[40] Hannaford, B. and Ryu, J. H., "Time-domain passivity control of haptic interfaces," *IEEE Transactions on Robotics and Automation*, vol. 18, no. 1, pp. 1-10, Feb. 2002.

[41] Ellis, R. E., Sarkar, N., and Jenkins, M. A., "Numerical methods for the haptic presentation of contact: theory, simulations, and experiments," in *Proceedings of the ASME Dynamic Systems and Control Division*, vol. 58, pp. 413-420, 1996.

[42] Goldfarb, M. and Wang, J., "Passive stiffness simulation with rate-independent hysteresis," in *Proceedings of ASME Dynamic Systems and Control Division*, vol. 67, pp. 345-350, 1999.

[43] Madill, D., Wang, D. and Ching, M., "A nonlinear observer for minimizing quantization effects in virtual walls," in *Proceedings of ASME Dynamic Systems and Control Division*, vol. 67, pp. 335-343, 1999.

[44] Mehling, J. S., Colgate, J. E., Peshkin, M. A., "Increasing the Impedance Range of a Haptic Display by Adding Electrical Damping", in *Proceedings of IEEE First Joint Eurohaptics Conference and Symposium on Haptic Interfaces for Virtual Environment and Teleoperator Systems*, pp. 257-262, 2005.

[45] Sanville, F. E., "Two-level Compressed Air Systems for Energy Saving," *The 7th International Fluid Control Symposium*, pp. 375-383, 1986.

[46] Quaglia, G. and Gastaldi, L., "The Design of Pneumatic Actuator with Low Energy Consumption," *The 4th Triennial International Symposium on Fluid Control, Fluid Measurement, and Visualization*, pp. 1061-1066, 1994.

[47] Quaglia, G. and Gastaldi, L., "Model and Dynamic of Energy Saving Pneumatic Actuator," *The 4th Scandinavian International Conference on Fluid Power*, vol. 1, 481-492, 1995.

[48] Pu, J., Wang, J. H., Moore, P. R., and Wong, C. B., "A New Strategy for Closed-loop Control of Servo-Pneumatic Systems with Improved Energy Efficiency and System Response," *The Fifth Scandinavian International Conference on Fluid Power*, pp. 339-352, 1997.

[49] Wang, J., Wang, J-D., Liau, V., "Energy Efficient Optimal Control of Pneumatic Actuator Systems," *Systems Science*, vol. 26, 3, pp. 109-123, 2000.

[50] Kawakami, Y., Terashima, Y., Kawai, S., "Application of Energy-saving to Pneumatic Driving Systems," in *Proceedings of 4th JHPS International Symposium*, pp. 201-206, 1999.

[51] Arinaga, T., Kawakami, Y., Terashima, Y., and Kawai, S., "Approach for Energy-Saving of Pneumatic Systems," in *Proceedings of the 1st FPNI-PhD Symposium*, pp. 49-56, 2000.

[52] Al-Dakkan, K. A., Barth, E. J., Goldfarb, M., "A Multi-Objective Sliding Mode Approach for the Energy Saving Control of Pneumatic Servo Systems," ASME International Mechanical Engineering Conference and Exposition, IMECE2003-42746, 2003.

[53] Margolis, D., "Energy Regenerative Actuator for Motion Control with Application to Fluid Power Systems," *Journal of Dynamic systems, Measurement and Control*, vol. 127, pp. 33-40, March 2005

CHAPTER II: MANUSCRIPT 1

PULSE WIDTH MODULATED SLIDING MODE CONTROL OF PNEUMATIC SERVO SYSTEMS

Xiangrong Shen, Jianlong Zhang, Eric J. Barth, Michael Goldfarb

Department of Mechanical Engineering

Vanderbilt University

Nashville, TN 37235

(Accepted by the *ASME Journal of Dynamic Systems, Measurement, and Control*)

Abstract

This paper presents a control methodology that enables nonlinear model based control of pulse width modulated (PWM) pneumatic servo actuators. An averaging approach is developed to describe the equivalent continuous-time dynamics of a PWM controlled nonlinear system, which renders the system, originally discontinuous and possibly non-affine in the input, into an equivalent system that is both continuous and affine in control input (i.e., transforms the system to nonlinear control canonical form). This approach is applied to a pneumatic actuator controlled by a pair of three-way solenoid actuated valves. The pneumatic actuation system is transformed into its averaged equivalent control canonical form and a sliding mode controller is developed based on the resulting model. The controller is implemented on an experimental system,

and the effectiveness of the proposed approach validated by experimental trajectory tracking.

Introduction

The servo control of pneumatic actuators is typically implemented by utilizing some type of servovalve to control the airflow into and out of the respective sides of a pneumatic cylinder. Several researchers have studied the design and control of such systems, including Shearer [1-3], Mannetje [4], Wang et al. [5], Bobrow and McDonell [6], and Richer and Hurmuzlu [7, 8], whose studies involved servocontrol via spool-type four-way servovalves, and Jacobsen et al. [9], Ben-Dov and Salcudean [10], and Henri et al. [11], whose studies involved control via flapper or jet-pipe type servovalves. In such systems, the cost of the servovalve in nearly all cases dominates the cost of the actuator.

Pulse width modulated (PWM) control offers the ability to provide servocontrol of pneumatic actuators at a significantly lower cost by utilizing binary solenoid valves in place of proportional servovalves. In a pneumatic servo system controlled by proportional servovalves, the power delivered to the pneumatic actuator is metered by continuously varying the flow resistance of the valve, which in turn continuously varies the fluid mass flow rate into and out of the respective sides of the cylinder. In a PWM-controlled system, the power delivered to the actuator is metered discretely by delivering packets or quanta of fluid mass via a valve that is either completely on or completely off. If delivery of these packets of mass occurs on a time scale that is significantly faster than the system dynamics (i.e., dynamics of the actuator and load), then the system will respond in essence to the average mass flow rate into and out of the cylinder, in a manner

similar to the continuous case. As is the case with control via servovalves, several researchers have investigated the use of PWM control of solenoid on/off valves for the servo control of pneumatic actuators. In particular, Noritsugu [12, 13], Kunt and Singh [14], Ye et al. [15], and Shih and Hwang [16] incorporate principally heuristic approaches for the PWM control of pneumatic servo systems. Though such approaches afford a level of control, they do not provide the stability or performance guarantees of approaches developed within a more rigorous analytical framework. The work of van Varseveld and Bone [17] proposes the use of discrete time linear controllers for the PWM control of pneumatic servo systems. Barth et al. [18] utilize a linear state-space averaging technique to enable the design of a linear compensator via a loop shaping approach that provides a prescribed degree of stability robustness in addition to a desired closed-loop bandwidth. Both of these prior works treat the PWM control of pneumatic servo systems within the context of linear control. Due to their highly nonlinear nature, pneumatic servo systems are better addressed by the use of nonlinear model-based control techniques. Paul et al. [19] proposed a switching controller (not technically a PWM controller) based on a "reduced-order" nonlinear model that provides stability in the sense of Lyapunov. The "reduced-order" aspect of their approach, however, requires simplifying assumptions that cannot accommodate the full nonlinear character of a pneumatic servo system. In particular, they neglect the nonlinearity in the chamber pressure dynamics, the change in pressure boundary conditions that results when switching the direction of control effort (i.e., the upstream and downstream pressures switch from supply and chamber, respectively, to chamber and atmosphere), and the

distinction between the choked and unchoked flow regimes through the solenoid valves. These combined effects constitute significant nonlinear behavior in such systems.

Unlike these prior works, this paper presents a method for nonlinear model based PWM control of a pneumatic servo actuator based on the full nonlinear model of such systems. Specifically, this paper extends the authors' previously published averaging techniques, which were developed in the context of linear systems [18], to nonlinear systems. The nonlinear averaging technique is then utilized as the basis for the development of a PWM-based sliding mode approach to the control of pneumatic servo systems, which is based on the full (i.e., non-reduced-order) nonlinear description of such systems. The controller is implemented on a single degree-of-freedom pneumatic servo system, and the effectiveness of the method verified by experimental trajectory tracking.

Average Model Based PWM-Control of Nonlinear Systems

A pulse width modulated control system meters the power delivered to an actuator from a power source in discrete packets, as opposed to the continuous delivery of power characteristic in a continuous control system (i.e., those treated in [1-11]). The "packets" of power delivered by a PWM system, however, are in essence averaged by the dynamics of the system being controlled. As such, the resulting dynamics, on the characteristic time-scale of interest for the closed-loop system, can be described by the average dynamics of such systems. Consider a general nonlinear dynamic system given in regular form as,

$$x^{(n)} = f(\mathbf{x}, \mathbf{u}) \tag{1}$$

where $x^{(n)}$ is the n^{th} derivative of x, $\mathbf{x} \in R^n$ is a vector of the continuous states of the system (i.e., all lower derivatives of x), $\mathbf{u} \in R^m$ is the vector of control inputs, and $f(\cdot,\cdot)$ describes the form of the system dynamics. In a PWM-controlled system, the elements of the control vector u_i are binary variables, such that they can only assume values of 0 or 1. Consider the case of p allowable combinations of the control vector $\mathbf{u}$, each referred to as input mode i, such that $\mathbf{u}_i : i \in \{1, 2, \ldots, p\}$. Since the elements of $\mathbf{u}_i$ are binary, selection of an input mode effectively selects a subset of the dynamics $f(\mathbf{x}, \mathbf{u})$. If $f_i(\mathbf{x})$ describes the dynamics corresponding to the input $\mathbf{u}_i$, then the system dynamics for a PWM-controlled system can assume p distinct forms, which correspond to its p distinct input modes. The dynamics of the system operating in each respective mode can be written as:

$$x^{(n)} = f_i(\mathbf{x}) \quad \text{for} \quad 1 \le i \le p \tag{2}$$

Within each PWM period, the control input can switch between modes 1 through p, where the fraction of the PWM period that any given mode is active is the duty cycle of that mode, or modal duty cycle, denoted as d_i. These modal duty cycles can be written in vector form as

$$D = \begin{bmatrix} d_1 & d_2 & \ldots & d_p \end{bmatrix}^T \tag{3}$$

where the 1-norm of this vector must satisfy

$$\|D\|_1 = 1 \tag{4}$$

which simply indicates that the duration of modes active must comprise the full duration of the PWM period. Collecting the system dynamics for each mode in the vector

$$F = \begin{bmatrix} f_1 & f_2 & \ldots & f_p \end{bmatrix}^T \tag{5}$$

the average system dynamics can be described by

$$x^{(n)} = F^T D \tag{6}$$

In the case of $p = 2$ (i.e., the minimum possible number of input modes), the input/output relationship is uniquely specified (i.e., it is the PWM equivalent of a single-input, single-output system). In this case, because of the constraint (4), the modal input vector can be written in terms of a single duty cycle as

$$D = \begin{bmatrix} d \\ 1-d \end{bmatrix} \tag{7}$$

and the state averaged model of this system written as,

$$x^{(n)} = f_1 d + f_2 (1-d) \tag{8}$$

The form of (8) can be recast in control canonical form, affine in the new continuous control variable *d* as

$$x^{(n)} = \tilde{f}(\mathbf{x}) + \tilde{b}(\mathbf{x}) d \tag{9}$$

where $\tilde{f}(\mathbf{x}) = f_2(\mathbf{x})$, $\tilde{b}(\mathbf{x}) = f_1(\mathbf{x}) - f_2(\mathbf{x})$, and the input is confined to a saturated range $d \in [0, 1]$. Since most control systems are generally symmetric in the control effort, in many cases it may be preferable to transform the control input *d* into a symmetric input *u* centered about zero (i.e., $u \in [-1, 1]$, though the amplitude may be other than unity if so desired). A simple linear transformation for the case $u \in [-1, 1]$ can be expressed as

$$u = 2d - 1 \tag{10}$$

such that (9) can be written as

$$x^{(n)} = \tilde{f}(\mathbf{x}) + \tilde{b}(\mathbf{x}) u \tag{11}$$

where the continuous input is confined to the symmetric range $u \in [-1, 1]$. Note that a nonlinear transformation could be used in place of (10) such that $u \in (-\infty, \infty)$, if so

desired. Equation (11) expresses a system dynamics, originally influenced by discontinuous control inputs, into an equivalent system that is affine in its single, continuous control input (i.e., the nonlinear system has been transformed into a control canonical form). Such a form is well suited to many nonlinear control approaches (e.g., sliding mode control, integrator back-stepping control).

In the case of $p > 2$ (i.e., three or more input modes), the mapping from the control inputs to system output (x) is non-unique, and as such constraints must be added in order to provide a unique dynamics (i.e., the case of $p > 2$ is the PWM equivalent of a multi-input, single-output system). Specifically, $p - 2$ constraints must be added to constraint (4) so that the vector of modal inputs can be described as a function of a single input (as described for the two-mode case by (7)). These constraints can be written in a general form as

$$D = \boldsymbol{\gamma}(d) \tag{12}$$

where $\boldsymbol{\gamma}(\cdot) \in R^p$. Given the constraints expressed by (12), along with (6) and (10), the system dynamics can be written in control canonical form as a function of the symmetric, continuous control input $u \in [-1, 1]$ as

$$x^{(n)} = \tilde{f}(\mathbf{x}) + \tilde{b}(\mathbf{x})u \tag{13}$$

where the exact forms of $\tilde{f}$ and $\tilde{b}$ depend upon the form of (12). Thus, a nonlinear system, originally discontinuous and possibly non-affine in the input, can be transformed into an equivalent system that is both continuous and affine in the single continuous control input. Various nonlinear model-based techniques may be applied directly to the resulting equivalent nonlinear control canonical model. Based on this approach, the

following two sections develop a nonlinear model and sliding mode controller for a pneumatic servo system.

A Nonlinear Averaged Model of a PWM-Controlled Pneumatic Servo System

In the case of a pneumatic servo system controlled by solenoid valves, the (previously mentioned) discrete inputs to the nonlinear system are the valve spool (or poppet) positions, and the continuous output is the motion of the load. In order to convert the discontinuous system inputs to an equivalent continuous input, the behavior of the system in each discrete mode must first be described. This section of the paper derives a model of the pneumatic servo system, defines and describes the discrete modes of operation of this system, and finally derives the equivalent description from (continuous) input to motion based on the averaging methods previously described.

Assuming air is a perfect gas undergoing an isothermal process, the rate of change of the pressure inside each chamber of the cylinder can be expressed as:

$$\dot{P}_{(a,b)} = \frac{RT}{V_{(a,b)}}\left(\dot{m}_{in(a,b)} - \dot{m}_{out(a,b)}\right) - \frac{P_{(a,b)}}{V_{(a,b)}}\dot{V}_{(a,b)} \tag{14}$$

where $P_{(a,b)}$ is the absolute pressure inside each side of the cylinder, $\dot{m}_{in(a,b)}$ and $\dot{m}_{out(a,b)}$ are the mass flow rates into and out of each side of the cylinder, R is the universal gas constant, T is the fluid temperature, and $V_{(a,b)}$ is the volume of each cylinder chamber. Based on isentropic flow assumptions, the mass flow rate though a valve orifice with effective area A_v for a compressible substance will reside in either a sonic (choked) or subsonic (unchoked) flow regime:

$$\dot{m}(P_u, P_d) = \begin{cases} \sqrt{\frac{k}{RT}\left(\frac{2}{k+1}\right)^{(k+1)/(k-1)}} C_f P_u A_v & \text{if } \frac{P_d}{P_u} \le C_r \text{ (choked)} \\ \sqrt{\frac{2k}{RT(k-1)}} \sqrt{1 - \left(\frac{P_d}{P_u}\right)^{(k-1)/k}} \left(\frac{P_d}{P_u}\right)^{(1/k)} C_f P_u A_v & \text{otherwise (unchoked)} \end{cases}$$

(15)

where C_f is the discharge coefficient of the valve, P_u and P_d are the upstream and downstream pressures, respectively, k is the ratio of specific heats, C_r is the pressure ratio that divides the flow regimes into unchoked and choked flow, and A_v is the cross-sectional area of the valve orifice. Assuming a combined inertial and viscous load, the motion dynamics of the system shown in Figure 2-1 can be written as:

$$M\ddot{x} + B\dot{x} = P_a A_a - P_b A_b - P_{atm} A_r \tag{16}$$

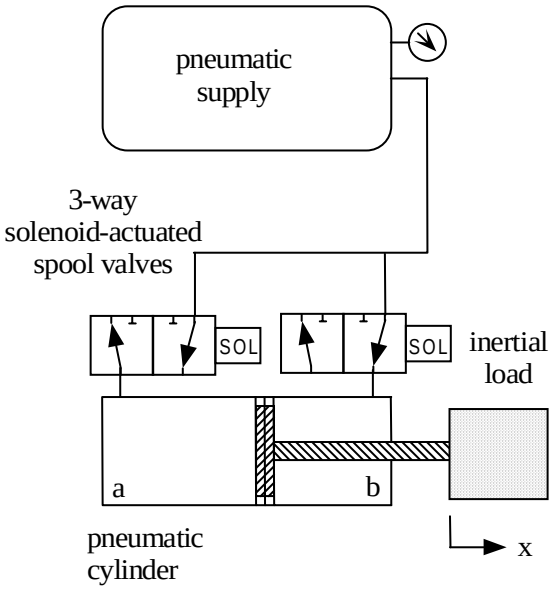

Figure 2-1. Solenoid valve controlled pneumatic servoactuator driving an inertial load.

where M is the payload plus the piston and rod assembly mass, B is the viscous friction coefficient, A_a and A_b are the effective areas of each side of the piston, and A_r is the cross-sectional area of the piston rod. The total dynamics from the valve area as input (which is an algebraic function of the spool position) to the motion output is given by the combination of (14-16):

$$\dddot{x} = \frac{A_a}{M}\left[\frac{RT}{V_a}\left(\dot{m}_{in,a} - \dot{m}_{out,a}\right) - \frac{P_a}{V_a}\dot{V}_a\right] - \frac{A_b}{M}\left[\frac{RT}{V_b}\left(\dot{m}_{in,b} - \dot{m}_{out,b)}\right) - \frac{P_b}{V_b}\dot{V}_b\right] - \frac{B}{M}\ddot{x} \qquad (17)$$

where $\dot{m}_{in,a}$, $\dot{m}_{out,a}$, $\dot{m}_{in,b}$, $\dot{m}_{out,b}$ are the mass flow rates into and out of the two sides of the cylinder, which are functions of the valve areas as expressed by (15). As such, the input vector is defined as:

$$\mathbf{u} = \begin{bmatrix} A_{v,in,a} & A_{v,out,a} & A_{v,in,b} & A_{v,out,b} \end{bmatrix}^{\mathrm{T}} \qquad (18)$$

where $A_{v,in,a}$ and $A_{v,in,b}$ are the valve areas between the pressure supply and chambers *a* and *b*, respectively, and $A_{v,out,a}$ and $A_{v,out,b}$ are the valve areas between the respective chambers and atmosphere. The pneumatic servo system under consideration in this paper incorporates two two-position three-way solenoid valves, such that at any given time, each chamber can either be connected to supply or exhaust (atmosphere). Assuming equal valve areas, the system has four possible modes as follows:

$$\text{Mode 1:}\quad \mathbf{u}_1 = A_v\begin{bmatrix} 1 & 0 & 0 & 1 \end{bmatrix}^{\mathrm{T}} \qquad (19)$$

$$\text{Mode 2:}\quad \mathbf{u}_2 = A_v\begin{bmatrix} 0 & 1 & 0 & 1 \end{bmatrix}^{\mathrm{T}} \qquad (20)$$

$$\text{Mode 3:}\quad \mathbf{u}_3 = A_v\begin{bmatrix} 0 & 1 & 1 & 0 \end{bmatrix}^{\mathrm{T}} \qquad (21)$$

$$\text{Mode 4:}\quad \mathbf{u}_4 = A_v\begin{bmatrix} 1 & 0 & 1 & 0 \end{bmatrix}^{\mathrm{T}} \qquad (22)$$

where Mode 1 corresponds to charging side *a* and discharging *b*, Mode 2 corresponds to discharging both, Mode 3 corresponds to charging side *b* and discharging *a*, Mode 4 corresponds to charging both, and A_v is the valve area of the open valves. Since, in the presence of Mode 2, Mode 4 does not offer significant utility with respect to tracking control, Mode 4 is not considered further (i.e., $d_4 = 0$). Thus, the controller can assume any of the first three modes, and as such, the modal duty cycle vector (as defined by (3)), is given by

$$D = \begin{bmatrix} d_1 & d_2 & d_3 \end{bmatrix}^T \tag{23}$$

Since the number of input modes for this system is three, a single constraint equation is required to properly constrain the system (as described in the last section). In this case, the constraint can be formulated by observing that, within a single PWM period, the controller will assume either a combination of Modes 1 and 2, which corresponds to a control effort in one direction, or a combination of Modes 2 and 3, which corresponds to a control effort in the opposite direction. Combining this constraint with the constraint of (4), the modal input vector can be written as a function of a single input (i.e., as in (7)) as

$$D^T = \begin{cases} \begin{bmatrix} 2d-1 & 2(1-d) & 0 \end{bmatrix} & \text{if } d \geq 0.5 \\ \begin{bmatrix} 0 & 2d & 1-2d \end{bmatrix} & \text{otherwise} \end{cases} \tag{24}$$

where $d \in [0, 1]$. Utilizing the transformation of (10) to provide control symmetry, the duty cycle vector can be rewritten as

$$D^T = \begin{cases} \begin{bmatrix} u & 1-u & 0 \end{bmatrix} & \text{if } u \geq 0 \\ \begin{bmatrix} 0 & 1+u & -u \end{bmatrix} & \text{otherwise} \end{cases} \tag{25}$$

where $u \in [-1, 1]$. Based on (15-21), and (25), the corresponding average model can be derived following the method presented in the last section as shown in the Appendix, which yields the following description:

$$\dddot{x} = \begin{cases} f(\mathbf{x}) + b^{+}(\mathbf{x})u & if \quad u \geq 0 \\ f(\mathbf{x}) + b^{-}(\mathbf{x})u & if \quad u < 0 \end{cases} \tag{26}$$

where

$$f(\mathbf{x}) = -\frac{A_a}{M}\left[\frac{RT}{V_a}\dot{m}(P_a, P_{atm}) + \frac{P_a}{V_a}\dot{V}_a\right] + \frac{A_b}{M}\left[\frac{RT}{V_b}\dot{m}(P_b, P_{atm}) + \frac{P_b}{V_b}\dot{V}_b\right] - \frac{B}{M}\ddot{x} \tag{27}$$

$$b^{+}(\mathbf{x}) = \frac{A_a}{M}\frac{RT}{V_a}[\dot{m}(P_s, P_a) + \dot{m}(P_a, P_{atm})] \tag{28}$$

$$b^{-}(\mathbf{x}) = \frac{A_b}{M}\frac{RT}{V_b}[\dot{m}(P_s, P_b) + \dot{m}(P_b, P_{atm})] \tag{29}$$

where the state vector consists of the pressure in each side of the cylinder, along with the position, velocity, and acceleration of the load:

$$\mathbf{x} = \begin{bmatrix} x & \dot{x} & \ddot{x} & P_a & P_b \end{bmatrix}^T \tag{30}$$

Note that, though not explicitly shown, the volume and rate of change of volume of each chamber are straightforward functions of the state (i.e., load displacement and velocity, respectively), while the mass flow rates are functions of the measured pressures, as given by (15). (26) through (29) describe the equivalent dynamics of the solenoid actuated pneumatic servo system in nonlinear control canonical form. As in a standard pneumatic servo system (i.e., one controlled via proportional servovalves), the dynamics of the system described (26) through (29) depend upon the sign of the control input (i.e., the pressure boundary conditions that drive the inlet or outlet mass flow rates depend upon whether the respective chambers are charging or discharging, as determined by the sign

of the input). That is, the split form of (26) is a byproduct of the pneumatic system dynamics, and not a result of the proposed PWM approach.

Pulse-Width-Modulated Sliding Mode Control

Having expressed the PWM system dynamics in a continuous input control canonical form, a sliding mode control approach can be applied to the control of the system. Selecting an integral sliding surface as:

$$s = (\frac{d}{dt} + \lambda)^3 \int_0^t e d\tau \tag{31}$$

where $e = x - x_{desired}$ and λ is a control gain, a robust control law can be developed based on a standard sliding mode approach, where the equivalent control component is derived by solving for the input for the case $\dot{s} = 0$, which gives:

$$u_{eq}{}^{+/-} = \frac{x_d - f(\mathbf{x}) - 3\lambda\ddot{e} - 3\lambda^2\dot{e} - \lambda^3 e}{b^{+/-}(\mathbf{x})} \tag{32}$$

where the superscript + or – denotes the corresponding value when *u* is positive or negative (i.e., as previously mentioned, the dynamics are sensitive to the sign of the input). The robust control law is obtained by adding a robustness component, such that

$$u = u_{eq}{}^{+/-} - K^{+/-}\,\mathrm{sgn}(s) \tag{33}$$

where the robustness gain *K* is time variant according to

$$K^{+/-} = \beta^{+/-}(F + \eta) + (\beta^{+/-} - 1)(x_d - f(\mathbf{x}) - 3\lambda\ddot{e} - 3\lambda^2\dot{e} - \lambda^3 e) \tag{34}$$

where $\beta^{+/-} = (\left|b^{+/-}\right|^{\max} / \left|b^{+/-}\right|^{\min})^{1/2}$, and $F = \alpha|f|$, where α characterizes the magnitude of the uncertainty in the homogeneous component of the system model (i.e., $\alpha = 0.1$ implies a ten percent uncertainty in the magnitude of $f(\mathbf{x})$). A greater degree of model

uncertainty effectively requires a higher gain. As previously mentioned, the dependence of the dynamics on the sign of the input is a characteristic of pneumatic servo systems. This dependence is accommodated by using the equivalent control component that corresponds to the proper direction of control effort, so that

$$u = u_{eq} - K\,\mathrm{sgn}(s) \tag{35}$$

where

$$u_{eq} = \begin{cases} u_{eq}^{+} & \text{if } u \geq 0 \\ u_{eq}^{-} & \text{otherwise} \end{cases} \tag{36}$$

and

$$K = \begin{cases} K^{+} & \text{if } u \geq 0 \\ K^{-} & \text{otherwise} \end{cases} \tag{37}$$

That is, if the resultant control effort is positive, the controller will be charging chamber *a* and discharging chamber *b*, and as such, the equivalent control law and the robustness gain corresponding to this assumption must be used. If the resultant control effort is negative, the equivalent control law and robustness gain corresponding to that assumption must be used. Recall additionally that, for the selected transformation between control effort and duty cycle (10), the sliding mode control command *u*, as given by (35), must be saturated at ±1. Finally, it should be noted that since the control law is a function of the state (i.e., a function of $f(\mathbf{x})$, $b^{+/-}(\mathbf{x})$, and *e*), computation of the control law requires knowledge (i.e., measurement or estimation) of the full state.

Experimental Results

Experiments were conducted to validate the proposed control approach. The experimental setup, which is shown schematically in Figure 2-1, incorporated a 2.7 cm (1-1/16 in) inner diameter, 10 cm (4-in) stroke pneumatic cylinder (Numatics 1062D04-04A) that was used to position a 10 kg mass. The airflow was controlled by a pair of pilot-assisted three-way solenoid-actuated valves (SMC VQ1200H-5B) operating at a PWM frequency of 25 Hz. The system was supplied with air at an absolute pressure of 584 kPa (85 psi). Implementation of the control law requires measurement of the model states, which is required specifically for the computation of $f(\mathbf{x})$ and $b^{+/-}(\mathbf{x})$ in (32) and (34), and for computation of the error used in (31-34). For these purposes, pressure transducers (Omega PX202-200GV) were used to measure the pressure in each cylinder chamber (i.e., P_a and P_b), and a linear potentiometer (Midori LP-100F) was used to measure the linear position of the load (x). The velocity and acceleration of the load ($\dot{x}$ and $\ddot{x}$), both of which are also states, were provided via filtered differentiation of the measured position with a filter roll-off at 25 Hz. The model and controller parameters used in the experiments are listed in Table 2-1.

Table 2-1. Model and controller parameters for experimental implementation of PWM controller.

Parameter	Value	Unit
Ps	584	kPa
A_a	572	mm^2
A_b	540	mm^2
A_r	32	mm^2
A_v	3.6	mm^2
C_f	0.8	
M	10.8	kg
B	13.1	kg-s
λ	20	s^{-1}
η	100	m/s^2
β	1.1	
α	0.1	

The tracking performance was assessed by sinusoidal tracking at various frequencies with a peak-to-peak motion amplitude of 40 mm (i.e., 40% of the full-scale cylinder motion). Specifically, Figures 2-2, 2-3, and 2-4 show the measured motion of the 10 kg mass for a commanded sinusoidal motion of 0.25, 0.5, and 1.0 Hz, respectively, along with the tracking error for each case. As shown, the control approach provides effective tracking of continuous motion via solenoid on/off valves. Tracking performance was degraded at higher frequencies, presumably due to some combination of choked flow through the valves (which limits the actuation power) and their limited switching response time. Regarding the latter, as with any PWM controlled system, the closed-loop system bandwidth is limited to approximately an order of magnitude below the PWM switching frequency, which in this case was 25 Hz, limited by the bandwidth of the valves. Thus, even without the mass flow saturation (i.e., choked flow), it is unlikely that this system could track frequencies much greater than 2 Hz. Figure 2-5 shows the (continuous, symmetric) control command, as generated by (31) through (37), corresponding to the 1.0

Hz sinusoidal tracking shown in Figure 2-4. Note that the control command is subject to a 25 Hz zero-order-hold, corresponding to the 25 Hz PWM period. Finally, Figure 2-6 shows the same control command for two cycles of the sinusoidal tracking, and Figures 2-7 and 2-8 show the resulting discrete valve commands corresponding to the control command of Figure 2-6. Recall that valve *a* is opened for a duty cycle corresponding to the control command when the command is positive, and valve *b* is opened for a duty cycle corresponding to the control command when the command is negative, as described by (25).

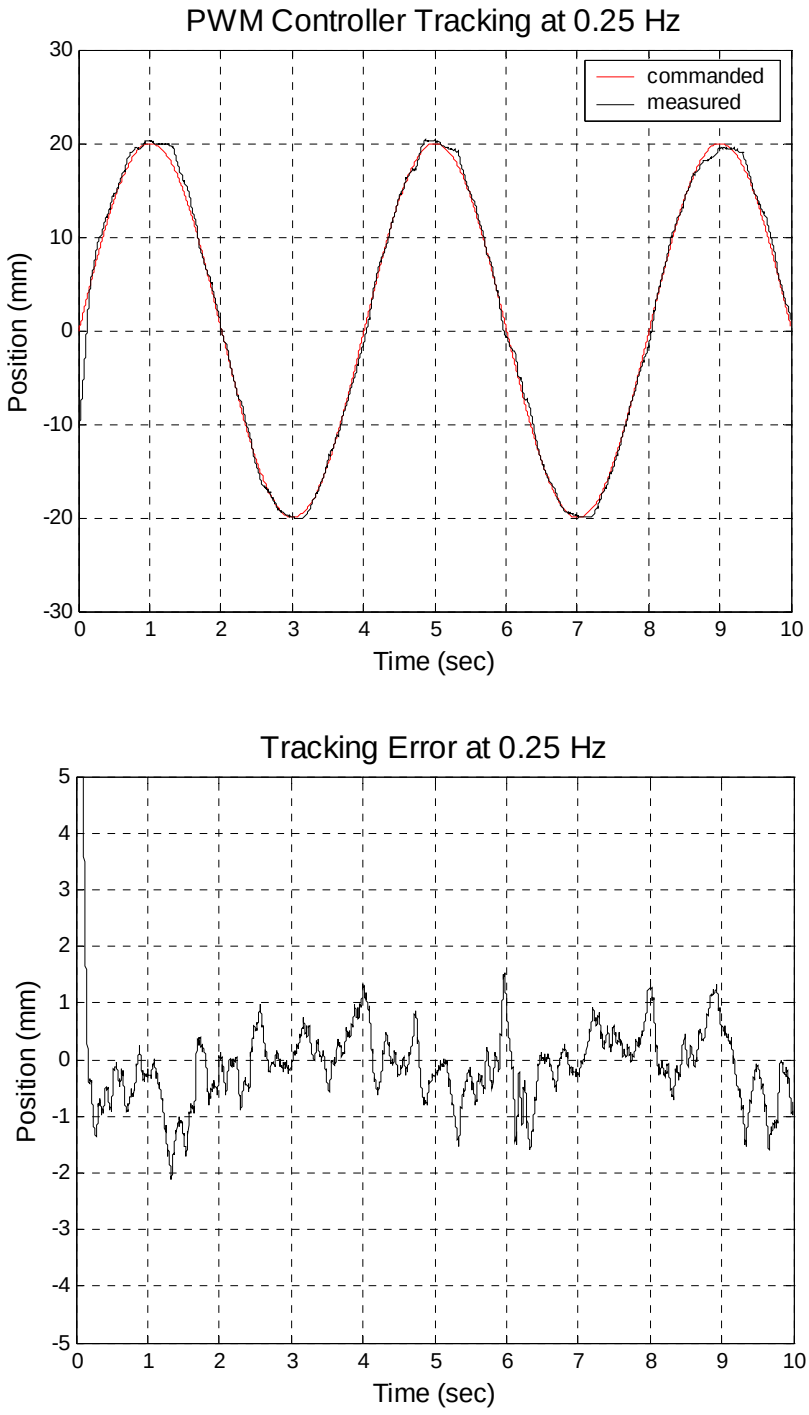

Figure 2-2. Command and measured motion (top) and tracking error (bottom) for sinusoidal tracking at 0.25 Hz.

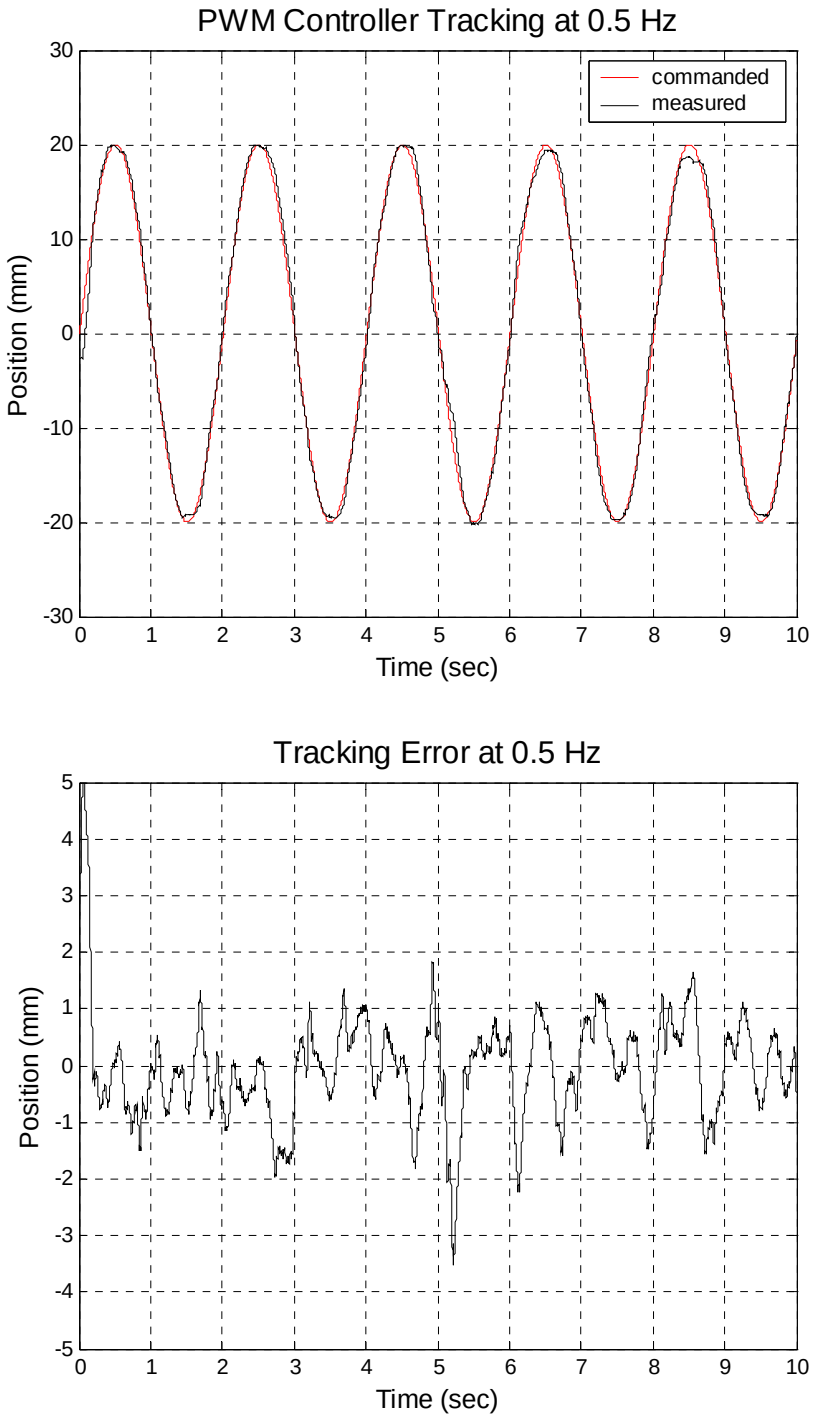

Figure 2-3. Command and measured motion (top) and tracking error (bottom) for sinusoidal tracking at 0.5 Hz.

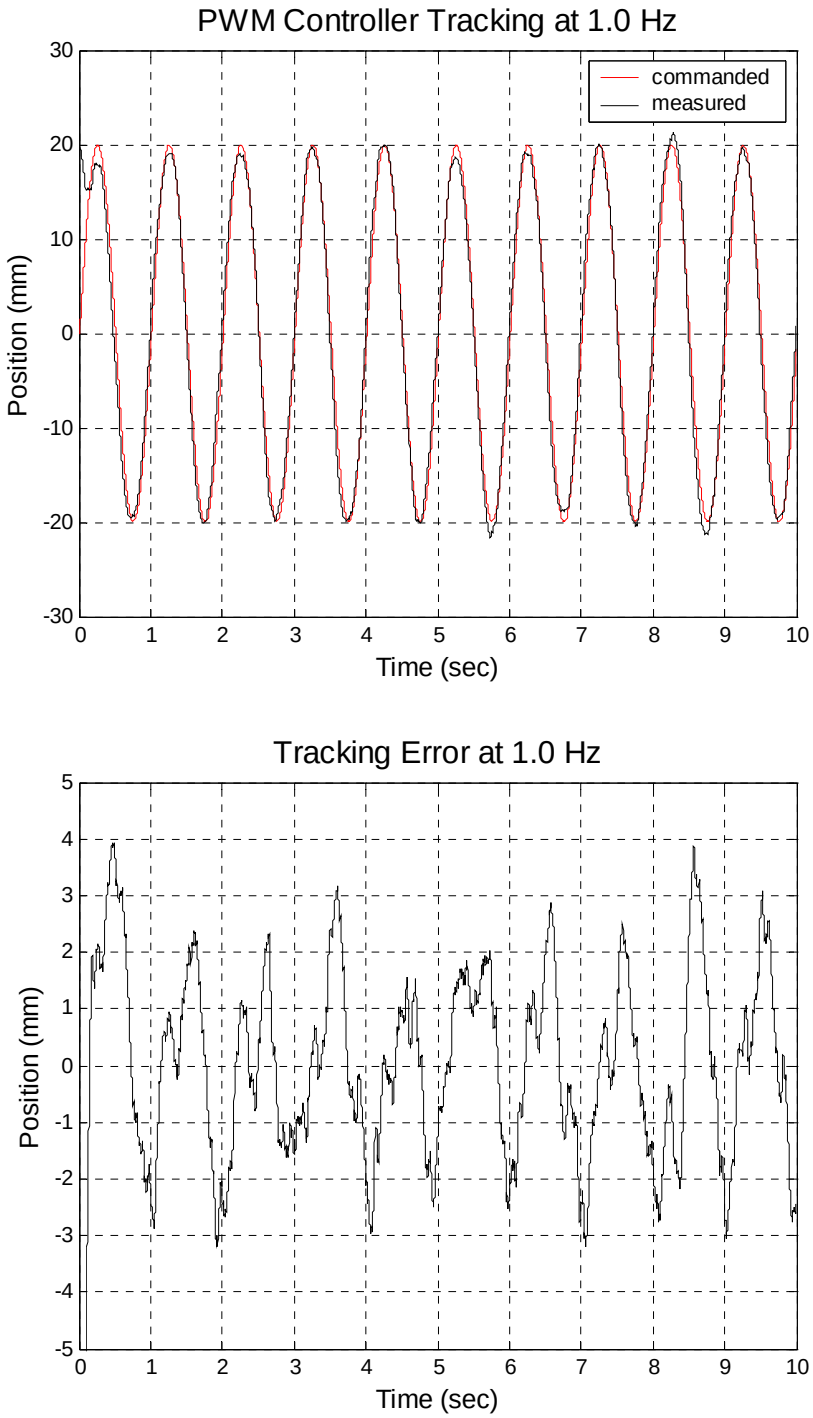

Figure 2-4. Command and measured motion (top) and tracking error (bottom) for sinusoidal tracking at 1.0 Hz.

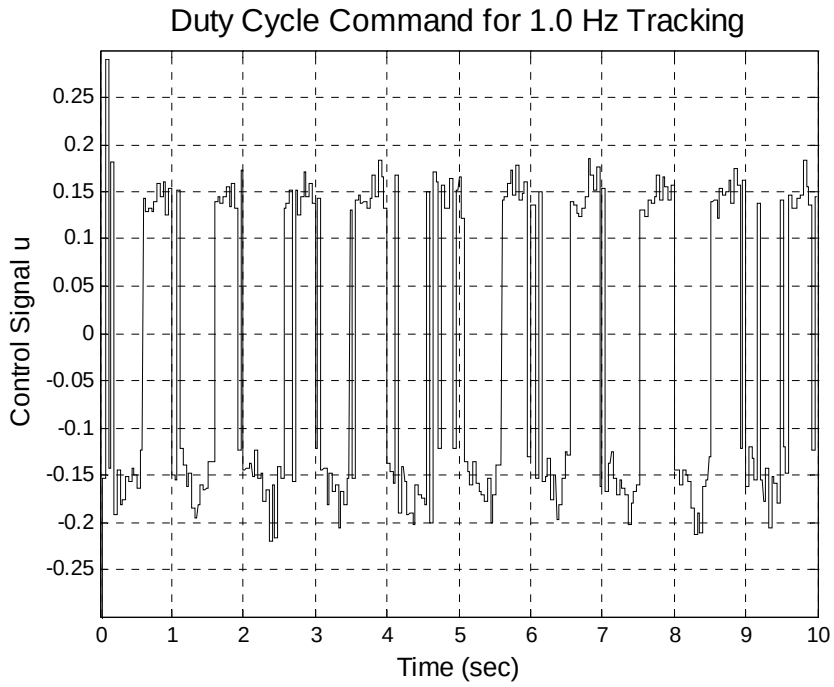

Figure 2-5. Continuous control command for 1.0 Hz sinusoidal tracking.

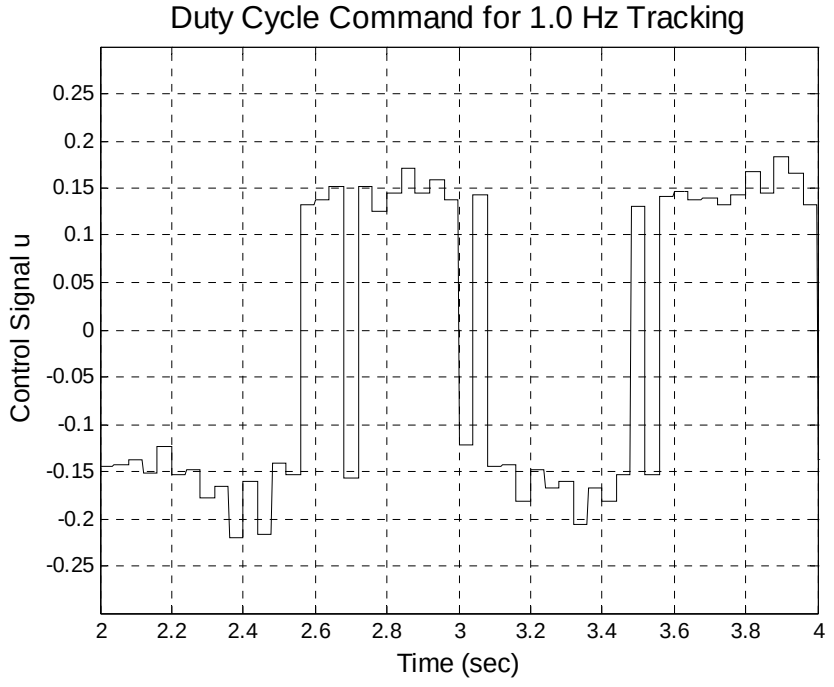

Figure 2-6. Continuous control command for two cycles of sinusoidal tracking.

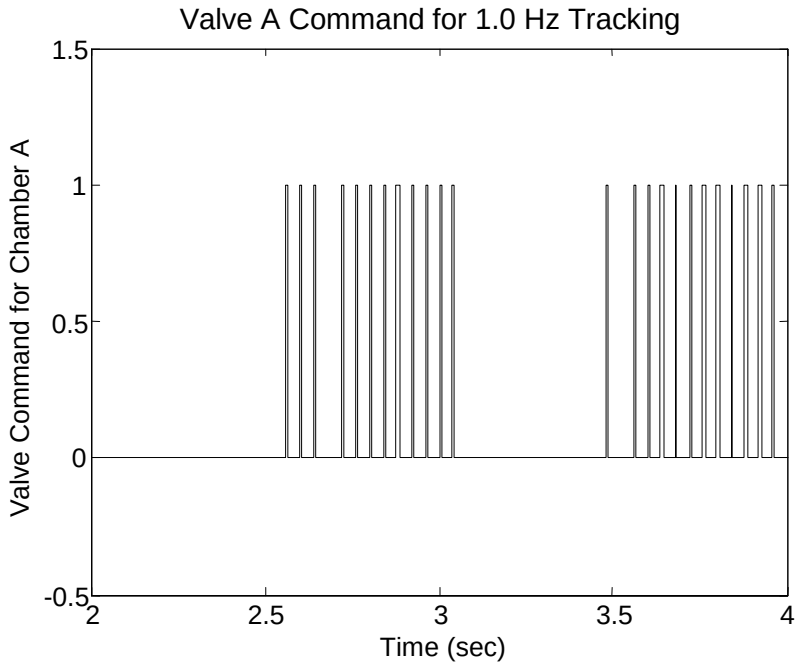

Figure 2-7. Binary (i.e., on/off) valve command for valve *a* corresponding to the control command in Figure 2-6 (1 corresponds to opening valve *a*, 0 to closing).

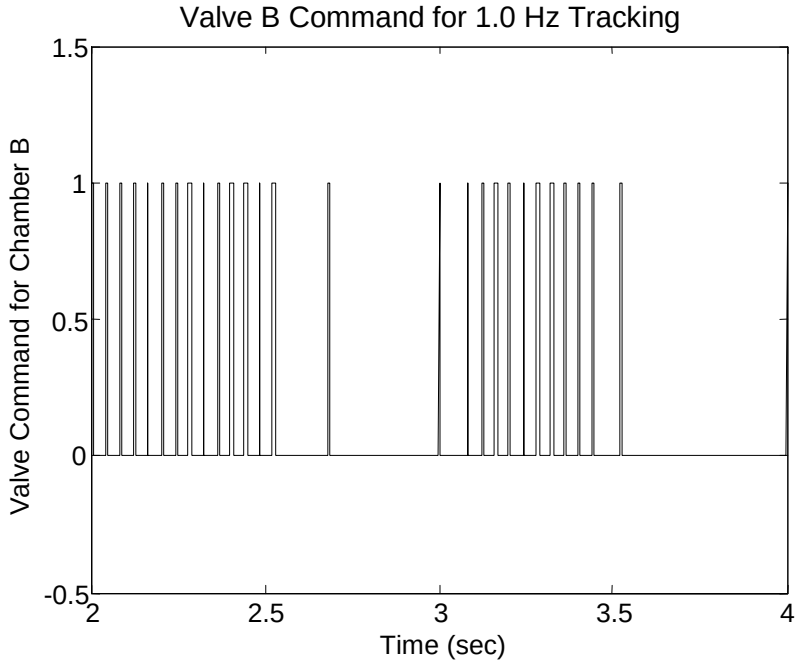

Figure 2-8. Binary (i.e., on/off) valve command for valve *b* corresponding to the control command in Figure 2-6 (1 corresponds to opening valve *b*, 0 to closing).

Conclusion

This paper presented a control approach capable of providing nonlinear servo control via relatively inexpensive on/off solenoid valves. A nonlinear model averaging approach was developed that enabled the use of a full (non-reduced-order) nonlinear model based control. This averaging method was applied to a PWM controlled pneumatic servo system, followed by the development of a sliding mode controller for that system. The proposed controller was implemented on an experimental setup, and shown via the resulting tracking performance to provide effective control of a continuous motion command.

Appendix

The single-input, single-output average model given by (26-29) is derived by first defining the modal system dynamics. Based on (18) and (19), the mass flow rates corresponding to Mode 1 are given by:

$$\begin{aligned} \dot{m}_{in,a} &= \dot{m}(P_s, P_a) \\ \dot{m}_{out,a} &= 0 \\ \dot{m}_{in,b} &= 0 \\ \dot{m}_{out,b} &= \dot{m}(P_b, P_{atm}) \end{aligned} \tag{A1}$$

where $\dot{m}(\cdot,\cdot)$ is given by (15). Substituting these into the generalized system dynamics of (17) yields the system dynamics of Mode 1, given by:

$$f_1(\mathbf{x}) = \frac{A_a}{M}\left[\frac{RT}{V_a}\dot{m}(P_s, P_a) - \frac{P_a}{V_a}\dot{V}_a\right] + \frac{A_b}{M}\left[\frac{RT}{V_b}\dot{m}(P_b, P_{atm}) + \frac{P_b}{V_b}\dot{V}_b\right] - \frac{B}{M}\ddot{x} \tag{A2}$$

Based on (18) and (20), the mass flow rates corresponding to Mode 2 are given by:

$$\begin{aligned} \dot{m}_{in,a} &= 0 \\ \dot{m}_{out,a} &= \dot{m}(P_a, P_{atm}) \\ \dot{m}_{in,b} &= 0 \\ \dot{m}_{out,b} &= \dot{m}(P_b, P_{atm}) \end{aligned} \tag{A3}$$

Substituting these into the generalized system dynamics of (17) yields the system dynamics of Mode 2, given by:

$$f_2(\mathbf{x}) = -\frac{A_a}{M}[\frac{RT}{V_a}\dot{m}(P_a, P_{atm}) + \frac{P_a}{V_a}\dot{V}_a] + \frac{A_b}{M}[\frac{RT}{V_b}\dot{m}(P_b, P_{atm}) + \frac{P_b}{V_b}\dot{V}_b] - \frac{B}{M}\ddot{x} \tag{A4}$$

Based on (18) and (21), the mass flow rates corresponding to Mode 3 are given by:

$$\begin{aligned} \dot{m}_{in,a} &= 0 \\ \dot{m}_{out,a} &= \dot{m}(P_a, P_{atm}) \\ \dot{m}_{in,b} &= \dot{m}(P_s, P_b) \\ \dot{m}_{out,b} &= 0 \end{aligned} \tag{A5}$$

Substituting these into the generalized system dynamics of (17) yields the system dynamics of Mode 3, given by:

$$f_3(\mathbf{x}) = -\frac{A_a}{M}[\frac{RT}{V_a}\dot{m}(P_a, P_{atm}) + \frac{P_a}{V_a}\dot{V}_a] - \frac{A_b}{M}[\frac{RT}{V_b}\dot{m}(P_s, P_b) - \frac{P_b}{V_b}\dot{V}_b] - \frac{B}{M}\ddot{x} \tag{A6}$$

As noted in the manuscript, Mode 4 is not used. Denoting the duty cycle vector as:

$$D = [d_1 \quad d_2 \quad d_3]^T, \tag{A7}$$

and the modal system dynamics vector as:

$$F = [f_1 \quad f_2 \quad f_3]^T, \tag{A8}$$

the average system dynamics are given by (6) as:

$$\ddot{x} = F^T D = f_1 d_1 + f_2 d_2 + f_3 d_3 \tag{A9}$$

Defining the duty cycle vector as given by (25) and substituting in (A9) yields:

$$\dddot{x} = \begin{cases} f_1 u + f_2(1-u) & \text{if } u \geq 0 \\ f_2(1+u) - f_3 u & \text{otherwise} \end{cases} \tag{A10}$$

Rearranging this in the standard control canonical form yields:

$$\dddot{x} = \begin{cases} f_2 + (f_1 - f_2)u & \text{if } u \geq 0 \\ f_2 + (f_2 - f_3)u & \text{otherwise} \end{cases} \tag{A11}$$

Thus, the respective terms in the average system dynamics of (26) are given by:

$$f(\mathbf{x}) = f_2 \tag{A12}$$

$$b^+(\mathbf{x}) = f_1 - f_2 \tag{A13}$$

and

$$b^-(\mathbf{x}) = f_2 - f_3 \tag{A14}$$

References

[1] Shearer, J. L., "Study of Pneumatic Processes in the Continuous Control of Motion with Compresses Air – I," *Transactions of the ASME*, vol. 78, pp. 233-242, 1956.

[2] Shearer, J. L., "Study of Pneumatic Processes in the Continuous Control of Motion with Compresses Air – II," *Transactions of the ASME*, vol. 78, pp. 243-249, 1956.

[3] Shearer, J. L., "Nonlinear Analog Study of a High-Pressure Servomechanism," *Transactions of the ASME*, vol. 79, pp. 465-472, 1957.

[4] Mannetje, J. J., "Pneumatic Servo Design Method Improves System Bandwidth Twenty-fold," *Control Engineering*, vol. 28, no. 6, pp. 79-83, 1981.

[5] Wang, J., Pu, J., and Moore, P., "A practical control strategy for servo-pneumatic actuator systems," *Control Engineering Practice*, vol. 7, pp. 1483-1488, 1999.

[6] Bobrow, J., and McDonell, B., "Modeling, Identification, and Control of a Pneumatically Actuated, Force Controllable Robot," *IEEE Transactions on Robotics and Automation*, vol. 14, no. 5, pp. 732-742, 1998.

[7] Richer, E. and Hurmuzlu, Y., "A High Performance Pneumatic Force Actuator System: Part I-Nonlinear Mathematical Model" *ASME Journal of Dynamic Systems, Measurement, and Control*, vol. 122, no. 3, pp. 416-425, 2000.

[8] Richer, E. and Hurmuzlu, Y., "A High Performance Pneumatic Force Actuator System: Part II-Nonlinear Control Design" *ASME Journal of Dynamic Systems, Measurement, and Control*, vol. 122, no. 3, pp. 426-434, 2000.

[9] Jacobsen, S.C., Iversen E.K., Knutti, D.F., Johnson, R.T., and Biggers, K.B., "Design of the Utah/MIT Dextrous Hand," *IEEE International Conference on Robotics and Automation*, pp. 1520-1532, 1986.

[10] Ben-Dov, D. and Salcudean, S.E., "A Force-Controlled Pneumatic Actuator," *IEEE Transactions on Robotics and Automation*, vol. 11, no. 6, pp. 906-911, 1995.

[11] Henri, P.D., Hollerbach, J.M., and Nahvi, A., "An Analytical and Experimental Investigation of a Jet Pipe Controlled Electropneumatic Actuator," *IEEE Transactions on Robotics and Automation*, vol. 14, no. 4, pp. 601-611, 1998.

[12] Noritsugu, T., "Development of PWM Mode Electro-Pneumatic Servomechanism. Part I: Speed Control of a Pneumatic Cylinder," *Journal of Fluid Control*, vol. 17, no. 1, pp. 65-80, 1986.

[13] Noritsugu, T., "Development of PWM Mode Electro-Pneumatic Servomechanism. Part II: Position Control of a Pneumatic Cylinder," *Journal of Fluid Control*, vol. 17, no. 2, pp. 7-31, 1986.

[14] Kunt, C., and Singh, R., "A Linear Time Varying Model for On-Off Valve Controlled Pneumatic Actuators," *ASME Journal of Dynamic Systems, Measurement, and Control*, vol. 112, no. 4, pp. 740-747, 1990.

[15] Ye, N., Scavarda, S., Betemps, M., and Jutard, A., "Models of a Pneumatic PWM Solenoid Valve for Engineering Applications," *ASME Journal of Dynamic Systems, Measurement, and Control*, vol. 114, no. 4, pp. 680-688, 1992.

[16] Shih, M., and Hwang, C., "Fuzzy PWM Control of the Positions of a Pneumatic Robot Cylinder Using High Speed Solenoid Valve," *JSME International Journal*, vol. 40, no. 3, pp. 469-476, 1997.

[17] van Varseveld, R. B., and Bone, G. M., "Accurate Position Control of a Pneumatic Actuator Using On/Off Solenoid Valves," *IEEE/ASME Transactions on Mechatronics*, vol. 2, no. 3, pp. 195-204, 1997.

[18] Barth E. J., Zhang, J., and Goldfarb, M., "Control Design for Relative Stability in a PWM-Controlled Pneumatic System." *ASME Journal of Dynamic Systems, Measurement, and Control*, vol. 125, no. 3, pp. 504-508, 2003.

[19] Paul, A. K., Mishra, J. K., Radke, M. G., "Reduced Order Sliding Mode Control for Pneumatic Actuator," *IEEE Transactions on Control Systems Technology*, vol. 2, no.3, pp. 271-276, 1994.

CHAPTER III: MANUSCRIPT 2

SIMULTANEOUS FORCE AND STIFFNESS CONTROL OF A PNEUMATIC ACTUATOR

Xiangrong Shen and Michael Goldfarb

Department of Mechanical Engineering

Vanderbilt University

Nashville, TN 37235

(Submitted to the *ASME Journal of Dynamic Systems, Measurement, and Control*)

Abstract

This paper proposes a new approach to the design of a robot actuator with physically variable stiffness. The proposed approach leverages the dynamic characteristics inherent in a pneumatic actuator, which behaves in essence as a series elastic actuator. By replacing the four-way servovalve used to control a typical pneumatic actuator with a pair of three-way valves, the stiffness of the series elastic component can be modulated independently of the actuator output force. Based on this notion, the authors propose a control approach for the simultaneous control of actuator output force and stiffness. Since the achievable output force and stiffness are coupled and configuration-dependent, the authors also present a control law that provides either maximum or minimum actuator output stiffness for a given displacement and desired force output. The general control and maximum/minimum stiffness approaches are

experimentally demonstrated and shown to provide high fidelity control of force and stiffness, and additionally shown to provide an order of magnitude dynamic range in stiffness.

Introduction

The modulation of actuator output stiffness can serve several purposes in robotic applications, many of these motivated by biological motor control strategies. For example, research suggests that humans achieve stable and effective interaction with a wide variety of environments by leveraging their ability to modulate joint impedance independently of joint torque [e.g., 1-4], and a significant body of research exists that highlights the role of variable compliance in enhancing the energetic efficiency of mammalian locomotion [e.g., 5-7]. As proposed by Salisbury [8] and generalized by Hogan [9], one means of modulating actuator output stiffness is via feedback control. Such an approach can effectively modulate actuator (or manipulator) output stiffness, but as with all feedback control systems, provides the desired characteristics in a limited frequency range, and can jeopardize system stability, especially in cases of non-collocated load sensing. Additionally, closed-loop strategies offer little with respect to energetic efficiency, since feedback control is generally energetically non-conservative. In order to provide variable compliance without these limitations, several researchers have developed robot actuators with physically variable stiffness, which incorporate some open-loop mechanism to enable simultaneous control of actuator force and stiffness. Specifically, in order to implement a biologically inspired strategy of interaction during robotic manipulation without the limitations imposed by feedback

control, Laurin-Kovitz et al. [10] proposed the design of a variable stiffness actuator that is loosely based on the configuration of the human musculoskeletal system. Their approach incorporates two (non-backdrivable) motors for a single joint (similar to the agonist/antagonist musculoskeletal relationships in animals), each actuating a tendon through a nonlinear spring. As with a biological motor control system, the joint torque is a function of the difference of the motor efforts, while the joint stiffness is a function of the sum of the motor efforts, thus providing simultaneous control of joint torque and stiffness. Koganezawa and Yamazaki [11], Koganezawa and Ban [12] and English and Russell [13, 14] proposed a variable stiffness actuator design of similar structure. In order to leverage the energetic benefits of variable compliance for robotic legged locomotion, Hurst et al. [15] presented a different design for a variable stiffness actuator. Like the previously described approaches, their design incorporates two motors for each (kinematic) degree-of-freedom, but unlike the agonist/antagonist approaches, the design of Hurst et al. is essentially a series elastic actuator, where the stiffness of the series elastic element is modulated by the second motor (i.e., the second motor adjusts a spring pretension, which modulates its stiffness). Tonietti et al. [16] presented the design of a variable stiffness actuator that is structurally different but conceptually similar to the design of Hurst et al. Finally, in order to enhance the intrinsic safety of human/robot interaction, Bicchi et al. [17] and Tonietti and Bicchi [18] proposed the use of an agonist/antagonist pair of McKibben artificial muscles to provide simultaneous control of position and (open-loop) stiffness in a similar manner to a biological motor control system. In essence they control the position via the difference of actuator pressures, while they control the stiffness with the sum.

This paper presents an alternate configuration for an actuator with a physically variable output stiffness that offers a more compact package and requires less mechanical complexity than the aforementioned motor-spring designs. Unlike the work presented in [17, 18], the proposed approach requires only a single actuator rather than two. Further, as subsequently shown, the proposed approach enables a greater dynamic range and bandwidth in the control of stiffness and force, relative to that demonstrated in [18]. Like the work presented in [17, 18], the proposed approach leverages the open-loop behavior of a pneumatic actuator, which inherently provides a series elastic component via the compressible gas dynamics. A typical pneumatic actuator is controlled via a single four-way spool valve, and as such, the actuator output stiffness is not controllable independently of the actuator force. By decoupling the single four-way spool valve into a pair of three-way valves, however, the pressure in each cylinder chamber can be independently controlled, and thus the actuator output stiffness of the cylinder actuator can be controlled independently of the output force. Like the agonist/antagonist systems previously described, the actuator force is a function of the difference between the chamber pressures, while the actuator output stiffness is a function of their sum. Thus, the only additional hardware required is an extra valve (for each actuator). As with the other (previously proposed) actuators, the stiffness is physical in nature (i.e., open-loop), and therefore maintains its constitutive behavior throughout the frequency spectrum, with no potential for unstable behavior. It should be noted that Raibert in [19] suggests an actuator configuration similar to the one proposed herein, but does not describe the simultaneous force and stiffness control of this configuration. Rather, as utilized by Raibert, the actuator alternates between a force source (when the valves are open) and a

spring (when the valves are closed). This paper presents an approach for the simultaneous stiffness and force control of the pneumatic actuator, and presents experimental results that characterize the force and stiffness tracking performance.

Modeling the Pneumatic Actuator

In order to implement simultaneous force and stiffness control, a two-input, two-output dynamic model of the actuator is briefly described. For the proposed variable stiffness actuator, the two model outputs are actuator force and output stiffness. The two inputs to the actuator are the respective valve commands. As in a typical pneumatic servo system, the commands are assumed to be valve areas, which are algebraically related to the valve spool displacement. Note that the servovalve spool dynamics are neglected, since these are typically significantly faster than the actuator dynamics. Finally, since mass flow rate through the valve is an algebraic function of the valve area, model formulation is simplified by assuming the model inputs are the respective mass flow rates into (positive) or out of (negative) the respective sides of the pneumatic cylinder. Specifically, modeling the flow through the valve as the isentropic flow of an ideal gas through a converging nozzle, the mass flow is algebraically related to the valve area command by the following relation:

$$\dot{m}(P_u, P_d) = A_v \Psi(P_u, P_d) \tag{1}$$

where

$$\Psi(P_u, P_d) = \begin{cases} \sqrt{\frac{\gamma}{RT}\left(\frac{2}{\gamma+1}\right)^{(\gamma+1)/(\gamma-1)}} C_f P_u \\ \qquad \text{if} \quad \frac{P_d}{P_u} \le C_r \quad \text{(choked)} \\ \sqrt{\frac{2\gamma}{RT(\gamma-1)}} \sqrt{1-\left(\frac{P_d}{P_u}\right)^{(\gamma-1)/\gamma}} \left(\frac{P_d}{P_u}\right)^{(1/\gamma)} C_f P_u \\ \qquad \text{otherwise} \quad \text{(unchoked)} \end{cases} \tag{2}$$

and A_v is the valve area command, P_u and P_d are the upstream and downstream pressures, respectively, k is the ratio of specific heats, R is the universal gas constant, T is the gas temperature at the orifice, C_f is the discharge coefficient of the valve, and C_r is the pressure ratio that divides the flow regimes into unchoked (sub-sonic) and choked (sonic) flow through the orifice. Thus, by commanding the valve orifice areas, the servovalves are algebraically commanding the mass flow rates into or out of each chamber of the cylinder, and as such, the mass flow rates through the respective valves are assumed to be the two actuator inputs. Note that, since the two valves are three-way valves, a positive valve command connects the pressure supply to the cylinder so that mass flows into the chamber (defined as positive mass flow), while a negative command connects the cylinder to exhaust, such that mass flows out of the chamber (defined as negative mass flow). The model is thus derived by describing the respective relationships between actuator force and chamber mass flow, and between actuator output stiffness and chamber mass flow. Based on the schematic of the pneumatic actuator shown in Fig. 1, the force generated by the actuator is given by:

$$F = P_a A_a - P_b A_b - P_{atm} A_r \tag{3}$$

where P_a and P_b are the absolute pressures inside each chamber of the actuator, A_a and A_b are the effective areas of each side of the piston, and A_r is the cross-sectional area of the

piston rod. In order to recover the mass flow rate inputs, the force equation is differentiated with respect to time:

$$\dot{F} = \dot{P}_a A_a - \dot{P}_b A_b \tag{4}$$

Assuming air is an ideal gas undergoing an isothermal process, the rate of change of the pressure inside each chamber of the cylinder can be expressed as a function of mass flow rate as:

$$\dot{P}_{(a,b)} = \frac{RT}{V_{(a,b)}} \dot{m}_{(a,b)} - \frac{P_{(a,b)}}{V_{(a,b)}} \dot{V}_{(a,b)} \tag{5}$$

where $P_{(a,b)}$ is the absolute pressure inside each side of the cylinder, $\dot{m}_{(a,b)}$ is the mass flow rate command (where as previously described, a positive command indicates mass flowing into the chamber, negative indicates mass flowing out), and $V_{(a,b)}$ is the volume of each cylinder chamber. Thus, the dynamics from mass flow input to the force output is given by:

$$\dot{F} = \frac{RTA_a}{V_a} \dot{m}_a - \frac{RTA_b}{V_b} \dot{m}_b - \frac{P_a A_a}{V_a} \dot{V}_a + \frac{P_b A_b}{V_b} \dot{V}_b \tag{6}$$

The volume in each chamber is a geometric function of piston displacement *x*, given by:

$$V_{(a,b)} = A_{(a,b)} (\frac{L}{2} \pm x) \tag{7}$$

where *L* is the stroke length of the actuator. Thus, the dynamics from mass flow input to force output can be written as a function of the measurable states (i.e., the chamber pressures and piston displacement) as:

$$\dot{F} = \frac{RT}{\frac{L}{2} + x} \dot{m}_a - \frac{RT}{\frac{L}{2} - x} \dot{m}_b - \frac{P_a A_a \dot{x}}{\frac{L}{2} + x} - \frac{P_b A_b \dot{x}}{\frac{L}{2} - x} \tag{8}$$

The output stiffness of the actuator is defined by:

$$K = -\frac{\partial F}{\partial x} \tag{9}$$

where the actuator force is given by (3). Substituting (3) into (9) yields:

$$K = -\frac{\partial (P_a A_a - P_b A_b - P_{atm} A_r)}{\partial x} = -A_a \frac{\partial P_a}{\partial x} + A_b \frac{\partial P_b}{\partial x} \tag{10}$$

The chamber pressures can be described as a function of displacement by assuming air is an ideal gas, such that

$$P_{(a,b)} = \frac{m_{(a,b)} RT}{V_{(a,b)}} \tag{11}$$

Substituting (7) into (11) yields an expression for pressures as a function of piston displacement:

$$P_{(a,b)} = \frac{m_{(a,b)} RT}{A_{(a,b)} (\frac{L}{2} \pm x)} \tag{12}$$

Differentiating with respect to *x* gives:

$$\frac{\partial P_{(a,b)}}{\partial x} = \mp \frac{m_{(a,b)} RT}{A_{(a,b)} (\frac{L}{2} \pm x)^2} \tag{13}$$

Thus, the stiffness can be written as a function of the respective masses of air in each cylinder chamber and the piston displacement as:

$$K = RT \left(\frac{m_a}{(\frac{L}{2} + x)^2} + \frac{m_b}{(\frac{L}{2} - x)^2} \right) \tag{14}$$

In order to recover the mass flow rate command inputs, (14) is differentiated with respect to time, which after simplification based on substitution from equation (12) yields the dynamics from mass flow input to the stiffness output as a function of measured states:

$$\dot{K} = \frac{RT}{(\frac{L}{2} + x)^2} \dot{m}_a + \frac{RT}{(\frac{L}{2} - x)^2} \dot{m}_b - \frac{2 P_a A_a \dot{x}}{(\frac{L}{2} + x)^2} + \frac{2 P_b A_b \dot{x}}{(\frac{L}{2} - x)^2} \tag{15}$$

Note that, the force dynamics (8) are influenced by the difference in valve commands (i.e., mass flow rates), while the stiffness dynamics (15) are influenced by the sum of the mass flow rates.

Sliding Mode Controller Design

Given the two-input, two-output model provided by (8) and (15), a standard multi-input-multi-output sliding mode approach can be utilized for the simultaneous control of actuator force and stiffness. In order to incorporate standard notation, let the input vector consist of the two mass flow rates such that $\mathbf{u} = [\dot{m}_a \quad \dot{m}_b]^T$ and let the output vector consist of the force and stiffness such that $\mathbf{x} = [F \quad K]^T$, so that the system dynamics can be expressed as:

$$\dot{\mathbf{x}} = \mathbf{f} + \mathbf{b}\mathbf{u} \tag{16}$$

where

$$\mathbf{f} = \begin{bmatrix} f_1 \\ f_2 \end{bmatrix} \tag{17}$$

and

$$\mathbf{b} = \begin{bmatrix} b_{11} & b_{12} \\ b_{21} & b_{22} \end{bmatrix} \tag{18}$$

where

$$f_1 = -\frac{P_a A_a \dot{x}}{\frac{L}{2} + x} - \frac{P_b A_b \dot{x}}{\frac{L}{2} - x} \tag{19}$$

$$f_2 = -\frac{2P_a A_a \dot{x}}{\left(\frac{L}{2} + x\right)^2} + \frac{2P_b A_b \dot{x}}{\left(\frac{L}{2} - x\right)^2} \tag{20}$$

$$b_{11} = \frac{RT}{\frac{L}{2} + x} \tag{21}$$

$$b_{12} = -\frac{RT}{\frac{L}{2} - x} \tag{22}$$

$$b_{21} = \frac{RT}{(\frac{L}{2} + x)^2} \tag{23}$$

$$b_{22} = \frac{RT}{(\frac{L}{2} - x)^2} \tag{24}$$

And we also assume that the bound for the uncertainty associated with the above model can be expressed by:

$$\left| \hat{f}_i - f_i \right| \le F_i \qquad i = 1,2 \tag{25}$$

$$\mathbf{b} = (\mathbf{I} + \mathbf{\Delta})\hat{\mathbf{b}} \qquad \left| \Delta_{ij} \right| \le D_{ij} \qquad i = 1,2 \qquad j = 1,2 \tag{26}$$

Where $\hat{f}_i$ is the estimated value of f_i, $\hat{\mathbf{b}}$ is the estimated matrix of $\mathbf{b}$, $\mathbf{I}$ is the 2×2 identity matrix and D_{ij} is a positive constant.

In order to develop an MIMO sliding mode controller for the system, first define a sliding surface vector $\boldsymbol{s}$ as

$$\mathbf{s} = \begin{bmatrix} s_1 \\ s_2 \end{bmatrix} = \begin{bmatrix} F - F_d \\ K - K_d \end{bmatrix} \tag{27}$$

where F_d and K_d are the desired actuator force and stiffness, respectively. The corresponding sliding conditions for the two states are:

$$\frac{1}{2}\frac{d}{dt} s_i^2 \le -\eta_i \left| s \right| \qquad i = 1,2 \tag{28}$$

where η_i is a strictly positive constant. In order to satisfy the sliding conditions in the presence of the model uncertainty, the MIMO sliding mode control law (as described in [20]) is given by:

$$\mathbf{u} = \mathbf{b}^{-1}(\dot{\mathbf{x}}_d - \mathbf{f} - \boldsymbol{\kappa}\,\mathrm{sgn}(\mathbf{s})) \tag{29}$$

where $\boldsymbol{\kappa}\,\mathrm{sgn}(\mathbf{s})$ is the robustness vector $[k_1\,\mathrm{sgn}(s_1) \quad k_2\,\mathrm{sgn}(s_2)]^T$, and $\dot{\mathbf{x}}_d$ is the time derivative of the desired input vector, which is defined as $\mathbf{x}_d = [F_d \quad K_d]^T$. k_1 and k_2 are chosen such that

$$(1 - D_{ii})k_i + \sum_{j \neq i} D_{ij}k_j = F_i + \sum_{j=1}^{2} D_{ij}\left|\dot{x}_{di} - \hat{f}_j\right| + \eta_i \quad i = 1,2 \tag{30}$$

The existence of a solution to these equations is guaranteed by the Frobenius-Perron theorem, as described in [20].

Finally, the commands to the control valves are calculated by:

$$A_{v,a} = \begin{cases} \dot{m}_a / \Psi(P_s, P_a) & \text{if } \dot{m}_a \geq 0 \\ \dot{m}_a / \Psi(P_a, P_{atm}) & \text{otherwise} \end{cases} \tag{31}$$

$$A_{v,b} = \begin{cases} \dot{m}_b / \Psi(P_s, P_b) & \text{if } \dot{m}_b \geq 0 \\ \dot{m}_b / \Psi(P_b, P_{atm}) & \text{otherwise} \end{cases} \tag{32}$$

where $\Psi(P_u, P_d)$ is defined by (2).

Force Control with Maximum/Minimum Output Stiffness

Many cases exist for the simultaneous control of force and stiffness for which one might desire either a maximum or a minimum actuator output stiffness. For example, during a kinematically constrained manipulation task (such as opening a drawer), a manipulator should ideally maintain a low output stiffness, which minimizes the effective

gain of the disturbance transfer function from position error normal to the kinematic constraint to the resulting force of interaction. Alternatively, for a manipulation task such as carving with a knife, the manipulator should ideally maintain a high output stiffness, which will minimize the effective gain from environmental disturbance force to a resulting error in desired trajectory. As described by (16-24), the actuator output stiffness and force are coupled, and thus the achievable stiffness at any given time depends on the actuator force and the actuator state. This coupling is expressed more explicitly by substituting (12) into (14), so that the stiffness can be expressed in terms of pressure and displacement as follows:

$$K = \frac{P_a A_a}{\frac{L}{2} + x} + \frac{P_b A_b}{\frac{L}{2} - x} \tag{33}$$

For a non-negative desired force F_d, the set of (3) and (33) can be solved explicitly for K and P_a, such that the expression for stiffness becomes:

$$K = \frac{F_d + P_b A_b + P_{atm} A_r}{\frac{L}{2} + x} + \frac{P_b A_b}{\frac{L}{2} - x} \tag{34}$$

Normally P_b is a positive value between atmospheric and supply pressure, and thus the minimum stiffness can be written as a function of desired force and displacement as:

$$K_{min} = \frac{F_d + P_{atm} A_a}{\frac{L}{2} + x} + \frac{P_{atm} A_b}{\frac{L}{2} - x} \qquad if \;\; F_d \geq 0 \tag{35}$$

since $A_a = A_b + A_r$. Further analysis of other cases gives the following expressions for the maximum and minimum stiffness:

$$K_{\max} = \begin{cases} \dfrac{P_s A_a}{\frac{L}{2} + x} + \dfrac{-F_d + P_s A_a - P_{atm} A_r}{\frac{L}{2} - x} & if \;\; F_d \geq (P_s - P_{atm}) A_r \\ \dfrac{F_d + P_s A_b + P_{atm} A_r}{\frac{L}{2} + x} + \dfrac{P_s A_b}{\frac{L}{2} - x} & otherwise \end{cases} \tag{36}$$

$$K_{min} = \begin{cases} \dfrac{F_d + P_{atm}A_a}{\frac{L}{2}+x} + \dfrac{P_{atm}A_b}{\frac{L}{2}-x} & if\ \ F_d \geq 0 \\ \dfrac{P_{atm}A_a}{\frac{L}{2}+x} + \dfrac{-F_d + P_{atm}A_b}{\frac{L}{2}-x} & otherwise \end{cases} \tag{37}$$

As such, the cases of minimum and maximum actuator stiffness could be implemented by utilizing either (36) or (37), respectively, to determine the desired stiffness command to the previously described MIMO controller for a given desired force. Such an approach, however, operates outside of the control loop, and thus does not account for disturbances or tracking error (i.e., does not take into consideration the actual force, or more accurately, the actual cylinder pressures).

In order to implement a more robust approach to obtaining a maximum/minimum actuator stiffness (i.e., one that is sensitive to disturbances and tracking error), the authors developed a control approach that operates inside the control loop on the control commands (i.e., on the mass flow rates), rather than the aforementioned command generator described by (36-37). Rather than specify a given stiffness at any given time, the proposed approach leverages the presence of saturation in stiffness (i.e., the presence of (36-37)) and the fact that stiffness is a strictly positive quantity. Given these, the stiffness can be made and maintained at its maximum (in general fluctuating) value by maximizing its time rate of change (i.e., driving it as quickly as possible to its maximum value). Similarly, the stiffness can be made and maintained at its minimum (in general fluctuating) value by minimizing its time rate of change (i.e., driving it as quickly as possible to its minimum value). As described by (15), the time rate of change of stiffness is linearly influenced by the (input) mass flow rates, and as such the maximum or minimum time derivative of stiffness can be obtained via the linear optimization of

$$J = b_{21}\dot{m}_a + b_{22}\dot{m}_b \tag{38}$$

where b_{21} and b_{22} are defined by (23) and (24). For stable force tracking, the mass flow rates should satisfy the sliding condition (28) for $i = 1$:

$$\frac{1}{2}\frac{d}{dt}s_1^{\,2} \le -\eta_1|s_1| \tag{39}$$

This condition can be satisfied by the following equation between the inputs:

$$b_{11}\dot{m}_a + b_{12}\dot{m}_b = -f_1 + \dot{F}_d - k_1\,\mathrm{sgn}(s_1) \tag{40}$$

where b_{11} and b_{12} are given by (21-22), f_1 is given by (19), $\dot{F}_d$ is the time derivative of the desired actuator force, and k_1 is the robustness gain satisfying (39). Moreover, the inputs $\dot{m}_a$ and $\dot{m}_b$ are bounded by an upper limit for which the corresponding valve is fully open to the air supply and a lower limit for which the corresponding valve is fully open to the exhaust. These constraints can be expressed as:

$$\dot{m}_{a,\min} \le \dot{m}_a \le \dot{m}_{a,\max} \tag{41}$$

$$\dot{m}_{b,\min} \le \dot{m}_b \le \dot{m}_{b,\max} \tag{42}$$

where $\dot{m}_{(a,b)(\min,\max)}$ are functions of the state as given by (1), evaluated at the maximum valve area. Specifically, $\dot{m}_{(a,b)(\min,\max)}$ are given by:

$$\dot{m}_{(a,b)max} = A_{v,max}\Psi(P_s, P_{(a,b)}) \tag{43}$$

and

$$\dot{m}_{(a,b)min} = -A_{v,max}\Psi(P_{(a,b)}, P_{atm}) \tag{44}$$

where P_s is the supply pressure and P_{atm} is the exhaust pressure. Note that the negative sign for $\dot{m}_{(a,b)\min}$ pertains to the direction of mass flow, as previously discussed. Thus,

the whole problem can be defined as maximizing or minimizing the objective function J as defined by (38) under the constraints (40), (41), and (42).

The optimization problem defined above can be solved with a linear programming approach. The control inputs for maximizing stiffness are given by:

$$\dot{m}_a = \begin{cases} \dot{m}_{a,\max} \\ \quad \text{if} \quad \dfrac{-f_1 + \dot{F}_d - k_1 \operatorname{sgn}(s_1) - b_{11}\dot{m}_{a,\max}}{b_{12}} \le \dot{m}_{b,\max} \\ \dfrac{-f_1 + \dot{F}_d - k_1 \operatorname{sgn}(s_1) - b_{12}\dot{m}_{b,\max}}{b_{11}} \\ \quad \text{otherwise} \end{cases} \tag{45}$$

and

$$\dot{m}_b = \begin{cases} \dfrac{-f_1 + \dot{F}_d - k_1 \operatorname{sgn}(s_1) - b_{11}\dot{m}_{a,\max}}{b_{12}} \\ \quad \text{if} \quad \dfrac{-f_1 + \dot{F}_d - k_1 \operatorname{sgn}(s_1) - b_{11}\dot{m}_{a,\max}}{b_{12}} \le \dot{m}_{b,\max} \\ \dot{m}_{b,\max} \\ \quad \text{otherwise} \end{cases} \tag{46}$$

The control inputs for minimizing stiffness are given by:

$$\dot{m}_a = \begin{cases} \dot{m}_{a,\min} \\ \quad \text{if} \quad \dfrac{-f_1 + \dot{F}_d - k_1 \operatorname{sgn}(s_1) - b_{11}\dot{m}_{a,\min}}{b_{12}} \ge \dot{m}_{b,\min} \\ \dfrac{-f_1 + \dot{F}_d - k_1 \operatorname{sgn}(s_1) - b_{12}\dot{m}_{b,\min}}{b_{11}} \\ \quad \text{otherwise} \end{cases} \tag{47}$$

and

$$\dot{m}_b = \begin{cases} \dfrac{-f_1 + \dot{F}_d - k_1 \operatorname{sgn}(s_1) - b_{11}\dot{m}_{a,\min}}{b_{12}} \\ \qquad \text{if} \quad \dfrac{-f_1 + \dot{F}_d - k_1 \operatorname{sgn}(s_1) - b_{11}\dot{m}_{a,\min}}{b_{12}} \geq \dot{m}_{b,\min} \\ \dot{m}_{b,\min} \\ \qquad \text{otherwise} \end{cases} \tag{48}$$

The corresponding commands to the control valves are calculated by (31) and (32).

Experimental Results

The force/stiffness controller was implemented on a pneumatic actuator used to drive a 10 kg inertial load. In order to test the proposed control approach throughout the dynamic workspace of the actuator, the controller was implemented within a servo control loop. Specifically, an outer proportional-derivative (PD) control loop was implemented on the position of the 10 kg mass, which in turn generated the desired force for the force portion of the force/stiffness controller to track. As such, rather than directly specify the desired force and stiffness trajectories, the desired position and stiffness trajectories were directly specified instead, and the desired force trajectory specified indirectly by the former (i.e., by the PD control loop). The experimental setup, which is shown schematically in Figure 3-1, consisted of a 2.7 cm (1-1/16 in) inner diameter, 10 cm (4 in) stroke pneumatic cylinder (Numatics 1062D04-04A) controlled by a pair of proportional servovalves (FESTO MPYE-5-M5-010-B), each configured as a three-way valve as shown in the figure, and each supplied with air at an absolute pressure of 653 kPa (95 psia). The output of the pneumatic cylinder was connected to a linear slide, upon which the mass was mounted. Displacement of the slide (and actuator) was measured with a linear potentiometer (Midori LP-100F). Pressure sensors (FESTO SDE-

16-10V/20mA) measured the pressure in each cylinder chamber, and in combination with the measured displacement, the actuator output stiffness was computed based on (33). The model and controller parameters used for both the inner (force/stiffness) and outer (position) loop are listed in Table 3-1.

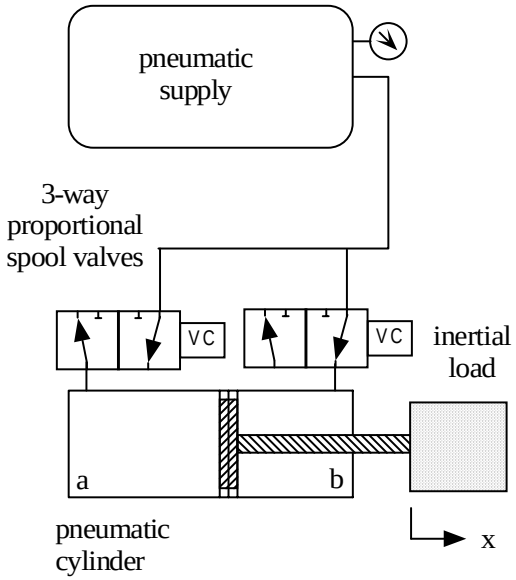

Figure 3-1. Pneumatic actuator controlled by a pair of three-way valves.

Table 3-1. Model and controller parameters for experimental implementation.

Parameter	Description	Value	Unit
P_s	Supply pressure	653	kPa
A_a	Piston area side a	572	mm^2
A_b	Piston area side b	540	mm^2
A_r	Rod area	32	mm^2
$A_{v,max}$	Maximum valve area	12.57	mm^2
C_f	Discharge coefficient	0.8	
C_r	Pressure ratio	0.5	
k	Ratio of specific heats	1.4	
R	Universal gas constant	0.287	kJ/kg·K
T	Gas temperature at the orifice	293	K
k_1	Force error robustness gain	6×10^3	$kg\text{-}m/sec^3$
k_2	Stiffness error robustness gain	1.5×10^5	kg/sec^3
K_p	Outer loop proportional gain	1000	N/m
K_d	Outer loop derivative gain	185	N·sec/m

The results of several tracking experiments are shown in Figures 3-2 through 3-5. Figure 3-2 shows the force and stiffness tracking performance corresponding to an (outer loop) 0.5 Hz sinusoidal command in motion at an amplitude of 20 mm, along with the tracking of a 0.5 Hz sinusoidal command in stiffness between 7.0 and 9.0 N/mm. Note that also the desired position and stiffness are both 0.5 Hz sinusoids, the shape of the force trajectory is quite different from that of the stiffness trajectory. Figure 3-3 shows the force and stiffness tracking performance corresponding to a 2.0 Hz sinusoidal command in motion and a 4.0 Hz sinusoidal command in stiffness, clearly illustrating the ability to simultaneously control stiffness and force. Figures 3-4 and 3-5 show the force tracking corresponding to a 0.5 Hz sinusoidal command in motion while maximizing stiffness and minimizing stiffness, respectively. Note that the variation in stiffness between the two conditions is approximately an order of magnitude, and as such provides a significant dynamic range in achievable stiffness.

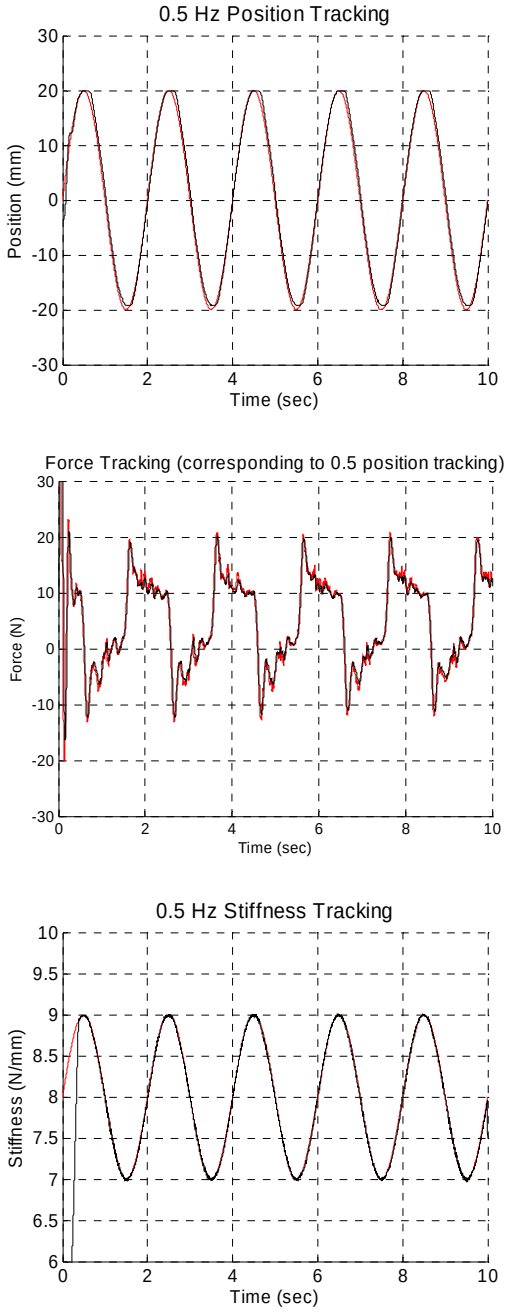

Figure 3-2. Actual and desired position (outer loop), force (inner loop), and stiffness (inner loop) tracking performance of a commanded motion of 0.5 Hz and commanded sinusoidal stiffness variation of 0.5 Hz.

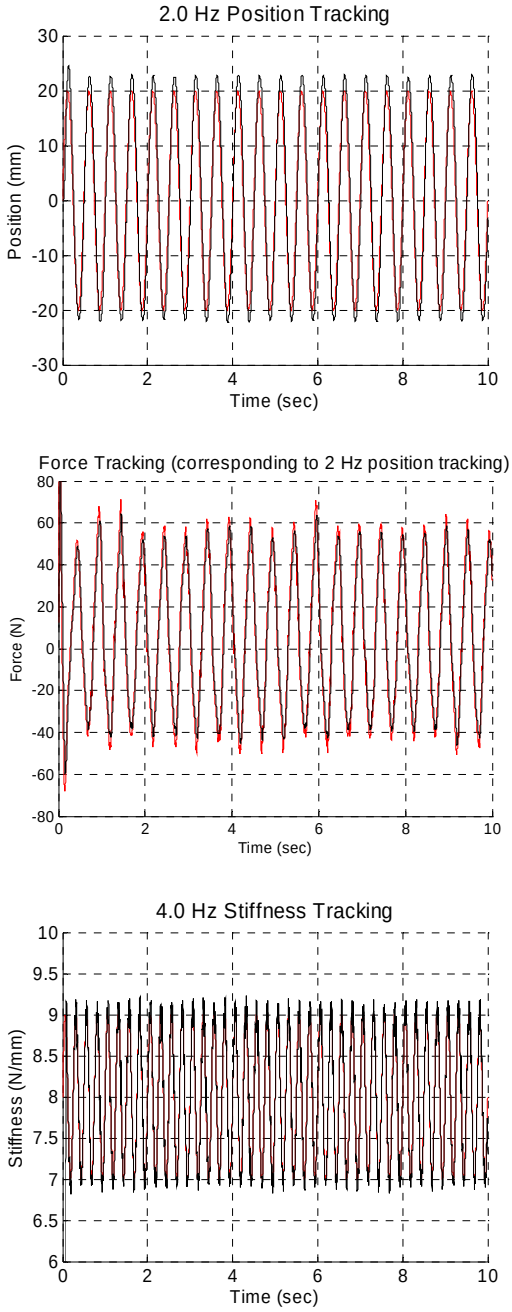

Figure 3-3. Actual and desired position (outer loop), force (inner loop), and stiffness (inner loop) tracking performance of a commanded motion of 2 Hz and commanded sinusoidal stiffness variation of 4 Hz.

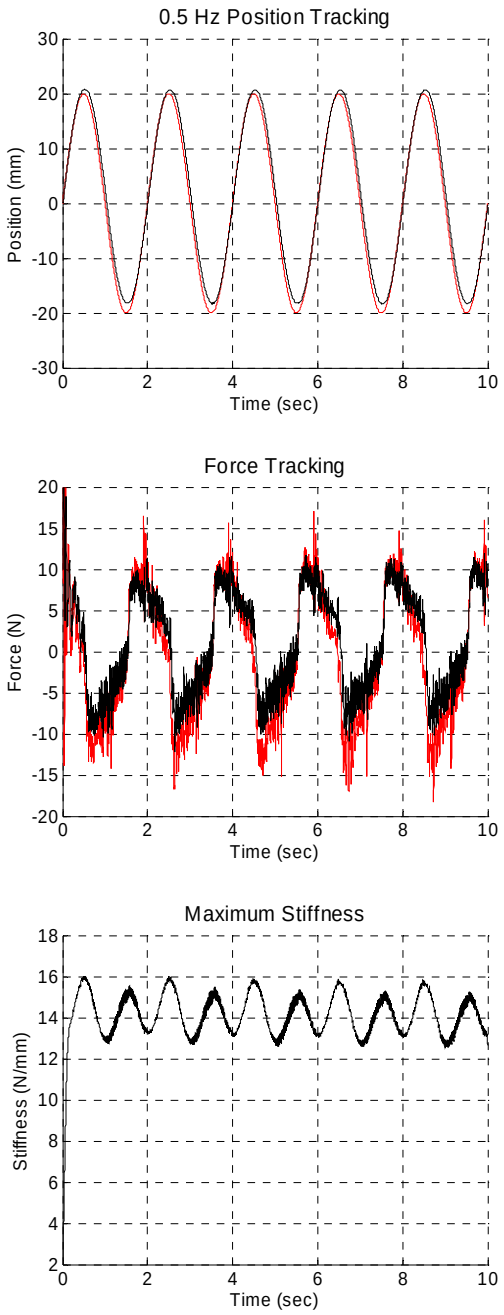

Figure 3-4. Position (outer loop), force (inner loop), and stiffness (inner loop) tracking for a sinusoidal command in motion while maximizing stiffness.

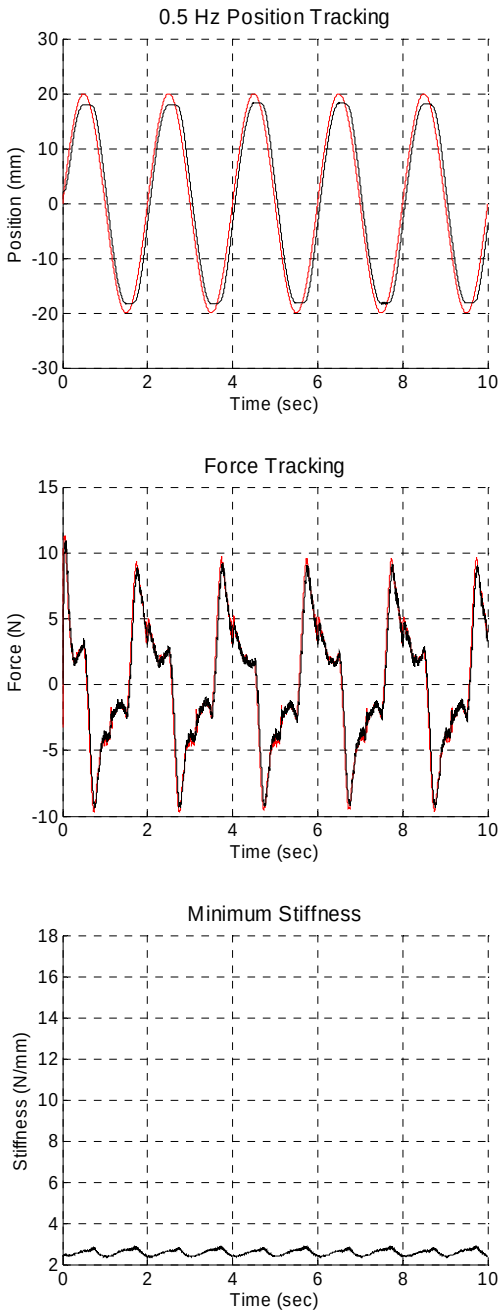

Figure 3-5. Position (outer loop), force (inner loop), and stiffness (inner loop) tracking for a sinusoidal command in motion while minimizing stiffness.

Conclusion

This paper proposes the use of a pneumatic actuator as a variable stiffness actuator. These actuators are well suited to such a task, since they are inherently series elastic actuators, and through the use of two three-way servovalves rather than a single four-way valve, the output stiffness can be modulated simultaneously of the actuation force. The net result is a robot actuator capable of physically (i.e., open-loop) variable stiffness with a minimal amount of associated hardware. This paper presented an approach to simultaneously control actuator force and stiffness, and presented experimental results that demonstrate the effectiveness of the proposed approach. In addition to enabling dynamic force tracking, experiments demonstrate stiffness tracking of equivalent bandwidth and with an order of magnitude ratio of maximum to minimum achievable stiffness (i.e., an order of magnitude dynamic range in stiffness).

References

[1] Hogan, N., "The mechanics of multi-joint posture and movement control," *Biological Cybernetics*, vol. 52, pp. 315-331, 1985.

[2] Hogan, N., "Adaptive control of mechanical impedance by coactivation of antagonist muscles," *IEEE Transactions on Automatic Control*, vol. 29, no. 8, pp. 681-690, 1984.

[3] Hogan, N., "Tuning muscle stiffness can simplify control of natural movement," in *Advances in Bioengineering*, ASME Winter Annual Meeting, pp. 279-282, 1980.

[4] Mussa-Ivaldi, F.A., Hogan, N., and Bizzi, E., "Neural, mechanical, and geometric factors subserving arm posture in humans," *Journal of Neuroscience*, vol. 5, pp. 2732-2743, 1985.

[5] Alexander, R. McN., "Three uses for springs in legged locomotion," *International Journal of Robotics Research*, vol. 9, no. 2, pp. 53-61, 1990.

[6] Cavagna, G. A., Heglund, N. C., and Taylor, C. R., "Mechanical work in terrestrial locomotion: two basic mechanisms for minimizing energy expenditure," *American Journal of Physiology*, vol. 223, pp. 243-261, 1977.

[7] Taylor, C. R., and Heglund, N. C., "Energetics and mechanics of terrestrial locomotion," *Annual Reviews of Physiology*, vol. 44, pp. 97-107, 1982.

[8] Salisbury, J.K., "Active stiffness control of a manipulator in cartesian coordinates," in *Proceedings of the IEEE Conference on Decision and Control*, pp. 383 – 388, 1980.

[9] Hogan, N., "Impedance Control: An Approach to Manipulation," *Journal of Dynamic Systems, Measurement, and Control*, pp. 1 – 24, 1985.

[10] Laurin-Kovitz, K. F., Colgate, J.E., and Carnes, S. D. R., "Design of components for programmable passive impedance," in *Proceedings of the IEEE International Conference on Robotics and Automation*, vol. 2, pp. 1476-1481, 1991.

[11] Koganezawa, K. and Yamazaki, M., "Mechanical stiffness control of tendon-driven joints," in *Proceedings of the IEEE/RSJ International Conference on Intelligent Robots and Systems*, pp. 818–825, 1999.

[12] Koganezawa, K. and Ban, S., "Stiffness Control of Antagonistically Driven Redundant DOF Manipulator," in *Proceedings of the IEEE/RSJ International Conference on Intelligent Robots and Systems*, pp. 2280-2285, 2002.

[13] English, C.E. and Russell, D., "Mechanics and stiffness limitations of a variable stiffness actuator for use in prosthetic limbs," *Mechanism and Machine Theory*, vol. 34, no. 1, pp. 7-25, 1999.

[14] English, C.E. and Russell, D., "Implementation of variable joint stiffness through antagonistic actuation using rolamite springs," *Mechanism and Machine Theory*, vol. 34, no. 1, pp. 27-40, 1999.

[15] Hurst, J.W., Chestnutt, J.E. and Rizzi, A.A., "An actuator with physically variable stiffness for highly dynamic legged locomotion," in *Proceedings of the IEEE International Conference on Robotics and Automation*, pp. 4662-4667, 2004.

[16] Tonietti, G., Schiavi, R. and Bicchi, A., "Design and control of a variable stiffness actuator for safe and fast physical human/robot interaction," in *Proceedings of the IEEE International Conference on Robotics and Automation*, pp. 528-533, 2005.

[17] Bicchi, A., Rizzini, S.L., and Tonietti, G., "Compliant design for intrinsic safety: general issues and preliminary design," in *Proceedings of the IEEE/RSJ International Conference on Intelligent Robots and Systems*, pp. 1864-1869, 2001.

[18] Tonietti, G. and Bicchi, A., "Adaptive simultaneous position and stiffness control for a soft robot arm," in *Proceedings of the IEEE/RSJ International Conference on Intelligent Robots and Systems*, pp. 1992-1997, 2002.

[19] Raibert, M.H., *Legged Robots that Balance*. MIT Press, Cambridge MA, pp. 33-34, 1986.

[20] Slotine, J.E. and Li, W., *Applied Nonlinear Control*, Prentice Hall, NJ, 1991.

Chapter IV: MANUSCRIPT 3

ON THE ENHANCED PASSIVITY OF PNEUMATICALLY-ACTUATED IMPEDANCE-TYPE HAPTIC INTERFACES

Xiangrong Shen and Michael Goldfarb

Department of Mechanical Engineering

Vanderbilt University

Nashville, TN 37235

(Accepted by the *IEEE Transactions on Robotics*)

Abstract

The stable simulation of high-stiffness surfaces remains a challenge in impedance-type haptic simulations of mechanical environments. In this paper, the authors propose an approach to achieving a stable, high-stiffness surface in a haptic interface by leveraging the open-loop properties of pneumatic actuators. By utilizing the open-loop component of the actuator stiffness as a primary component of stiffness simulation in a haptic interface, the system requires a comparatively small component of simulated stiffness from the closed-loop control of the actuator. A passivity analysis is presented describing how the presence of an open-loop stiffness enhances the range of passivity of haptically simulated high-stiffness surfaces. Experimental results both with and without a human operator are presented that demonstrate the effectiveness of the approach and its enhanced passivity relative to motor-actuated devices.

Introduction

Stiffness is a defining characteristic of rigid objects and surfaces, and as such is one of the most fundamental components of their haptic simulation. Though many realistic objects and surfaces are characterized by relatively high stiffnesses, most haptic simulations are limited to significantly lower stiffnesses due to issues of stability and noise. Specifically, haptic simulations utilize either an admittance-type or impedance-type structure. In the former, the haptic interface measures the force imposed by the human operator and outputs a motion (i.e., position) as described by the desired admittance of the environment. In the latter, the haptic interface measures the motion imposed by the human operator and outputs a force as described by the desired impedance of the environment. Admittance type simulations require a high gain to effectively simulate free space, while impedance type simulations require a high gain to simulate a hard surface. As such, both have narrow stability margins in their respective high-gain states. Most haptic interfaces are implemented with an impedance approach, possibly due in part to the fact that free space is often the default environment in a haptic environment, and in part to the fact that free space is typically the energetically stable equilibrium state in the absence of user input. One could additionally argue that instability in the simulation is preferable when the user is in a high impedance state, which is more likely to occur when in contact with a surface than when in free space.

A considerable amount of research has been conducted on the stability of impedance-type haptic simulation, focused on the simulation of hard surfaces, since that is the regime of instability as previously discussed. Much of this work has focused on the simulation of springs, since springs (i.e., constitutive behavior relating force to

displacement) are the defining characteristic of a solid material (e.g., Hooke's laws). Despite the fact that such behavior (i.e., a single-valued algebraic relationship between force and displacement) is energetically passive, impedance-type simulations of haptic surfaces generally result in active behavior, which in turn can result in instability of the device. The active behavior of simulated surfaces is due primarily to the disproportionality between displacement and force introduced by discretization, digital quantization, and phase lag introduced by sensor filtering and the mechanical dynamics of the haptic interface [1], which have been collectively referred to as "energy leaks" [2]. This issue has been studied and treated by several researchers [1-16]. Colgate et al. [3] and Colgate and Schenkel [4, 5] derive a condition for the passivity of a discretely simulated wall that indicates that the maximum stiffness to preserve passivity of the haptic interface is proportional to the ratio of open-loop damping in the device to the sampling period of the simulation. Abbott and Okamura [6] and Diolaiti et al. [7] have generalized this result by additionally considering the effects of quantization. Love and Book [8] also present an analysis for the stability of a discretely simulated haptic surface, but incorporate a classical stability analysis of the discrete-time characteristic equation rather than a passivity-based approach.

Several control approaches have been proposed to address the energy leaks in a haptic simulation. Based on the passivity analysis presented by Colgate and Schenkel, Colgate et al. [9] proposed the use of a "virtual coupling," which is in essence a filter placed between the haptic device and the simulated environment. The "virtual coupling" in effect modifies the simulated environment to ensure that it preserves passivity of the system (as given by the condition derived in [4, 5]. Adams and Hannaford [10] and

Stramigioli et al. [11] further developed virtual coupling methods. Hannaford and Ryu [12] proposed a time-based approach to the design of a virtual coupling that monitors the net power flow and adjusts the properties of the coupling to ensure energetically passive behavior of the haptic system over time. Finally, Gillespie and Cutkosky [2], Ellis et al. [13], Goldfarb and Wang [14], and Madill et al. [15] propose other algorithms, not explicitly based on passivity, that compensate for the energy leaks in a haptic simulation.

The aforementioned approaches address energy leaks via software modification. In their 1997 paper, Colgate and Schenkel [5] propose modifying the haptic interface hardware design in order to enhance the passivity of surface simulation. Specifically, they found that the maximum surface stiffness that maintains passivity is proportional to the open-loop damping present in the haptic device. Thus, by adding open-loop damping to the design of the device, higher stiffness simulations can be obtained without sacrificing the dynamic character of the simulation. This approach was experimentally demonstrated by Colgate and Brown [1], who showed that a mechanical damper coupled to the output shaft of a motor-actuated haptic display increased significantly the range of simulated impedances that maintain passive behavior. Based on a similar notion, Mehling et al. [16] proposed a variation on this theme that utilized an electrical resistance across the motor leads rather than a mechanical damper. Specifically, a resistor in parallel with the motor is the energetic equivalent of a mechanical damper reflected into the electrical domain, and thus an equivalent damper can be implemented with less hardware and with more ideal damping behavior. The work described herein is a related approach to that proposed by Colgate and Schenkel and implemented in various incarnations by Colgate and Brown and Mehling et al., but rather than add open-loop damping to the device, the

proposed approach leverages the open-loop stiffness of pneumatic actuators to enhance the passivity of the haptic simulation of a stiff surface. The following section discusses the presence of open-loop stiffness in a pneumatic actuator, which is followed by the presentation of a passivity analysis similar to that of Colgate and Schenkel, in which it is shown that the presence of an open-loop stiffness in the haptic device increases the region of passivity for the haptic simulation of a stiff surface. The implementation of force control in a pneumatic actuator is briefly described, followed by the experimental implementation of the proposed approach. Experimental results are presented that indicate the enhanced passivity of the proposed approach.

Open Loop Stiffness in a Pneumatic Actuator

The output impedance of an electromagnetic motor consists primarily of inertial and damping behavior. The output impedance of a pneumatic actuator, however, includes a stiffness term in addition to the typical inertial and damping terms. Specifically, a pneumatic actuator exhibits an open-loop stiffness, relative to ground, where the equilibrium point of the stiffness is controllable (i.e., depends on the relative mass of air occupying the opposing chambers of a double-acting cylinder). The open-loop stiffness of the actuator is a function of the chamber pressures and piston displacement, and is easily derived as follows. The output stiffness of the actuator is given by:

$$k = -\frac{\partial F}{\partial x} \tag{1}$$

where the actuator force is a function of the relative chamber pressures given by:

$$F = P_a A_a - P_b A_b - P_{atm} A_r \tag{2}$$

where P_a and P_b are the absolute pressures inside each chamber of the actuator, A_a and A_b are the effective areas of each side of the piston, P_{atm} is atmospheric pressure, and A_r is the cross-sectional area of the piston rod. Substituting (2) into (1) yields:

$$k = -\frac{\partial(P_a A_a - P_b A_b - P_{atm} A_r)}{\partial x} = -A_a \frac{\partial P_a}{\partial x} + A_b \frac{\partial P_b}{\partial x} \tag{3}$$

The chamber pressures can be described as a function of displacement by assuming air is an ideal gas, such that

$$P_{a/b} = \frac{m_{a/b} RT}{V_{a/b}} \tag{4}$$

where $m_{a/b}$ is the mass of air in either chamber *a* or *b*, *R* is the universal gas constant, and *T* is the temperature of the air. The volume in each chamber is a geometric function of piston displacement *x*, given by:

$$V_{a/b} = A_{a/b}(\frac{L}{2} \pm x) \tag{5}$$

where *L* is the stroke length of the actuator. Substituting (5) into (4) yields an expression for pressures as a function of piston displacement:

$$P_{a/b} = \frac{m_{a/b} RT}{A_{a/b}(\frac{L}{2} \pm x)} \tag{6}$$

Differentiating with respect to *x* gives:

$$\frac{\partial P_{a/b}}{\partial x} = \mp \frac{m_{a/b} RT}{A_{a/b}(\frac{L}{2} \pm x)^2} \tag{7}$$

Thus, the stiffness can be written as a function of the respective masses of air in each cylinder chamber and the piston displacement as:

$$k = RT\left(\frac{m_a}{(\frac{L}{2} + x)^2} + \frac{m_b}{(\frac{L}{2} - x)^2}\right) \tag{8}$$

The equilibrium position of the actuator stiffness x_e is given by (2) when $F = 0$. Substituting (4) and (5) into (2) with the condition that $F = 0$, the equilibrium position is given by the solution of the quadratic equation:

$$x_e^2 - \frac{RT}{P_{atm}A_r}(m_a + m_b)x_e - \frac{L^2}{4} + \frac{RT}{P_{atm}A_r}\frac{L}{2}(m_a - m_b) = 0 \qquad (9)$$

Passivity Analysis of a Pneumatically Actuated Haptic Interface

Stiffness is both the defining component of a haptic surface simulation, and the component for which the (impedance-based) haptic system is most susceptible to instability. As previously described, the instability is largely a result of phase lag between motion and force in the high-gain feedback loop. Using an actuator with an output impedance characterized by inertia and damping (e.g., an electromagnetic motor), all stiffness in the haptic simulation must result from the sampled-data feedback loop. Since a pneumatic actuator exhibits an open-loop stiffness with a controllable equilibrium point, however, one could in theory create a desired stiffness primarily with open-loop behavior, thus reducing significantly the feedback gain of the sampled-data feedback loop. Like the addition of open-loop damping proposed by Colgate and Schenkel, the proposed approach leverages a change in the open-loop dynamics to enhance the passivity of a simulated surface. Rather than add damping, however, the proposed approach adds (primarily) stiffness via the natural behavior of pneumatic actuators. In order to assess the effect of the open-loop stiffness of a pneumatic actuator on the passivity of a haptic simulation of stiffness, the authors incorporate a passivity analysis for a sampled-data system based on the one originally presented by Colgate and Schenkel

[5]. As described in [5], in order for the haptic interface system depicted by Figure 4-1 to remain passive, the system must satisfy the following condition:

$$\int_0^t f(\tau)v(\tau)d\tau > 0, \qquad \forall\, t > 0, \text{ admissible } f(t) \tag{10}$$

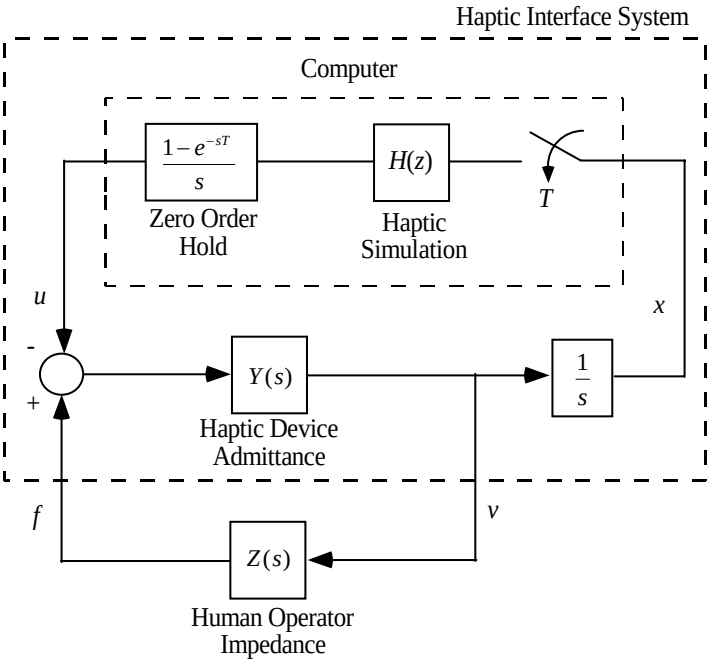

Figure 4-1. Block diagram of haptic interface.

For the assumed electric motor actuator output admittance of

$$Y(s) = \frac{1}{ms + b} \tag{11}$$

used in [5], and for the haptic simulation of a spring (i.e., $H(z) = K$), the maximum achievable simulated stiffness to ensure passivity is limited by:

$$K < \frac{2b}{T} \tag{12}$$

where b is the open-loop damping in the device and T is the sampling period. In order to assess the passivity of a pneumatically actuated haptic device, the actuator output admittance is modified to include a stiffness term in addition to the inertial and damping terms. Since the equilibrium of the stiffness term is variable (as previously shown), it requires a representation based on displacement rather than velocity. Thus, rather than describing the pneumatic actuator admittance as:

$$Y(s) = \frac{1}{ms + b + k/s}, \tag{13}$$

which omits the presence of a variable equilibrium point, the dynamic character of the actuator is instead described by the block diagram shown in Figure 4-2, which explicitly addresses the change in equilibrium point in the actuator stiffness. The local approximation of the steady-state force generated by the actuator results from a combination of the actuator stiffness and the equilibrium position of that stiffness, which is represented in Figure 4-2 and can be expressed as

$$f_{ss} = k(x - x_e) \tag{14}$$

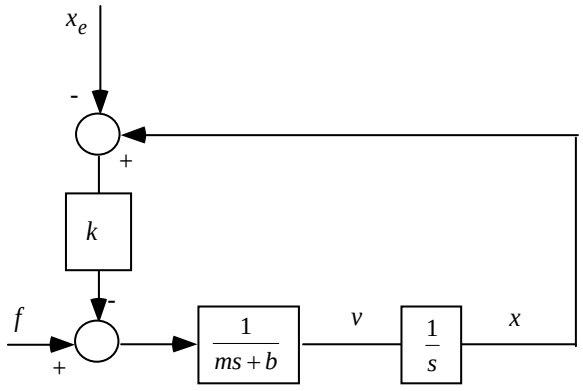

Figure 4-2. Open-loop dynamic behavior of pneumatically actuated haptic device.

where k is the actuator stiffness as described by (8) and x_e is the equilibrium position given by (9). In the case of implementing a desired stiffness (i.e., for the impedance-type haptic simulation of a surface), the commanded actuator force is given by:

$$u = K(x - x_w)\delta(x, x_w) \tag{15}$$

where K is the desired stiffness of the surface, x_w is the location of the surface (or wall), and $\delta(x, x_w)$ represents a unilateral constraint which specifies that the haptic device should only impose a force when the operator is inside the surface. As discussed in [5], presence of the unilateral constraint $\delta(x, x_w)$ does not affect the sufficient condition for passivity of the haptic system, and the position of the surface can be assumed to be zero without loss of generality. Equating (14) and (15) in the absence of the unilateral constraint and with $x_w = 0$ yields the equilibrium position required for the haptic simulation of a stiffness:

$$x_e = \left(1 - \frac{K}{k}\right)x \tag{16}$$

One can thus close the loop in the block diagram of Figure 4-2 with (16) to represent the discrete-time implementation of an impedance type simulation of stiffness with a pneumatic actuator, which is shown in Figure 4-3. By "migrating" the open-loop stiffness of the pneumatic actuator k backward through the summing junction, one can arrive at the representation shown in Figure 4-4. Finally, by collapsing the parallel paths prior to the zero order hold, as shown in Figure 4-5, one can arrive at a representation in the form of that shown in Figure 4-1, where $H(z) = K - k = \Delta K$. Though the actuator admittance is not shown as a single block, the representation is easily collapsed to that of Figure 4-1, yielding an actuator admittance $Y(s)$ as given in (13). Rather than show the actuator

admittance in collapsed form, the stiffness in Figure 4-5 is separated from the rest of the actuator admittance block to make clear that the commanded actuator force consists of two components, one resulting from the open-loop properties and one resulting from the closed-loop command.

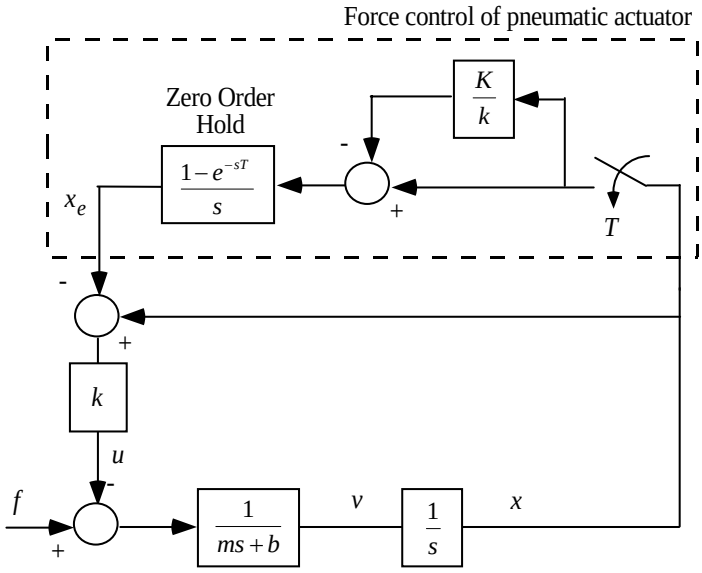

Figure 4-3. Discretely-implemented stiffness simulation with a force-controlled pneumatic actuator.

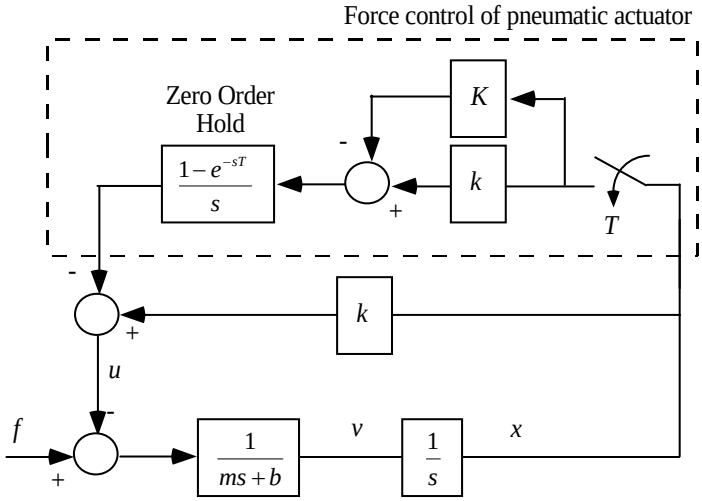

Figure 4-4. Rearrangement of Figure 4-3.

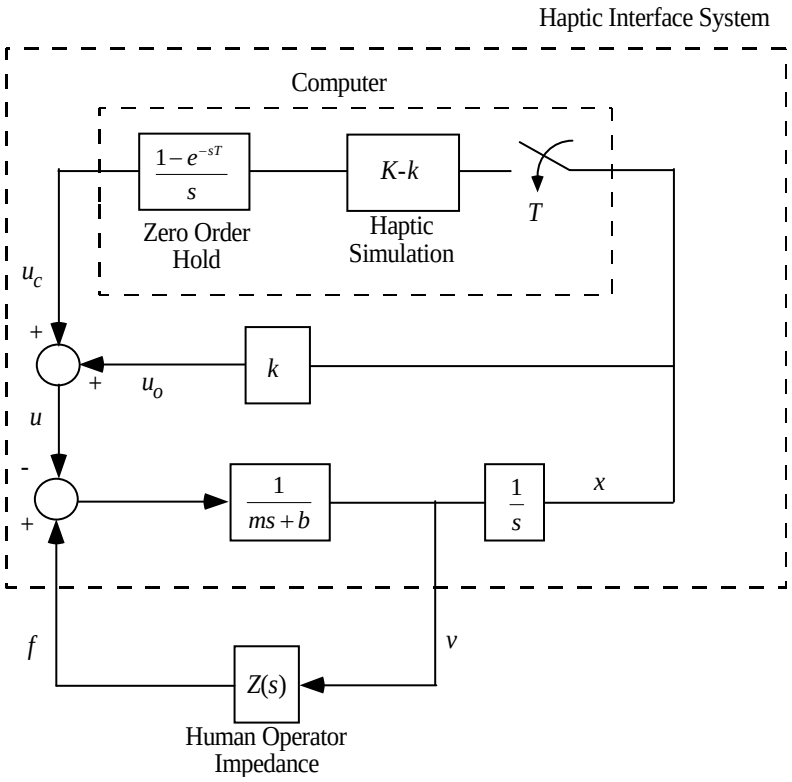

Figure 4-5. Pneumatically actuated impedance-type stiffness simulation, omitting the force control dynamics of the pneumatic actuator.

Note that, in the passivity analysis performed in [5], Colgate and Schenkel quite reasonably assumed that the dynamics between the commanded force and the actual force in the electric motor were negligible. These dynamics are typically not negligible in a pneumatic actuator, and rather are typically first order in nature (i.e., the pressure is an integration of mass flow rate, as discussed in the following section). Therefore, the closed-loop dynamics between commanded and actual force must also be considered in a passivity analysis of the pneumatic haptic interface. As such, the haptic interface model shown in Figure 4-5 must be modified to include the dynamics of the force-controlled pneumatic actuator, which for purposes of analysis are approximated as first order and

linear with time constant τ_c, acting on the closed-loop component of the actuator force, as shown in Figure 4-6.

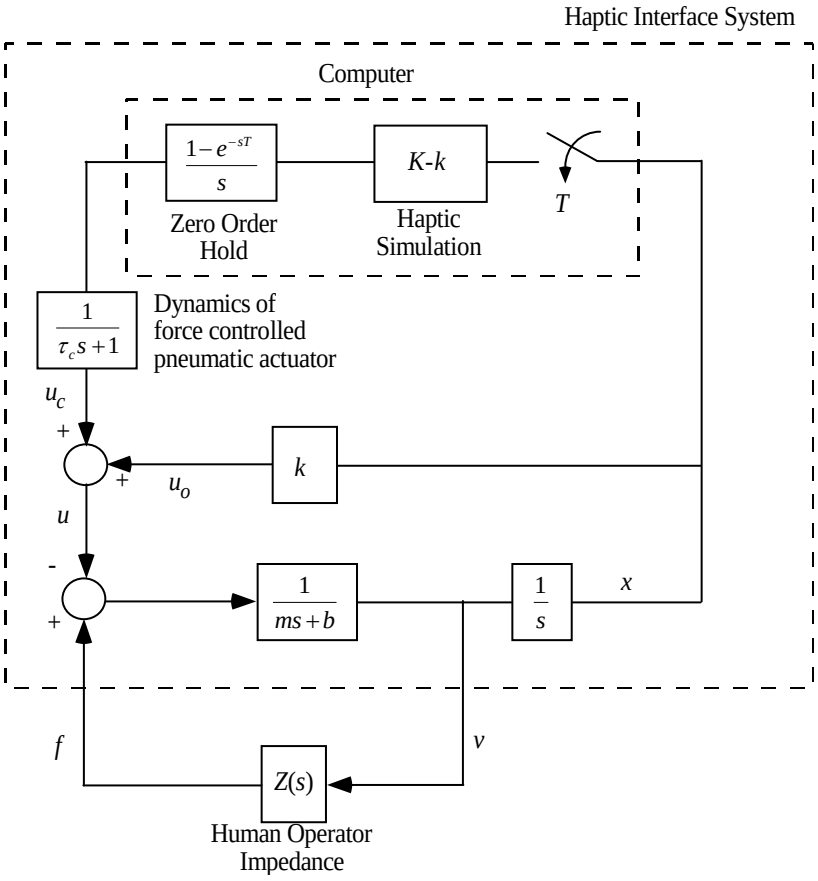

Figure 4-6. Pneumatically actuated impedance-type stiffness simulation.

Based on this model of the system dynamics, a passivity analysis similar to that conducted in [5] provides insight into the effect of the open-loop stiffness on the passivity of haptic simulation. The system is assumed to be at rest initially and without potential energy. To ensure passivity, the total energy stored in the system (i.e., kinetic and potential) should be less than the total energy input to the system by the operator, mathematically stated as:

$$\frac{1}{2}mv^2(t)+\frac{1}{2}kx^2(t)<\int_0^t f(\tau)v(\tau)d\tau \tag{17}$$

Conservation of energy for the haptic device yields

$$\frac{1}{2}mv^2(t)=\int_0^t f(\tau)v(\tau)d\tau-\int_0^t u(\tau)v(\tau)d\tau-\int_0^t bv(\tau)v(\tau)d\tau \tag{18}$$

where the left-hand-side term is the energy stored in the device inertia, the first term on the right-hand-side is the energy imposed by the operator, the second term is the energy absorbed by the actuator, and the third term the energy absorbed by the damping in the device. The actuator force u results from the combination of the open-loop component u_o and the closed-loop component u_c:

$$\frac{1}{2}mv^2(t)=\int_0^t f(\tau)v(\tau)d\tau-\int_0^t u_c(\tau)v(\tau)d\tau-\int_0^t u_o(\tau)v(\tau)d\tau-\int_0^t bv(\tau)v(\tau)d\tau \tag{19}$$

The open-loop component of the actuator force u_o results from potential energy storage, and thus can be brought to the left-hand-side:

$$\frac{1}{2}mv^2(t)+\frac{1}{2}kx^2(t)=\int_0^t f(\tau)v(\tau)d\tau-\int_0^t u_c(\tau)v(\tau)d\tau-\int_0^t bv(\tau)v(\tau)d\tau \tag{20}$$

Thus, the total energy input by the operator can be represented by:

$$\int_0^t f(\tau)v(\tau)d\tau=\frac{1}{2}mv^2(t)+\frac{1}{2}kx^2(t)+\int_0^t u_c(\tau)v(\tau)d\tau+\int_0^t bv(\tau)v(\tau)d\tau \tag{21}$$

In order to ensure passivity, (21) must satisfy (17), which results in the following condition for passivity:

$$\int_0^t u_c(\tau)v(\tau)d\tau+\int_0^t bv(\tau)v(\tau)d\tau>0 \tag{22}$$

Based on the work presented in [5], this condition is satisfied when

$$b > \frac{T}{2(1-\cos\omega T)} \mathrm{Re}\left\{(1-e^{-j\omega t})H(e^{j\omega t})\right\}, 0 \le \omega \le \omega_n \tag{23}$$

where $H(e^{j\omega t})$ represents the (discrete-time) dynamics of the haptic simulation. In the case of a pneumatic actuator, the dynamics of closed-loop force control become an unwanted component of the haptic simulation, and as such

$$H(e^{j\omega t}) = \frac{\Delta K}{\tau_c s + 1}\bigg|_{s=\frac{e^{j\omega t}-1}{Te^{j\omega t}}} = \frac{\Delta K \cdot Te^{j\omega t}}{(\tau_c + T)e^{j\omega t} - \tau_c} \tag{24}$$

Combining (23) and (24) yields a sufficient condition for passivity of the system as follows:

$$\Delta K < \frac{2b}{T + 2\tau_c} \tag{25}$$

Since the simulated stiffness *K* is given by

$$K = k + \Delta K, \tag{26}$$

the simulated stiffness that will ensure passivity of the haptic interface is given by

$$K < \frac{2b}{T + 2\tau_c} + k \tag{27}$$

Equation (27) indicates that the presence of an open-loop stiffness (i.e., *k*) increases the range of passively achievable stiffness relative to an electric motor actuator as described by (12), while the presence of the force control dynamics in the actuator (i.e., τ_c) decreases the range of passively achievable stiffness. Since the time constant of a typical pneumatic force controller is on the order of 100 milliseconds and a typical sampling period is on the order of one millisecond, the denominator of the first term is increased by approximately two orders of magnitude relative to an electric motor-actuated system. The viscous damping coefficient of a typical (direct-drive) motor-actuated haptic

interface is on the order of 0.01 N-s/m [7], while a typical viscous damping coefficient for a pneumatic actuator is on the order of 10 N-s/m [17], and thus is approximately three orders of magnitude greater. As such, the net effect on the first term in (27) is a significant increase in magnitude relative to typical values of simulated stiffness reported for motor-actuated haptic interfaces (e.g., [7, 13, 14, 18]). The second term in (27), the open loop stiffness, is on the order of 10 N/mm (for typical pressures in a pneumatic actuator), which is also larger than typical values of simulated stiffness reported for motor-actuated interfaces. As such, one would expect that the use of a pneumatic actuator would provide a net positive and significant benefit with regard to the passive simulation of stiffness, due both to the increased amount of damping and the presence of an open-loop stiffness. When simulating free space (i.e., $K = 0$), the condition for passivity becomes:

$$0 < \frac{2b}{T + 2\tau_c} + 2k \tag{28}$$

which is clearly always satisfied since all terms on the right-hand-side are positive. Thus passivity is enhanced when simulating a stiffness with a pneumatic actuator, and always guaranteed when simulating free space.

Force Control of Pneumatic Actuators

Implementation of an impedance-type haptic interface requires control of the output force. In the case of an electric motor, control of the actuator force output is afforded by the use of feedback control, either based on current measurement and feedback (as in the case of a servoamplifier), or based on the direct measurement and feedback of force. Since the dynamics between valve area command input and force

output of a pneumatic actuator are more involved than a typical electric motor, a method of force control based on feedback of the measured force is described here. A model from input valve command to output force of a pneumatic actuator is derived by differentiating (2) with respect to time, which gives:

$$\dot{F} = \dot{P}_a A_a - \dot{P}_b A_b \tag{29}$$

Assuming air is an ideal gas undergoing an isothermal process, the rate of change of the pressure inside each chamber of the cylinder can be expressed as:

$$\dot{P}_{(a,b)} = \frac{RT}{V_{(a,b)}} \dot{m}_{(a,b)} - \frac{P_{(a,b)}}{V_{(a,b)}} \dot{V}_{(a,b)} \tag{30}$$

Based on the isentropic flow of an ideal gas through a converging nozzle, the relationship between the mass inflow/outflow rate and the valve opening area is given by

$$\dot{m}(P_u, P_d) = A_v \Psi(P_u, P_d) \tag{31}$$

where P_u and P_d represent the upsteam and downstream pressures across the valve, respectively, A_v represents the valve orifice area, and $\Psi(\cdot,\cdot)$ is a nonlinear algebraic function of the state given by:

$$\Psi(P_u, P_d) = \begin{cases} \sqrt{\dfrac{\gamma}{RT}\left(\dfrac{2}{\gamma+1}\right)^{(\gamma+1)/(\gamma-1)}} C_f P_u \\ \qquad \text{if} \quad \dfrac{P_d}{P_u} \le C_r \quad \text{(choked)} \\ \sqrt{\dfrac{2\gamma}{RT(\gamma-1)}} \sqrt{1 - \left(\dfrac{P_d}{P_u}\right)^{(\gamma-1)/\gamma}} \left(\dfrac{P_d}{P_u}\right)^{(1/\gamma)} C_f P_u \\ \qquad \text{otherwise} \quad \text{(unchoked)} \end{cases} \tag{32}$$

In this equation, C_f is the discharge coefficient of the valve, γ is the ratio of specific heats, and C_r is the pressure ratio that divides the flow regimes into unchoked and choked flow. Substituting (30) and (31) into (29) gives:

$$\dot{F} = \frac{A_a RT}{V_a}\Psi_a A_{v,a} - \frac{P_a A_a}{V_a}\dot{V}_a - \frac{A_b RT}{V_b}\Psi_b A_{v,b} + \frac{P_b A_b}{V_b}\dot{V}_b \tag{33}$$

where

$$\Psi_a = \begin{cases} \Psi(P_s, P_a) & for\ A_{v,a} \geq 0 \\ \Psi(P_a, P_{atm}) & for\ A_{v,a} < 0 \end{cases} \tag{34}$$

and

$$\Psi_b = \begin{cases} \Psi(P_s, P_b) & for\ A_{v,b} \geq 0 \\ \Psi(P_b, P_{atm}) & for\ A_{v,b} < 0 \end{cases} \tag{35}$$

Thus, a positive "signed area" represents the area between the pressure supply and the cylinder, while a negative signed area represents the area between the cylinder and exhaust. The use of a four-way spool valve constrains the effective valve areas such that:

$$A_{v,a} = -A_{v,b} = A_v \tag{36}$$

Thus, the system dynamics from single signed valve area command to the actuator force output are given by:

$$\dot{F} = (\frac{A_a RT}{V_a}\Psi_a + \frac{A_b RT}{V_b}\Psi_b)A_v - \frac{P_a A_a}{V_a}\dot{V}_a + \frac{P_b A_b}{V_b}\dot{V}_b \tag{37}$$

which is affine in the control input A_v.

Having expressed the actuation force dynamics in a control canonical form, a sliding mode control approach can be applied to the force control of the system. Selecting a sliding surface

$$e = F - F_d \tag{38}$$

where F_d is the desired actuation force, a robust control law can be developed based on a standard sliding mode control approach, where the equivalent control component is derived by solving for the input for the case $\dot{e} = 0$, which gives:

$$A_{v,eq} = \frac{\dot{F}_d + \frac{P_a A_a}{V_a}\dot{V}_a - \frac{P_b A_b}{V_b}\dot{V}_b}{\frac{A_a RT}{V_a}\Psi_a + \frac{A_b RT}{V_b}\Psi_b} \tag{39}$$

or

$$A_{v,eq} = \begin{cases} \dfrac{\dot{F}_d + \frac{P_a A_a}{V_a}\dot{V}_a - \frac{P_b A_b}{V_b}\dot{V}_b}{\frac{A_a RT}{V_a}\Psi(P_s, P_a) + \frac{A_b RT}{V_b}\Psi(P_b, P_{atm})} & \text{for } A_v \geq 0 \\ \dfrac{\dot{F}_d + \frac{P_a A_a}{V_a}\dot{V}_a - \frac{P_b A_b}{V_b}\dot{V}_b}{\frac{A_a RT}{V_a}\Psi(P_a, P_{atm}) + \frac{A_b RT}{V_b}\Psi(P_s, P_b)} & \text{for } A_v < 0 \end{cases} \tag{40}$$

The robust control law is obtained by adding a robustness component, such that

$$A_v = A_{v,eq} - \eta \,\mathrm{sgn}(e) \tag{41}$$

where η is the robustness gain.

Experiments

Experiments were conducted to demonstrate the performance of the proposed controller while simulating a high stiffness surface. The experimental setup, which is shown schematically in Figure 4-7 and in photograph in Figure 4-8, consisted of a 2.7 cm (1-1/16 in) inner diameter, 10 cm (4 in) stroke pneumatic cylinder (Numatics 1062D04-04A) controlled by a four-way proportional servovalve (FESTO MPYE-5-M5-010-B, which has a bandwidth of approximately 125 Hz) supplied with air at an absolute pressure of 653 kPa (95 psia). The output of the pneumatic cylinder was connected to a linear slide via a load cell (Transducer Techniques MLP-50), which was used to measure the actuator force. A human operator grasped a handle on the linear slide, which enabled

application of significant forces (relative to a stylus-type device). Displacement of the slide (and actuator) was measured with a linear potentiometer (Midori LP-100F). The model and controller parameters used in the experiments are listed in Table 4-1.

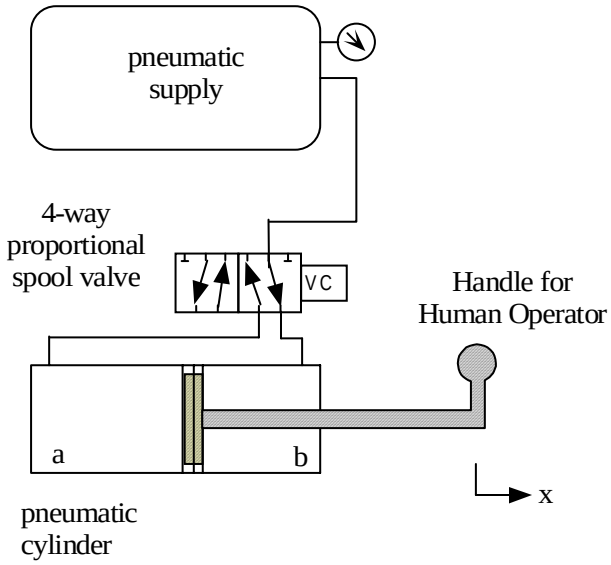

Figure 4-7. Schematic of pneumatically actuated haptic interface.

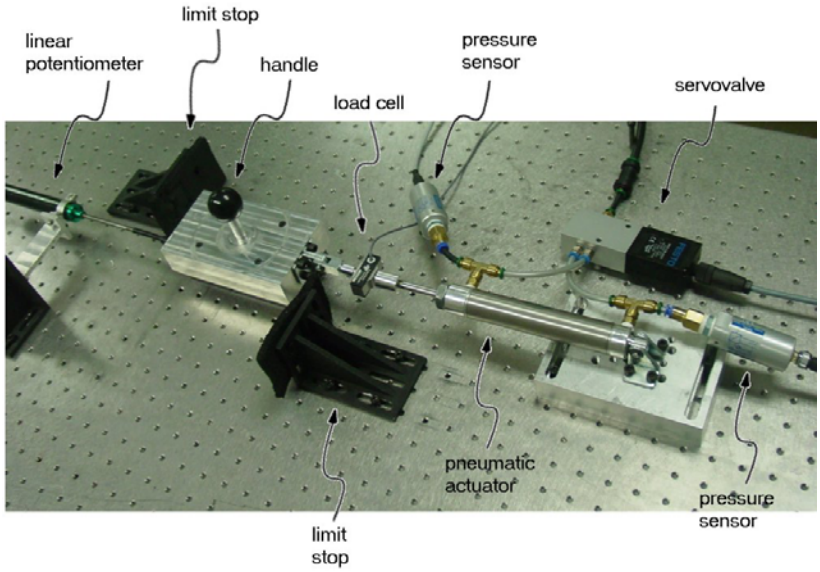

Figure 4-8. Experimental setup for assessment of pneumatically actuated haptic interface.

Table 4-1. Model and controller parameters for experimental implementation.

Parameter	Value	Unit
P_s	653	kPa
A_a	572	mm^2
A_b	540	mm^2
A_r	32	mm^2
L	102	mm
C_f	0.8	
C_r	0.5	
R	0.287	kJ/kg-K
T	293	K
γ	1.4	
η	2.0	mm^2

The performance of the pneumatically-implemented impedance-type haptic display is indicated by the data shown in Figures 4-9 through 4-13, which shows the simulation of a surface stiffness of K=10 N/mm at a "wall" position of 10mm and at a sampling rate of 1000 Hz. Note that in order to isolate the effects of the open-loop actuator behavior on the passivity of the system, all surface simulations presented in this paper consisted only of a simple stiffness, and did not involve any stabilizing algorithms such as a virtual coupling. Figure 4-9 shows the motion imposed by the human operator, Figure 4-10 shows the resulting force imposed by the haptic interface, and Figure 4-11 shows the constitutive behavior simulated by the system (i.e., the force plotted versus displacement). Note that the bandwidth of the actuator, though not explicitly shown, is implicitly indicated by the slope of the position data in Figure 4-9, which indicates an "impact" velocity of approximately 0.1 m/s, combined with the single-valued nature of Figure 4-11, which indicates a lack of significant phase lag when impacting a surface at that velocity. Figures 4-12 and 4-13 show the open and closed-loop contributions to the stiffness, respectively. The open-loop contribution to the stiffness was computed by

substituting (6) into (8), which yields an expression for actuator stiffness in terms of measurable quantities (i.e., pressure and displacement):

$$k = \frac{P_a A_a}{\frac{L}{2} + x} + \frac{P_b A_b}{\frac{L}{2} - x} \tag{41}$$

Pressure sensors (FESTO SDE-16-10V/20mA) measured the pressure in each cylinder chamber, and in combination with the measured displacement, the open-loop stiffness was computed. The closed-loop contribution was simply the difference between the desired stiffness and the open-loop contribution. As can be seen from Figure 13, the closed-loop portion, which is the one that affects the passivity of the simulation as described by (25), is a fraction of the desired stiffness, and often remains negative, in which case passivity is guaranteed.

Note that, when simulating free space, the closed-loop force controller effectively masks the presence of the open-loop stiffness in the actuator. As with any closed-loop force control, a higher feedback gain provides a higher bandwidth of control, but magnifies the sensor noise. The single feedback gain η was chosen to be just below the point at which noise was noticeable to the user in “free space.”

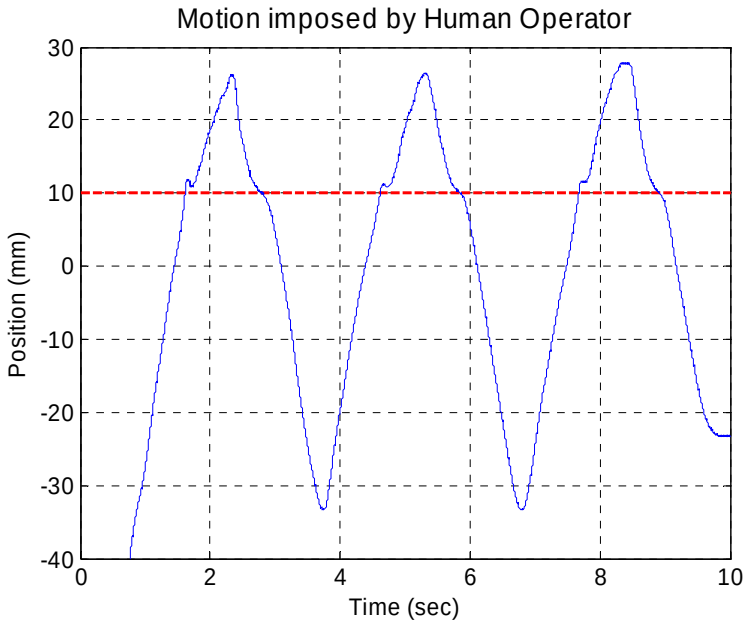

Figure 4-9. Motion imposed by human operator for simulated stiffness of K=10 N/mm and wall located at 10 mm.

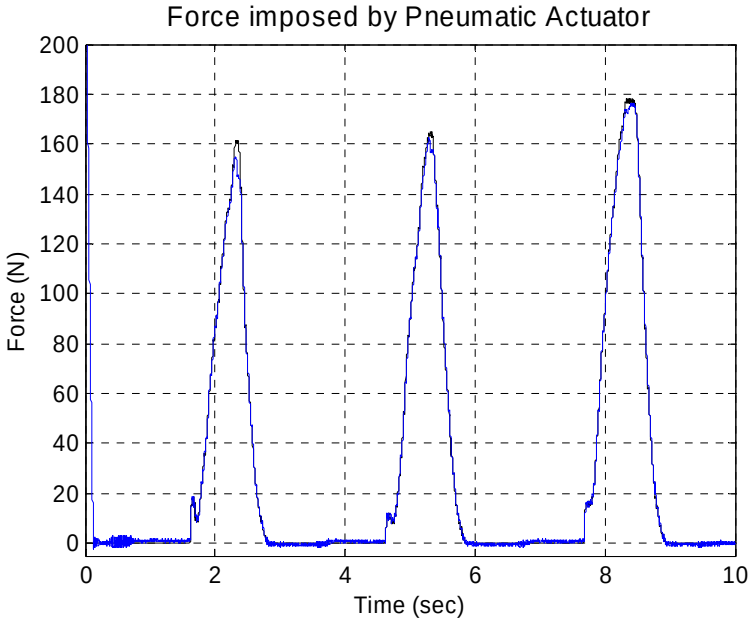

Figure 4-10. Desired (taller peaks) and actual force corresponding to motion shown in Figure 4-9 (K=10 N/mm).

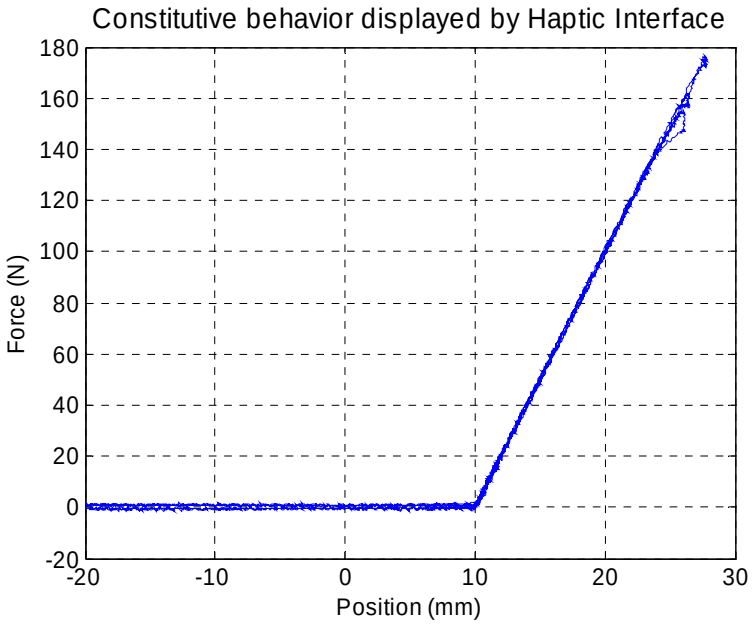

Figure 4-11. Constitutive behavior displayed by haptic interface for K=10 N/mm (i.e., force of Figure 4-10 plotted versus motion of Figure 4-9).

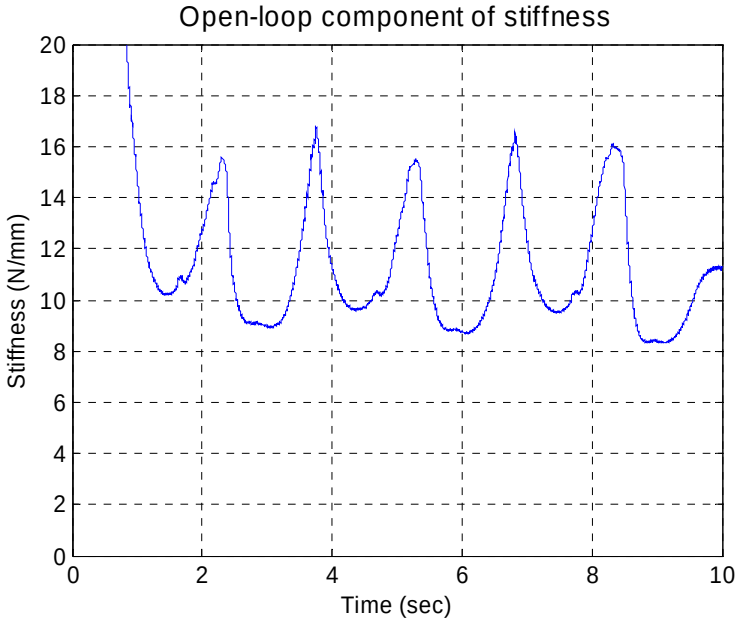

Figure 4-12. Open-loop component of stiffness during simulation of K=10 N/mm.

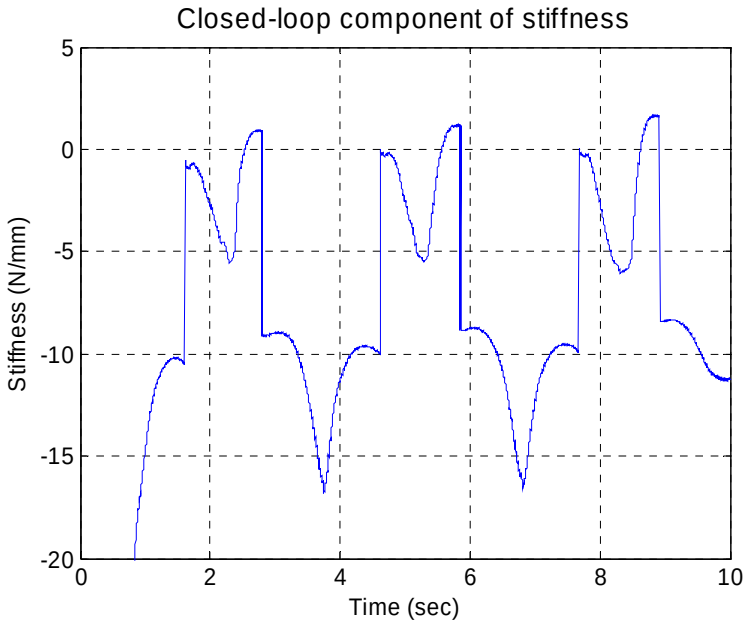

Figure 4-13. Closed-loop component of stiffness during simulation of K=10 N/mm.

The ability of the pneumatically-actuated system to impose a moving wall is indicated by the experimental data shown in Figures 4-14 through 4-16. Specifically, in a multi-degree-of-freedom haptic interface, the simulation of a static wall in a task space often requires the simulation of "moving" walls in the joint space. The ability to simulate a "moving" wall was demonstrated by resting a 4.5 kg (10 lb) mass against the surface. This was implemented by tying a cable to the handle of the haptic interface, routing the cable over a pulley on the edge of the table, and hanging the mass vertically from the cable. In essence the hanging mass imposed a roughly constant gravitational force against the wall, with a smaller oscillating inertial component superimposed onto the constant gravitational force. As with the "static" wall simulation, the surface was simulated with a stiffness of K=10 N/mm at a sampling rate of 1000 Hz. Unlike the static simulation, the wall was commanded to move sinusoidally about the 10 mm position at a

frequency of 0.5 Hertz and with an amplitude of 5 mm, as shown by the dashed line in Figure 4-14. As seen in Figure 4-14, the mass (solid line) oscillates smoothly along with the motion of the wall. Note that the initial oscillation results from the impact between the mass and the wall, since the mass initially starts somewhat "above" the surface, while damping of the initial oscillation is due to the open-loop damping, since the simulation includes only a stiffness component. Finally, Figures 4-15 and 4-16 show the measured open-loop stiffness and the required closed-loop component. The closed-loop component clearly remains either very small or negative, thus ensuring passivity of the haptic system.

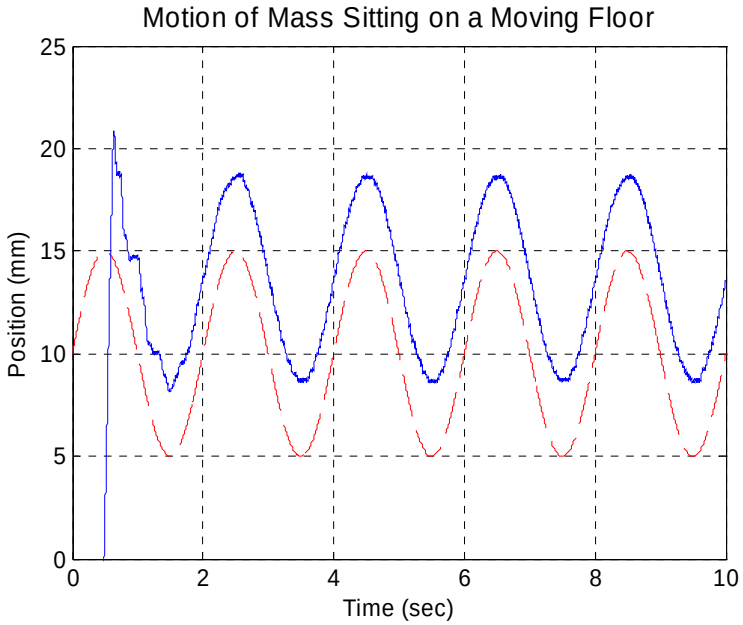

Figure 4-14. Motion of mass which is "sitting" on a moving floor of stiffness K=10 N/mm (floor position indicated by dashed line, mass position by solid line).

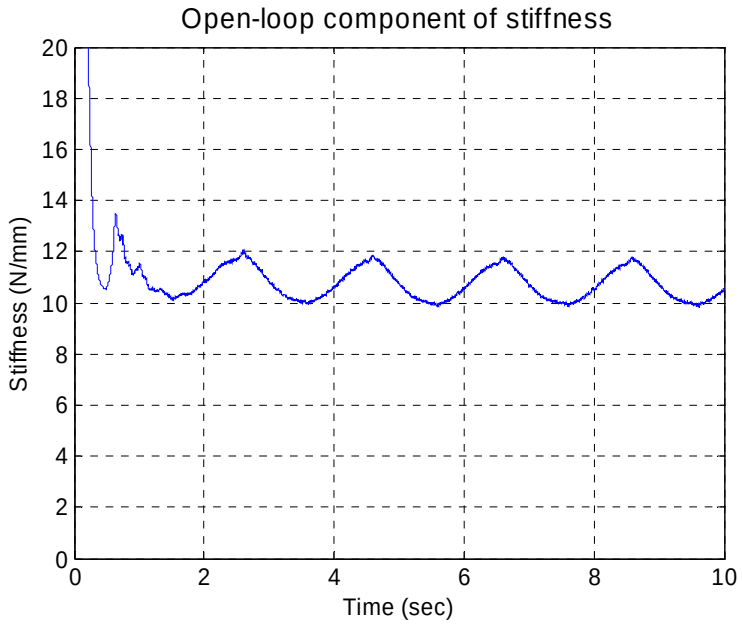

Figure 4-15. Open-loop stiffness corresponding to moving floor.

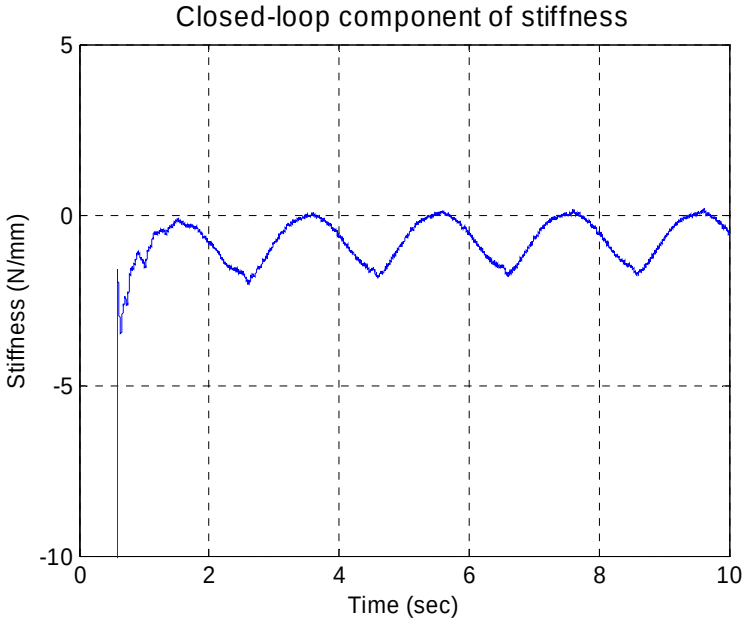

Figure 4-16. Closed-loop stiffness corresponding to moving floor.

In order to assess the maximum stiffness the device could simulate, the 4.5 kg (10 lb) mass used in the previously described experiment was “dropped” on a simulated surface, in a manner similar to that previously described (i.e., a pulley and cable). At a sampling frequency of 1000 Hz, the simulated stiffness was increased until the response became metastable. The experimental data show that the maximum attainable stiffness for a stable response is 30 N/mm, which is significantly larger than previously published impedance-type haptic simulations of pure stiffness with a motor-actuated haptic interface at comparable sampling rates without explicit stability compensation (i.e., in the absence of virtual couplings or other energy leak compensation algorithms) [7, 13, 14, 18]. Figure 4-17 shows the motion of the mass after the mass is released in the free space. Following the initial impact between the mass and the surface, the mass oscillates at a decreasing magnitude until it comes to a rest, due to the existence of the damping in the device. Figure 4-18 shows the motion of the mass when the simulated stiffness is 35 N/mm, which results in a metastable response (i.e., sustained oscillation). Note that the enhanced passivity (relative to motors) evidenced by Figure 4-17 is due both to the presence of open-loop stiffness and to the increased open-loop damping of the pneumatic actuator relative to electric motors.

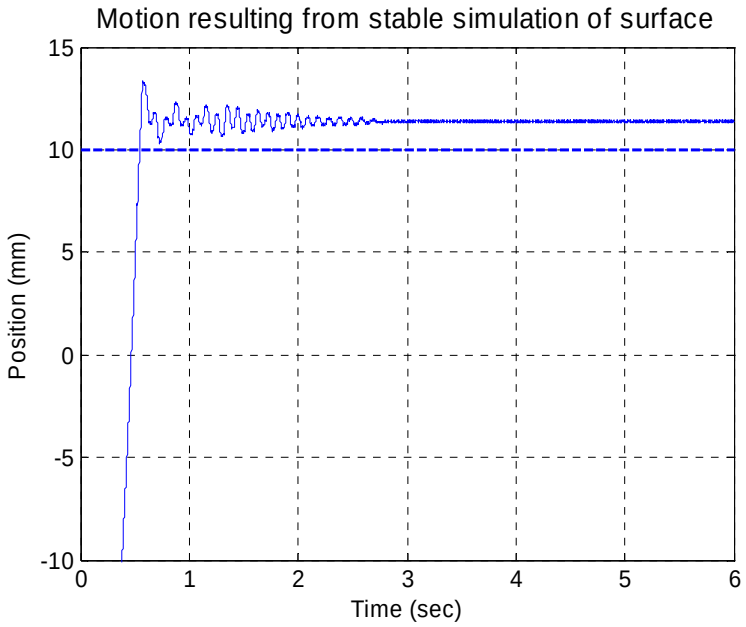

Figure 4-17. Stable motion of the mass resulting from simulated stiffness of K=30 N/mm.

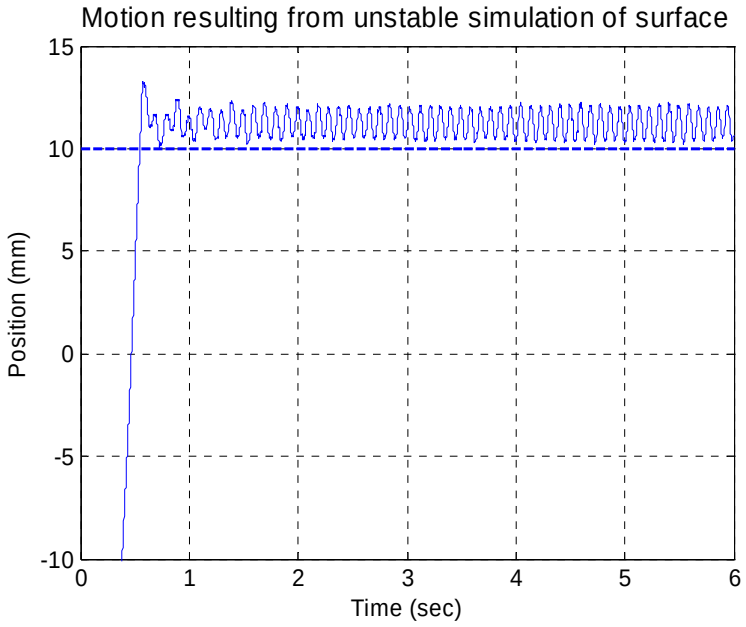

Figure 4-18. Limit cycling of the mass resulting from simulated stiffness of K=35 N/mm.

Conclusion

The authors proposed the use of pneumatic actuation for an impedance-type haptic device. Due to the inherent open-loop stiffness of a pneumatic actuator under force control, the stiffness component from computer-based feedback control required to simulate a stiff surface is significantly reduced. The authors show that the presence of open-loop stiffness in the pneumatic actuator enhances the range of achievable surface stiffnesses relative to an electric motor actuated system, and additionally show that the system is always stable in free space. Experiments indicate that the enhanced range of passivity enables a pneumatically actuated impedance-type haptic device to simulate a greater surface stiffness than a typical motor-actuated device.

References

[1] Colgate, J. E., and Brown, J. M., "Factors affecting the Z-width of a haptic display," in *Proceedings of the IEEE International Conference on Robotics and Automation*, pp. 3205-3210, 1994.

[2] Gillespie, R. B., and Cutkosky, M. R., "Stable user-specific haptic rendering of the virtual wall," in *Proceedings of ASME Dynamic Systems and Control Division*, vol. 58, pp. 397-406, 1996.

[3] Colgate, J. E., Grafing, P. E., Stanley, M. C., and Schenkel, G., "Implementation of stiff virtual walls in force reflecting interfaces," in *Proceedings of IEEE Virtual Reality Annual International Symposium*, pp. 202-207, 1993.

[4] Colgate, J. E., and Schenkel, G., "Passivity of a class of sampled-data systems: Application to haptic interfaces," in *Proceedings of the American Control Conference*, pp. 3236-3240, 1994.

[5] Colgate, J. E., and Schenkel, G., "Passivity of a class of sampled-data systems: Application to haptic interfaces," *Journal of Robotic Systems*, vol. 14, no. 1, pp. 37-47, Jan. 1997.

[6] Abbott, J., and Okamura, A., "A sufficient condition for passive virtual walls with quantization effects," in *Proceedings of ASME International Mechanical Engineering Congress and Exposition*, pp. 1065-1073, 2004.

[7] Diolaiti, N., Niemeyer, G., Barbagli, F., and Salisbury, J. K., "A criterion for the passivity of haptic devices," in *Proceedings of the IEEE International Conference on Robotics and Automation*, pp. 2463-2467, 2005.

[8] Love, L., and Book, W., "Contact stability analysis of virtual walls," in *Proceedings of ASME Dynamic Systems and Control Division*, vol. 57, pp. 689-694, 1995.

[9] Colgate, J. E., Stanley, M. C., and Brown, J. M., "Issues in the haptic display of tool use," in *Proceedings of the IEEE/RSJ International Conference on Intelligent Robots and Systems*, vol. 3, pp. 140-145, 1995.

[10] Adams, R. J., and Hannaford, B., "Stable haptic interaction with virtual environments," *IEEE Transactions on Robotics and Automation*, vol. 15, no. 3, pp. 465-474, June 1999.

[11] Stramigioli, S., Secchi, C., van der Schaft, A., and Fantuzzi, C., "A novel theory for sample data system passivity," in *Proceedings of the IEEE/RSJ International Conference on Intelligent Robots and Systems*, pp. 1936-1941, 2002.

[12] Hannaford, B., and Ryu, J. H., "Time-domain passivity control of haptic interfaces," *IEEE Transactions on Robotics and Automation*, vol. 18, no. 1, pp. 1-10, Feb. 2002.

[13] Ellis, R. E., Sarkar, N., and Jenkins, M. A., "Numerical methods for the for reflection of contact," *ASME Journal of Dynamic Systems, Measurement, and Control*, vol. 119, no. 4, pp. 768-774, Dec. 1997.

[14] Goldfarb, M., and Wang, J., "Passive stiffness simulation with rate-independent hysteresis," in *Proceedings of ASME Dynamic Systems and Control Division*, vol. 67, pp. 345-350, 1999.

[15] Madill, D., Wang, D., and Ching, M., "A nonlinear observer for minimizing quantization effects in virtual walls," in *Proceedings of ASME Dynamic Systems and Control Division*, vol. 67, pp. 335-343, 1999.

[16] Mehling, J. S., Colgate, J. E., Peshkin, M. A., "Increasing the Impedance Range of a Haptic Display by Adding Electrical Damping", in *Proceedings of IEEE First Joint Eurohaptics Conference and Symposium on Haptic Interfaces for Virtual Environment and Teleoperator Systems*, pp. 257-262, 2005.

[17] Wang, J., Wang, J. D., Daw, N., and Wu, Q. H., "Identification of Pneumatic Cylinder Friction Parameters Using Genetic Algorithms," *IEEE/ASME Transactions on Mechatronics*, vol. 9, no. 1, pp. 100-107, Mar. 2004.

[18] O'Malley, M., and Goldfarb, M., "The Effect of Virtual Surface Stiffness on the Haptic Perception of Detail," *IEEE/ASME Transactions on Mechatronics*, vol. 9, no. 2, pp. 448-453, June 2004.

CHAPTER V: MANUSCRIPT 4

ENERGY SAVING IN PNEUMATIC SERVO CONTROL UTILIZING INTER-CHAMBER CROSS-FLOW

Xiangrong Shen and Michael Goldfarb

Department of Mechanical Engineering

Vanderbilt University

Nashville, TN 37235

Submitted to the *ASME Journal of Dynamic Systems, Measurement, and Control*

Abstract

This paper proposes a structure and control approach for the energy saving servo control of a pneumatic servo system. The energy saving approach is enabled by supplementing a standard four-way spool valve controlled pneumatic actuator with an additional two-way valve that enables flow between the cylinder chambers. The "crossflow" valve enables recirculation of pressurized air, and thus enables the extraction of stored energy that would otherwise be exhausted to atmosphere. A control approach is formulated that supplements, to the extent possible, the mass flow required by a sliding mode controller with the recirculated mass flow provided by the crossflow valve. Following the control formulation, experimental results are presented that indicate energy savings of 25% to 52%, with essentially no compromise in tracking performance relative

to the standard sliding mode control approach (i.e., relative to control via a standard four-way spool valve, without the supplemental flow provided by the crossflow valve).

Introduction

A typical pneumatic servo system consists of a proportionally controllable four-way spool valve and a pneumatic cylinder, as depicted in Figure 5-1. In this system, the position of the valve spool controls the airflow into and out of each side of the cylinder, which in turn results in a pressure differential across the piston that imposes an actuation force on the load. In such a system, feedback control is incorporated to command the valve spool motion input that will result in a desired output motion of the piston and associated load. A considerable amount of work has been conducted in the modeling and feedback control of such systems, including the work by Shearer [1, 2, 3], Mannetje [4], Ben-Dov and Salcudean [5], Wang et al. [6], Maeda et al. [7], Ning and Bone [8], Bobrow and McDonell [9], and Richer and Hurmuzlu [10, 11], among others.

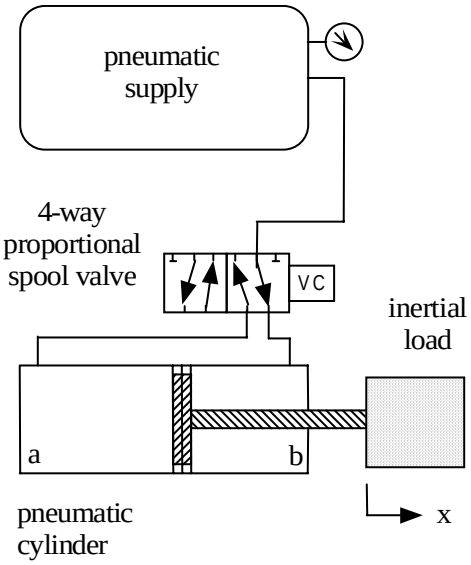

Figure 5-1. Configuration of a typical pneumatic servo system.

Most applications involving servoactuation draw energy from an essentially limitless reservoir of power (i.e., from a power plant). In many applications, however, the available energy may be considerably more limited (e.g., in the case of a mobile robot), and in such cases, the energetic efficiency of the system is significant. Because pneumatic actuators generally contain a considerable amount of stored energy due to their compressibility, and since this stored energy can in theory be moved from one part of the actuator to another in a controlled fashion via valves, pneumatic systems offer unique possibilities with regard to the energetic efficiency of control.

Some of the prior work that treats energy saving in a pneumatic actuation system includes that by Sanville [12], Quaglia and Gestaldi [13, 14], Pu et al. [15], Wang et al. [16], Kawakami et al. [17], Arinaga et al. [18], and Al Dakkan et al. [19, 20]. Specifically, Sanville [12] proposes the use of a secondary reservoir in an open-loop system to collect exhaust air rather than vent it to atmosphere, then reuse the stored air on

the return stroke. Quaglia and Gestaldi [13, 14] propose a non-conventional pneumatic cylinder that incorporates multiple cylinder chambers embedded into a single actuator with the intent of recycling compressed air. Pu et al. [15] describe a pneumatic arrangement that incorporates a standard four-way spool valve controlled pneumatic servoactuator, with an additional two-way valve between the two sides of the cylinder. Wang et al. [16] studied the use of input shaping to choose a command profile for point-to-point motions that would result in energy savings for closed loop pneumatic servoactuators, and showed that some velocity profiles could reduce energy demand relative to other profiles. Kawakami et al. [17] and Arinaga et al. [18] utilized metering circuits to reduce the airflow requirements for open-loop point-to-point motions. Al Dakkan et al. [19, 20] decouple a standard four-way valve into a pair of three-way servovalves, and present a method of energy saving in the context of a servocontrolled pneumatic actuator.

Like the work of Al Dakkan et al., this paper presents an approach to energy saving in the context of a servocontrolled pneumatic actuator. The decoupled configuration (utilized in Al Dakkan et al.) enables independent control of cylinder chamber pressures, but does not enable the reuse or recycling of pressurized air. Unlike that work, the work presented herein utilizes a crossflow configuration rather than a decoupled configuration, such that pressurized air can be recycled. The valve configuration utilized in this work is similar to that used in the work of Pu et al. [15]. The control approach, however, is quite different. Specifically, Pu et al. utilize a linear control approach that assumes for simplicity that the command to the crossflow valve is linearly related to the command to the standard (four-way) valve. Further, the results

presented by Pu et al. do not quantify the energy savings provided by their approach (relative to a standard approach), and thus the effectiveness of the proposed approach is unclear. The work presented in this paper incorporates a nonlinear control approach that constrains the valves only by the tracking and energy saving objectives, and experimentally demonstrates the effectiveness of the proposed approach relative to a standard (four-way valve) approach.

Crossflow Configuration

As previously mentioned, the introduction of a crossflow valve in a pneumatic servo actuator enables the recycling of pressurized air, and thus the potential for energy saving control. The crossflow configuration is shown in Figure 5-2.

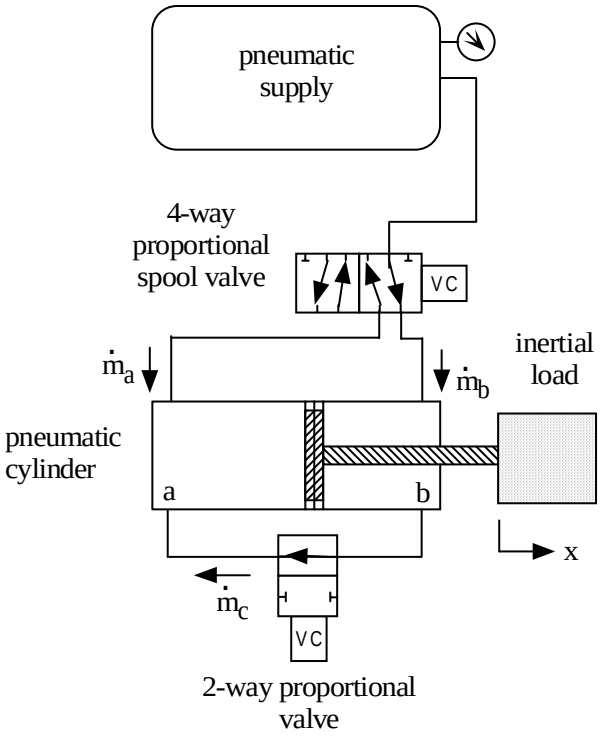

Figure 5-2. Modifying the configuration of a typical pneumatic servo system to add an additional inter-chamber flow path.

Assuming the input to this system is the valve area command to each valve, and that the output of interest is the piston motion, the input/output behavior of the crossflow configuration can be described as follows. Assuming a combined inertial and viscous load, the motion dynamics of the system can be described as:

$$M\ddot{x} + B\dot{x} = P_a A_a - P_b A_b - P_{atm} A_r \tag{1}$$

where M is the mass of the piston and rod assembly, B is the viscous friction coefficient, A_a and A_b are the effective areas of each side of the piston, and A_r is the cross-sectional area of the piston rod. Differentiating (1) with respect to time gives:

$$M\dddot{x} + B\ddot{x} = \dot{P}_a A_a - \dot{P}_b A_b$$

or

$$\dddot{x} = \frac{1}{M}(-B\ddot{x} + \dot{P}_a A_a - \dot{P}_b A_b) \tag{2}$$

Assuming air is a perfect gas undergoing an isothermal process, the rate of change of the pressure inside each chamber of the cylinder can be expressed as:

$$\dot{P}_{(a,b)} = \frac{RT}{V_{(a,b)}}\dot{m}_{t(a,b)} - \frac{P_{(a,b)}}{V_{(a,b)}}\dot{V}_{(a,b)} \tag{3}$$

where $P_{(a,b)}$ is the absolute pressure inside each side of the cylinder, $\dot{m}_{t(a,b)}$ is the total mass flow rate into or out of each side of the cylinder, R is the universal gas constant, T is the fluid temperature, and $V_{(a,b)}$ is the volume of each cylinder chamber. Substituting (3) into (2) gives:

$$\dddot{x} = \frac{A_a}{M}[\frac{RT}{V_a}\dot{m}_{t,a} - \frac{P_a}{V_a}\dot{V}_a] - \frac{A_b}{M}[\frac{RT}{V_b}\dot{m}_{t,b} - \frac{P_b}{V_b}\dot{V}_b] - \frac{B}{M}\ddot{x} \tag{4}$$

The mass flow rate into or out of each chamber $\dot{m}_{t(a,b)}$ is the combination of the mass

flow from the four-way valve, $\dot{m}_{(a,b)}$, and the mass flow through the crossflow valve, $\dot{m}_c$. Given a crossflow mass flow rate defined as positive from chamber *b* to chamber *a* (as shown in Figure 5-2), the relationship can be expressed mathematically as:

$$\dot{m}_{t,a} = \dot{m}_a + \dot{m}_c \tag{5}$$

$$\dot{m}_{t,b} = \dot{m}_b - \dot{m}_c \tag{6}$$

Substituting (5) and (6) into (4) gives:

$$\ddot{x} = \frac{A_a}{M}[\frac{RT}{V_a}(\dot{m}_a + \dot{m}_c) - \frac{P_a}{V_a}\dot{V}_a] - \frac{A_b}{M}[\frac{RT}{V_b}(\dot{m}_b - \dot{m}_c) - \frac{P_b}{V_b}\dot{V}_b] - \frac{B}{M}\ddot{x} \tag{7}$$

The volume in each chamber is a geometric function of piston displacement *x*, given by:

$$V_{(a,b)} = A_{(a,b)}(\frac{L}{2} \pm x) \tag{8}$$

The rate of change of the chamber volume is likewise given by:

$$\dot{V}_{(a,b)} = \pm A_{(a,b)}\dot{x} \tag{9}$$

Substituting (8) and (9) into (7) gives the following equation:

$$\ddot{x} = \frac{RT}{M}(\frac{\dot{m}_a + \dot{m}_c}{\frac{L}{2} + x} - \frac{\dot{m}_b - \dot{m}_c}{\frac{L}{2} - x}) - \frac{A_a}{M}(\frac{P_a\dot{x}}{\frac{L}{2} + x}) - \frac{A_b}{M}(\frac{P_b\dot{x}}{\frac{L}{2} - x}) - \frac{B}{M}\ddot{x} \tag{10}$$

Assuming the mass flow rate through each valve can be described by the isentropic flow of an ideal gas through a converging nozzle, the mass flow rate though each valve orifice with effective area A_v is given by:

$$\dot{m}(P_u, P_d) = A_v\Psi(P_u, P_d) \tag{11}$$

where

$$\Psi(P_u, P_d) = \begin{cases} \sqrt{\frac{k}{RT}\left(\frac{2}{k+1}\right)^{(k+1)/(k-1)}} C_f P_u & \text{if } \frac{P_d}{P_u} \le C_r \text{ (choked)} \\ \sqrt{\frac{2k}{RT(k-1)}} \sqrt{1 - \left(\frac{P_d}{P_u}\right)^{(k-1)/k}} \left(\frac{P_d}{P_u}\right)^{(1/k)} C_f P_u & \text{otherwise (unchoked)} \end{cases} \tag{12}$$

where C_f is the discharge coefficient of the valve, P_u and P_d are the upstream and downstream pressures, respectively, k is the ratio of specific heats, C_r is the pressure ratio that divides the flow regimes into unchoked (subsonic) and choked (sonic) flow. As such, the mass flow rates can be expressed as:

$$\dot{m}_a = \begin{cases} A_{v,1}\Psi(P_s, P_a) & \text{if } A_{v,1} \ge 0 \\ A_{v,1}\Psi(P_a, P_{atm}) & \text{if } A_{v,1} < 0 \end{cases} \tag{13}$$

$$\dot{m}_b = \begin{cases} -A_{v,1}\Psi(P_b, P_{atm}) & \text{if } A_{v,1} \ge 0 \\ -A_{v,1}\Psi(P_s, P_b) & \text{if } A_{v,1} < 0 \end{cases} \tag{14}$$

$$\dot{m}_c = \begin{cases} A_{v,2}\Psi(P_b, P_a) & \text{if } P_a \le P_b \\ -A_{v,2}\Psi(P_a, P_b) & \text{if } P_a > P_b \end{cases} \tag{15}$$

where $A_{v,1}$ is the signed effective area of the four-way control valve, and $A_{v,2}$ is the nonnegative effective area of the two-way crossflow valve. Note that when $A_{v,1}$ is positive, chamber *a* is connected to the supply and chamber *b* is connected to the exhaust; when $A_{v,1}$ is negative, chamber *a* is connected to the exhaust and chamber *b* is connected to the supply. Combining (10) with (13-15) gives the full input/output model of the pneumatic servoactuator in a crossflow configuration from the effective valve area inputs, $A_{v,1}$ and $A_{v,2}$, to the load position output, x.

Controller Design

Based on this model, an energy-saving controller can be developed to minimize the consumption of compressed air. Specifically, tracking of a given trajectory with a given load will dictate a given mass flow rate into or out of the respective sides of the pneumatic cylinder. In cases where the pressure in the chamber being depressurized is greater than the pressure in the chamber being pressurized, the required mass flow rate can be supplemented via use of the crossflow valve. As such, the proposed controller can be developed by first calculating the control effort (i.e., differential mass flow rate) required for tracking, and second by calculating the extent to which the crossflow can contribute to that differential mass flow.

Calculation of the Differential Mass Flow Rate

The first term on the right-hand side of (10) is the only term affected by the system inputs. In order to simplify the controller design, an intermediate input called the *control effort* is defined in such a way that the system dynamics are affine in the intermediate control variable. The intermediate control effort is therefore defined as:

$$u = \frac{\dot{m}_a + \dot{m}_c}{\frac{L}{2} + x} - \frac{\dot{m}_b - \dot{m}_c}{\frac{L}{2} - x} \tag{16}$$

such that substitution into (10) gives:

$$\dddot{x} = \frac{RT}{M}u - \frac{A_a}{M}\left(\frac{P_a \dot{x}}{\frac{L}{2} + x}\right) - \frac{A_b}{M}\left(\frac{P_b \dot{x}}{\frac{L}{2} - x}\right) - \frac{B}{M}\ddot{x} \tag{17}$$

or

$$\dddot{x} = f + bu \tag{18}$$

where

$$f = -\frac{A_a}{M}\left(\frac{P_a \dot{x}}{\frac{L}{2}+x}\right) - \frac{A_b}{M}\left(\frac{P_b \dot{x}}{\frac{L}{2}-x}\right) - \frac{B}{M}\ddot{x} \tag{19}$$

$$b = \frac{RT}{M} \tag{20}$$

Thus expressing the system dynamics in control canonical form, a sliding mode approach can be utilized for the control of the intermediate system. An integral sliding surface is defined as:

$$s = \left(\frac{d}{dt} + \lambda\right)^3 \int_0^t e d\tau \tag{21}$$

where $e = x - x_d$, x_d is the desired position, and λ is a control gain. The corresponding sliding condition is

$$\frac{1}{2}\frac{d}{dt}s^2 \le -\eta|s| \tag{22}$$

where η is a positive constant. In order to satisfy the sliding condition in the presence of the model uncertainty, a sliding mode control law is developed as described in [21]:

$$\hat{u} = \frac{1}{\hat{b}}\left(\dddot{x}_r - \hat{f} - \hat{k}\,\mathrm{sgn}(s)\right) \tag{23}$$

where

$$\dddot{x}_r = \dddot{x}_d - 3\lambda\ddot{e} - 3\lambda^2\dot{e} - \lambda^3 e \tag{24}$$

The robustness gain $\hat{k}$ is determined by the following condition:

$$\hat{k} \ge \beta(F + \beta U + \eta) + (\beta - 1)|\hat{u}| \tag{25}$$

where the bounds of uncertainty associated with the model of (18-20) are given by:

$$\left|\hat{f} - f\right| \le F \tag{26}$$

$$\beta^{-1} \le b/\hat{b} \le \beta \tag{27}$$

$$\left|\hat{u} - u\right| \le U \tag{28}$$

where $\hat{f}$, $\hat{b}$ and $\hat{u}$ are the nominal values of *f*, *b* and *u*, respectively, thus rendering *F*, β and U as positive constants. Note that the intermediate control effort, *u*, includes parametric uncertainty, since it must be calculated based on (12) and (16).

Relative Contributions of Crossflow and Direct Flow

As discussed previously, the total control effort is composed of a direct flow portion (i.e., mass flow rate from the four-way valve) and a crossflow portion, and as such the control input can be expressed as:

$$\hat{u} = u_{ab} + u_c \tag{29}$$

where

$$u_{ab} = \frac{\dot{m}_a}{\frac{L}{2} + x} - \frac{\dot{m}_b}{\frac{L}{2} - x} \tag{30}$$

$$u_c = \dot{m}_c \frac{L}{(\frac{L}{2})^2 - x^2} \tag{31}$$

where u_{ab} is the direct flow component of the intermediate control effort and u_c is the crossflow component. From (31) it can be observed that the crossflow contribution to the control effort u_c has the same sign as the crossflow rate $\dot{m}_c$, which in turn depends solely on the difference between the chamber pressures, $\Delta P = P_a - P_b$, as indicated by (15). Since effective recycling of the mass flow requires that the crossflow component always add constructively to the intermediate control effort (i.e., the differential mass flow rate), the relationship between the crossflow and the intermediate differential flow control input can be considered in two cases:

Case 1: $\hat{u} \cdot \Delta P < 0$ (32)

Case 2: $\hat{u} \cdot \Delta P \geq 0$ (33)

In Case 1, the crossflow u_c has the same sign as the control effort $\hat{u}$, and thus the recycled crossflow is constructive with regard to the desired tracking effort. As such, the crossflow valve is opened and the valve area computed by combining (15) and (31) such that:

$$A_{v,2} = \begin{cases} \dfrac{\hat{u} \cdot [(\frac{L}{2})^2 - x^2]}{\Psi_c \cdot L} & \text{if } \dfrac{\hat{u} \cdot [(\frac{L}{2})^2 - x^2]}{\Psi_c \cdot L} \leq A_{v,\max} \\ A_{v,\max} & \text{otherwise} \end{cases} \tag{34}$$

where

$$\Psi_c = \Psi[\max(P_a, P_b), \min(P_a, P_b)] \tag{35}$$

The remainder of the intermediate control effort $\hat{u}$ (i.e., the remainder of the required differential mass flow rate) must be provided by the four-way valve, and thus its commanded area is given by combining (13-14), (29-31), and (34-35):

$$A_{v,1} = \frac{\hat{u} \cdot [(\frac{L}{2})^2 - x^2] - A_{v,2}\Psi_c L}{\Psi_a(\frac{L}{2} - x) + \Psi_b(\frac{L}{2} + x)} \tag{36}$$

where

$$\Psi_a = \begin{cases} \Psi(P_s, P_a) & \text{if } \hat{u} \geq 0 \\ \Psi(P_a, P_{atm}) & \text{otherwise} \end{cases} \tag{37}$$

$$\Psi_b = \begin{cases} \Psi(P_b, P_{atm}) & \text{if } \hat{u} \geq 0 \\ \Psi(P_s, P_b) & \text{otherwise} \end{cases} \tag{38}$$

In Case 2, the contribution of the crossflow u_c would be in the opposite direction of the control effort $\hat{u}$ (i.e., non-constructive recycling), and thus the two-way valve should remain closed:

$$A_{v,2} = 0 \tag{39}$$

The entire differential mass flow must in this case be provided by the four-way valve, such that the signed area is given by:

$$A_{v,1} = \frac{\hat{u} \cdot [(\frac{L}{2})^2 - x^2]}{\Psi_a(\frac{L}{2} - x) + \Psi_b(\frac{L}{2} + x)} \tag{40}$$

Note that (40) is also the control law for a standard sliding mode controller (i.e., in the absence of a two-way crossflow valve). The two-input control law can be summarized as follows: if (32) is satisfied, calculate the valve inputs with (34) and (36); otherwise calculate the valve inputs with (39) and (40).

Experiments

The proposed controller was implemented on an experimental setup to demonstrate the tracking performance and to quantify the energy saving, relative to a standard configuration (i.e., four-way valve). The experimental setup, which is shown schematically in Figure 5-2, consists of a 2.7 cm (1-1/16 in) inner diameter, 10 cm (4 in) stroke pneumatic cylinder (Numatics 1062D04-04A) controlled by a pair of proportional servovalves (FESTO MPYE-5-M5-010-B), configured as a four-way valve and a two-way (crossflow) valve, respectively. The output of the pneumatic cylinder was connected to a linear slide, upon which a mass of 10 kg was mounted. Displacement of the slide (and actuator) was measured with a linear potentiometer (Midori LP-100F), while the pressure in each cylinder chamber was measured by a pressure sensor (FESTO SDE-16-10V/20mA). For the evaluation of the energy (i.e., pressurized supply mass) expenditure, a mass flow meter (Hastings HFC-202) was used to measure the mass flow rate from the

air supply, which was integrated over the duration of the experiment to obtain the cumulative compressed air consumption. A comparison was performed for this setup between a standard pneumatic servo system and the proposed crossflow energy saving servo system. The standard system, which was controlled by a single four-way spool valve, utilized a sliding mode controller where the control law is given by (23) and (40). The model and controller parameters used for the sliding mode controller are given in Table 5-1. The crossflow system, which was controlled by a four-way spool valve in combination with a two-way crossflow valve, utilized the same model and control parameters as those used on the standard setup (i.e., the parameters listed in Table 5-1).

Table 5-1. Model and controller parameters for experimental implementation.

Parameter	Description	Value	Unit
P_s	Supply pressure	653	kPa
A_a	Piston area side a	572	mm^2
A_b	Piston area side b	540	mm^2
A_r	Rod area	32	mm^2
$A_{v,max}$	Maximum valve area	12.57	mm^2
C_f	Discharge coefficient	0.8	
C_r	Pressure ratio	0.5	
k	Ratio of specific heats	1.4	
R	Universal gas constant	0.287	kJ/kg·K
T	Gas temperature at the orifice	293	K
λ	Control bandwidth	30	mm/sec^2
k	Robustness gain	4×10^5	mm/sec^3

Figures 5-3 through 5-5 show a comparison of tracking performance of the crossflow approach with the standard sliding mode approach corresponding to sinusoidal desired position trajectories of 0.25 Hz, 1.0 Hz, and 1.5 Hz, respectively, indicating that both approaches provide similar tracking performance. Figure 5-6 shows the valve

commands for the crossflow configuration corresponding to tracking at 1.0 Hz (i.e., Figure 5-4), while Figure 5-7 shows for comparison the corresponding single valve command for the standard approach. Figures 5-8 and 5-9 show the same commands over a single cycle. Figure 5-10 shows the cylinder chamber pressures corresponding to the crossflow configuration for tracking at 1.0 Hz. Note that the energy saving is enabled when the pressure trajectories cross, enabling the constructive recycling of the mass from one chamber to the other. The average pressure in chamber *a* is in general lower than the average pressure in chamber *b*, since the tracking task is symmetric, but the piston areas are asymmetric, requiring a higher pressure in chamber *b* to provide the same actuator force. Since crossflow recycling is enabled when the pressure traces cross, a symmetric cylinder (i.e., either rodless or double rod cylinder) would provide considerably greater opportunity for crossflow energy saving. Figure 5-11 shows the energy (i.e., mass flow) expenditure of the crossflow and standard approaches corresponding to the 1.0 Hz trajectory tracking, indicating significantly less required mass flow for the crossflow approach. The relative energy expenditure of the crossflow approach versus the standard approach at various tracking frequencies, and for a step input, is summarized in Table 5-2. As indicated in the table, the proposed approach reduces the air consumption 25% to 40% for sinusoidal tracking at frequencies between 0.25 Hz and 1.5 Hz, and 52% for step input tracking. It can be further observed that the energy saving effect tends to decrease with the increase of the tracking frequency, which is due primarily to the (area) saturation of the two-way valve. Higher tracking frequency requires a larger control effort, which effectively saturates the two-way valve and thus requires the additional mass flow from the supply. Note that, as seen from Figure 5-6, the valve area required of the crossflow

valve is much larger than that of the four-way valve, since the driving pressure difference across the valve is in general much smaller.

Table 5-2. Energy saving of crossflow relative to standard controller.

Frequency (Hz)	Energy Saving (%)
0.25	36
0.5	38
0.75	40
1.0	31
1.25	25
1.5	26
step	52

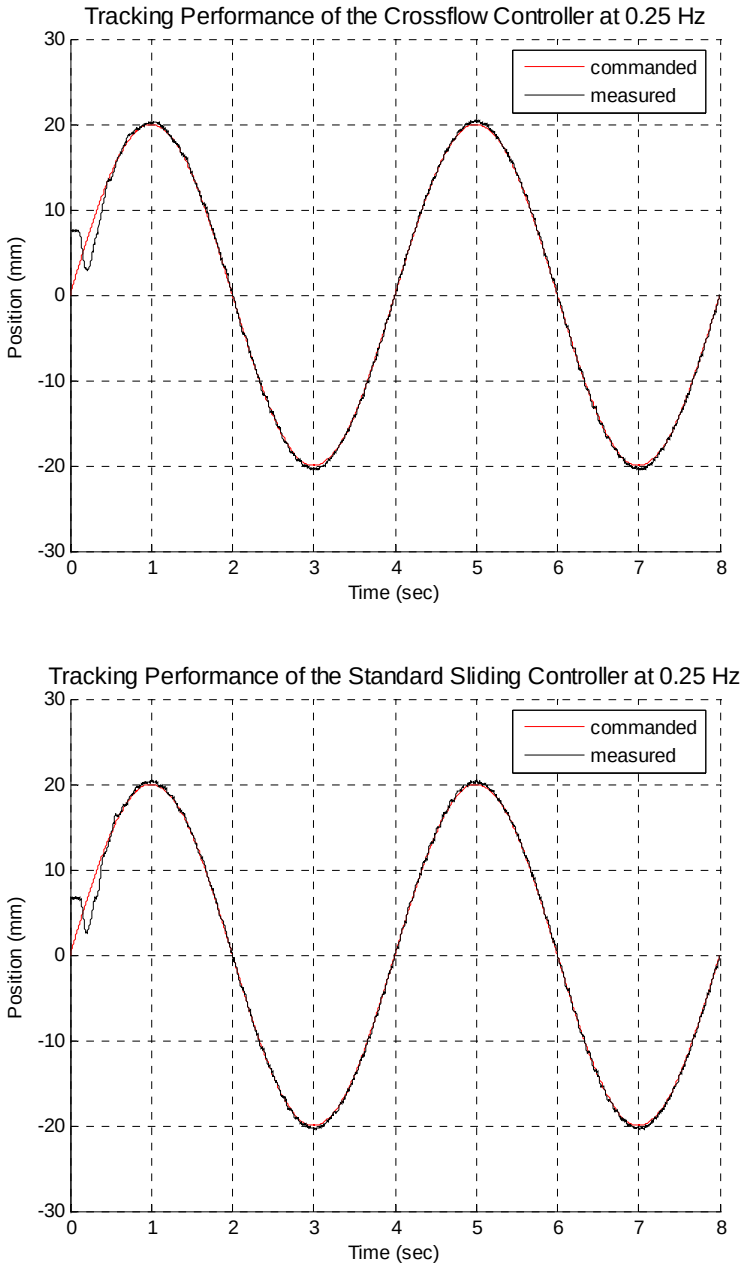

Figure 5-3. Tracking performance comparison of the crossflow controller and the standard sliding controller corresponding to 0.25 Hz sinusoidal command.

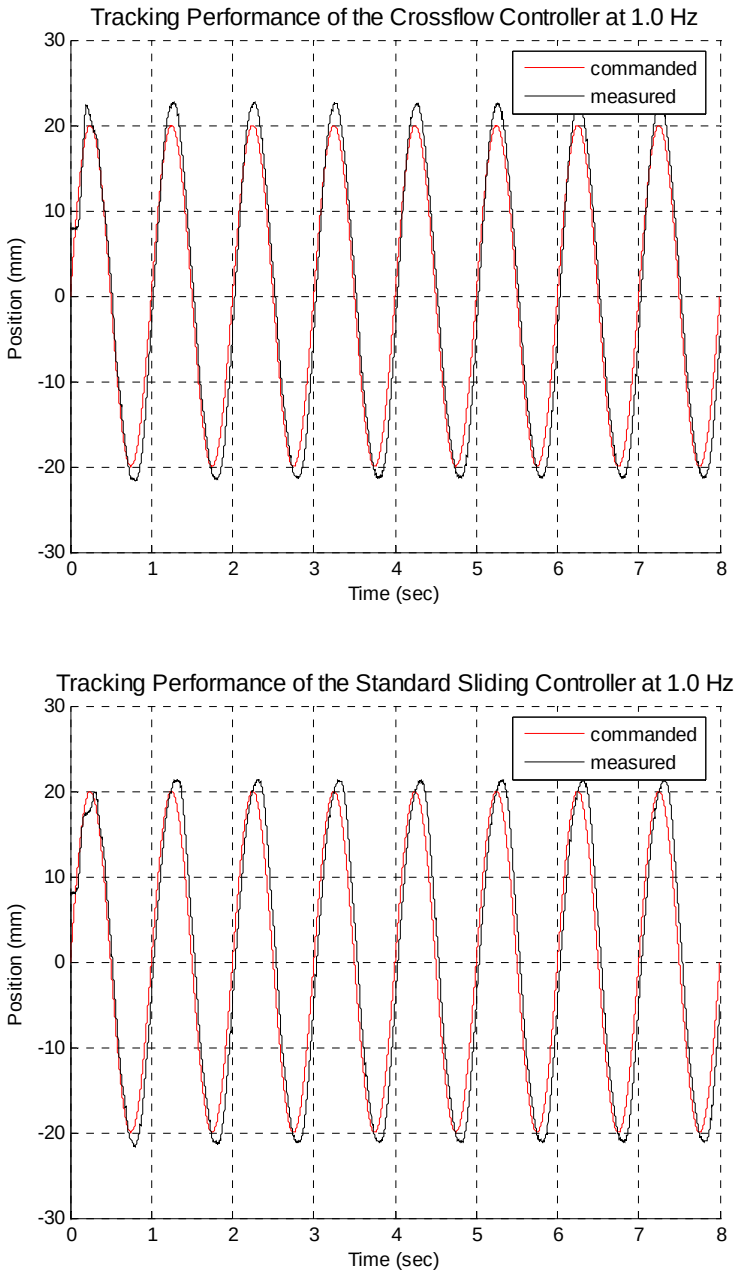

Figure 5-4. Tracking performance comparison of the crossflow controller and the standard sliding controller corresponding to 1.0 Hz sinusoidal command.

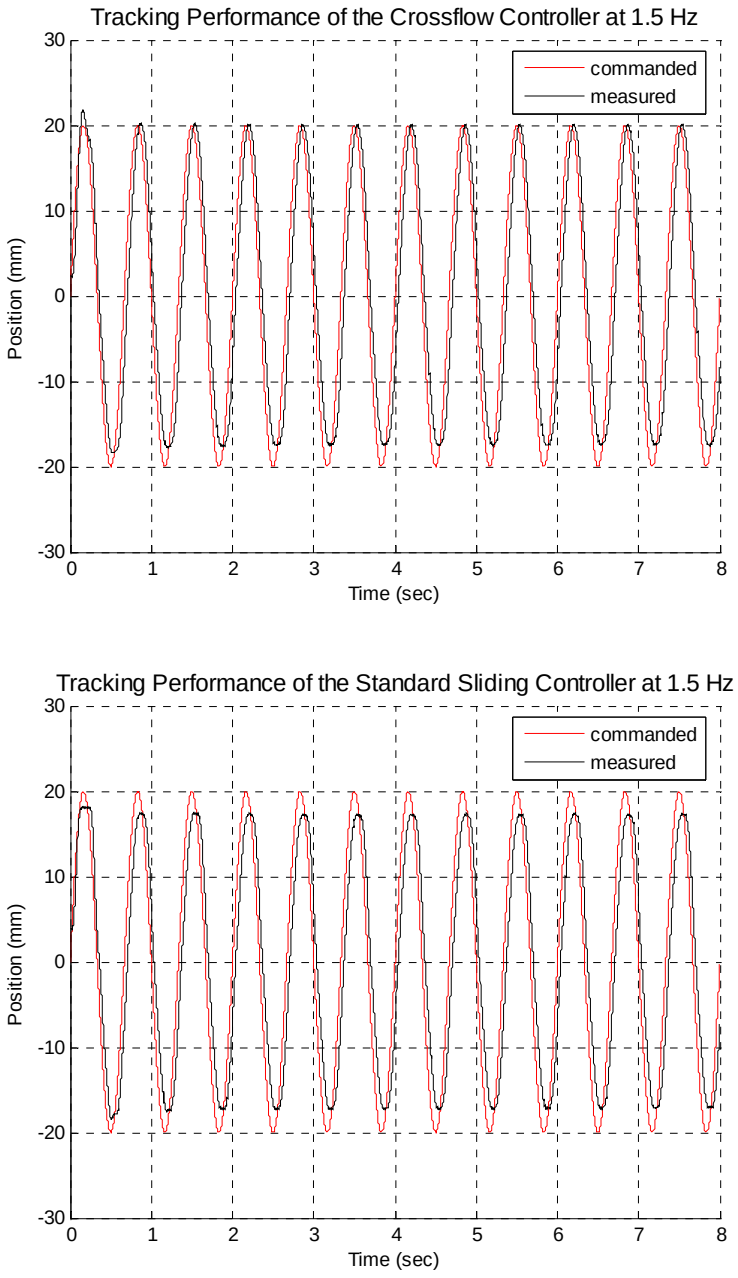

Figure 5-5. Tracking performance comparison of the crossflow controller and the standard sliding controller corresponding to 1.5 Hz sinusoidal command.

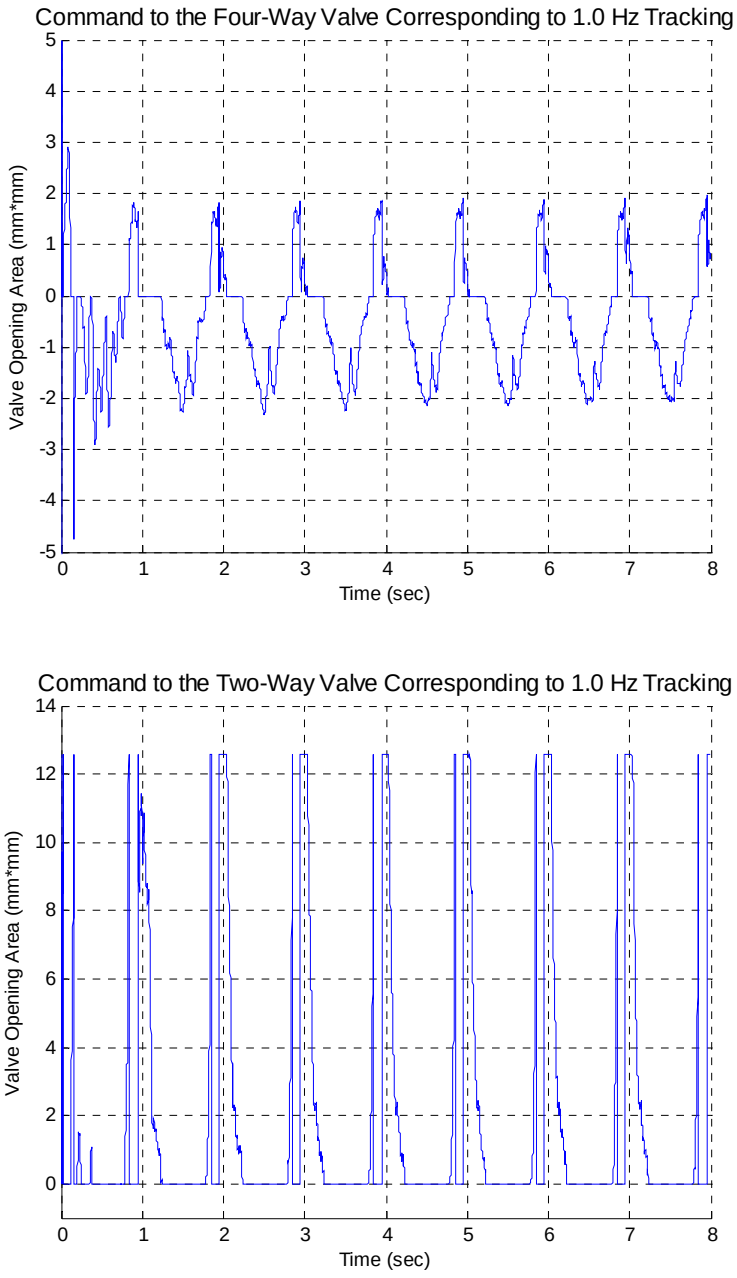

Figure 5-6. Control (valve) commands for crossflow controller corresponding to 1.0 Hz sinusoidal tracking.

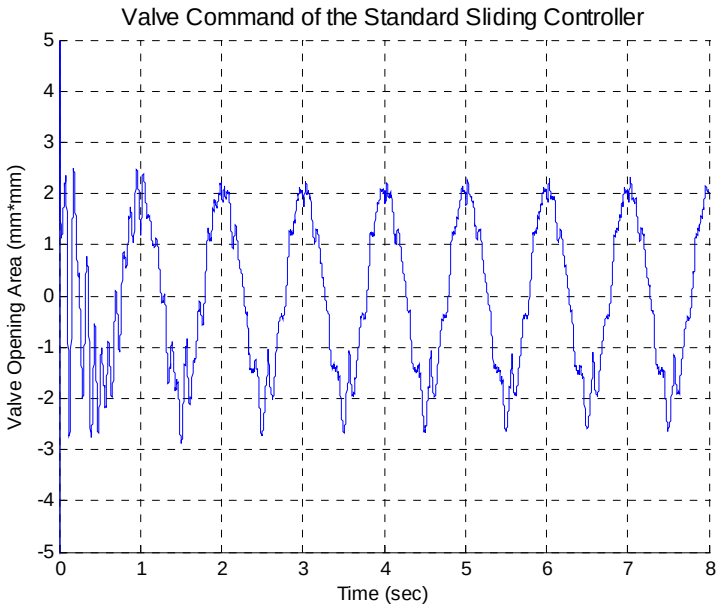

Figure 5-7. Control (valve) command for standard controller corresponding to 1.0 Hz sinusoidal tracking.

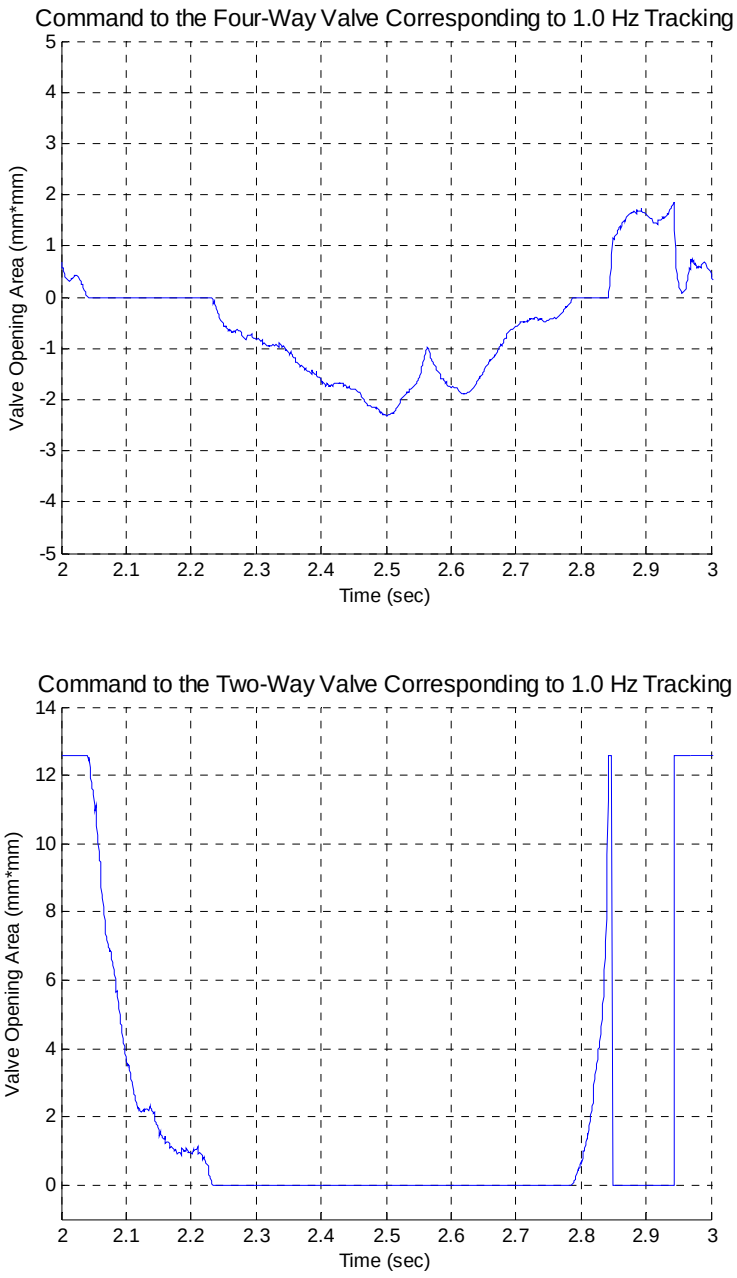

Figure 5-8. One cycle of control (valve) commands for crossflow controller corresponding to 1.0 Hz sinusoidal tracking.

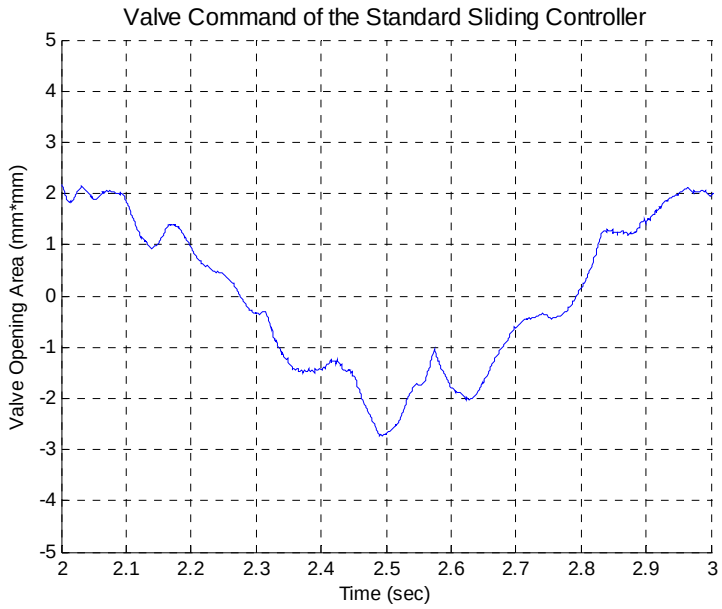

Figure 5-9. One cycle of control (valve) command for standard controller corresponding to 1.0 Hz sinusoidal tracking.

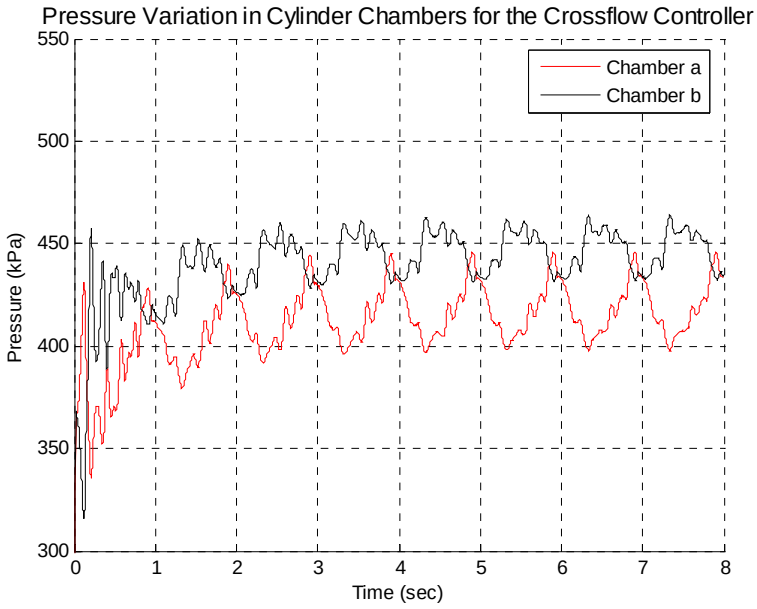

Figure 5-10. Cylinder pressures for crossflow controller corresponding to 1.0 Hz sinusoidal tracking.

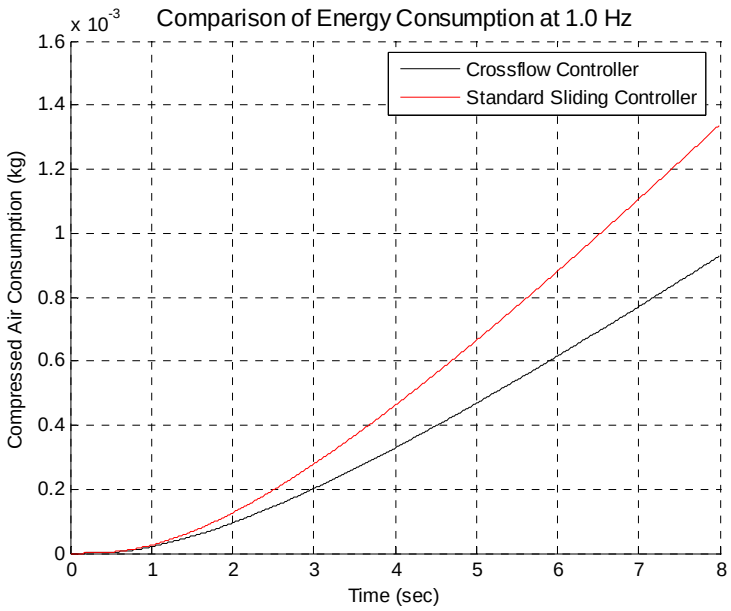

Figure 5-11. Comparison of supply mass expenditure between crossflow and standard approaches corresponding to 1.0 Hz sinusoidal tracking.

Conclusion

This paper presents a crossflow energy saving approach that enables significant energy saving for a pneumatic actuator in the context of servo actuation. Experimental results were presented that demonstrate reduced energy consumption by 25% to 52% relative to a standard four-way valve configuration, with essentially no sacrifice in tracking performance.

References

[1] Shearer, J. L., "Study of Pneumatic Processes in the Continuous Control of Motion with Compressed Air – I," *Transactions of the ASME*, vol. 78, pp. 233-242, 1956.

[2] Shearer, J. L., "Study of Pneumatic Processes in the Continuous Control of Motion with Compressed Air – II," *Transactions of the ASME*, vol. 78, pp. 243-249, 1956.

[3] Shearer, J. L., "Nonlinear Analog Study of a High-Pressure Servomechanism," *Transactions of the ASME*, vol. 79, pp. 465-472, 1957.

[4] Mannetje, J. J., "Pneumatic Servo Design Method Improves System Bandwidth Twenty-fold," *Control Engineering*, vol. 28, no. 6, pp. 79-83, 1981.

[5] Ben-Dov, D. and Salcudean, S. E., "A Force Controlled Pneumatic Actuator," *IEEE Transactions on Robotics and Automation,* vol. 14, no. 5, pp. 732-742, 1998.

[6] Wang, J., Pu, J., and Moore, P., "A practical control strategy for servo-pneumatic actuator systems," *Control Engineering Practice*, vol. 7, pp. 1483-1488, 1999.

[7] Maeda, S., Kawakami, Y., and Nakano, K., "Position Control of Pneumatic Lifters," *Transactions of Japan Hydraulic and Pneumatic Society*, vol. 30, no. 4, pp. 89-95, 1999.

[8] Ning, S. and Bone, G. M., "High Steady-State Accuracy Pneumatic Servo Positioning System with PVA/PV Control and Friction Compensation," *Proceeding of the 2002 IEEE International Conference on Robotics & Automation, pp. 2824-2829, 2002.*

[9] Bobrow, J., and McDonell, B., "Modeling, Identification, and Control of a Pneumatically Actuated, Force Controllable Robot," *IEEE Transactions on Robotics and Automation,* vol. 14, no. 5, pp. 732-742, 1998.

[10] Richer, E. and Hurmuzlu, Y., "A High Performance Pneumatic Force Actuator System: Part I-Nonlinear Mathematical Model" *ASME Journal of Dynamic Systems, Measurement, and Control*, vol. 122, no. 3, pp. 416-425, 2000.

[11] Richer, E. and Hurmuzlu, Y., "A High Performance Pneumatic Force Actuator System: Part II-Nonlinear Control Design" *ASME Journal of Dynamic Systems, Measurement, and Control*, vol. 122, no. 3, pp. 426-434, 2000.

[12] Sanville, F. E., "Two-level Compressed Air Systems for Energy Saving," The 7th International Fluid Control Symposium, pp. 375-383, 1986.

[13] Quaglia, G. and Gastaldi, L., "The Design of Pneumatic Actuator with Low Energy Consumption," The 4th Triennial International Symposium on Fluid Control, Fluid Measurement, and Visualization, pp. 1061-1066, 1994.

[14] Quaglia, G. and Gastaldi, L., "Model and Dynamic of Energy Saving Pneumatic Actuator," The 4th Scandinavian International Conference on Fluid Power, vol. 1, 481-492, 1995.

[15] Pu, J., Wang, J. H., Moore, P. R., and Wong, C. B., "A New Strategy for Closed-loop Control of Servo-Pneumatic Systems with Improved Energy Efficiency and System Response," The Fifth Scandinavian International Conference on Fluid Power, pp. 339-352, 1997.

[16] Wang, J., Wang, J-D., Liau, V., "Energy Efficient Optimal Control of Pneumatic Actuator Systems," *Systems Science*,Vol. 26, 3, pp. 109-123, 2000.

[17] Kawakami, Y., Terashima, Y., Kawai, S., "Application of Energy-saving to Pneumatic Driving Systems," Proc. 4th JHPS International Symposium, pp. 201-206, 1999.

[18] Arinaga, T., Kawakami, Y., Terashima, Y., and Kawai, S., "Approach for Energy-Saving of Pneumatic Systems," Proceedings of the 1st FPNI-PhD Symposium, pp. 49-56, 2000.

[19] Al-Dakkan, K.A., Goldfarb, M., and Barth, E.J. "Energy Saving Control for Pneumatic Servo Systems," ASME/IEEE International Conference on Advanced Intelligent Mechatronics, vol. 1, pp. 284 –289, 2003.

[20] Al-Dakkan, K.A., Barth, E.J., and Goldfarb, M. "A Multi-Objective Sliding Mode Approach for the Energy Saving Control of Pneumatic Servo Systems," *ASME International Mechanical Engineering Congress and Exposition*, IMECE2003-42746, 2003.

[21] Slotine, J.J.E., and Li, W. *Applied Nonlinear Control*. Prentice-Hall, Inc., New Jersey, 1991.

CHAPTER VI

CONCLUSIONS

This dissertation explored several control applications of pneumatic systems by exploiting the natural characteristics of such systems. The first manuscript presented a control approach capable of providing nonlinear servo control via relatively inexpensive on/off solenoid valves. Based on a full nonlinear model derived by applying averaging method to the PWM controlled pneumatic servo system, a sliding mode controller was developed which provides effective control of a continuous motion command. The second manuscript presented an approach for the simultaneous control of output force and stiffness of a pneumatic actuator. As a result, the pneumatic actuator can be used as a robotic actuator capable of physically (i.e., open-loop) variable stiffness with a minimal amount of associated hardware. The third manuscript proposed the use of pneumatic actuation for an impedance-type haptic device. The presence of the open-loop stiffness in a pneumatic actuator reduced the requirement for the stiffness component from computer-based feedback control, thus enhances the passivity of the haptic device and the range of achievable surface stiffnesses relative to an electric motor actuated system. The fourth manuscript presented a crossflow energy saving approach that enables significant energy saving for a pneumatic actuator in the context of servo actuation. The proposed control approach reduced energy consumption by 25% to 52%, with essentially no compromise in tracking performance, relative to a standard four-way valve configuration controlled by a standard sliding mode control approach.